Report of Energy Frontier Topical Groups 5, 6, 7 submitted to the US Community Study
on the Future of Particle Physics (Snowmass 2021)

Precision QCD, Hadronic Structure & Forward QCD, Heavy Ions

M. Begel,[1, *] S. Höche,[2, *] M. Schmitt,[3, *] H.-W. Lin,[4, 5, †] P.M. Nadolsky,[2, 6, †] C. Royon,[7, †]
Y-J. Lee,[8, ‡] S. Mukherjee,[1, ‡] C. Baldenegro,[9] J. Campbell,[2] G. Chachamis,[10]
F.G. Celiberto,[11, 12, 13] A. M. Cooper-Sarkar,[14] D. d'Enterria,[15] M. Diefenthaler,[16]
M. Fucilla,[17, 18, 19] M. V. Garzelli,[20] M. Guzzi,[21] M. Hentschinski,[22] T. J. Hobbs,[23, 24]
J. Huston,[4] J. Isaacson,[2] S.R. Klein,[25] F. Kling,[26] P. Kotko,[27] Yu. V. Kovchegov,[28]
G. Krintiras,[7] A.S. Kronfeld,[2] K. Kutak,[29] B. Mistlberger,[30] I. Moult,[31] S. Mrenna,[2]
B. Nachman,[25] M. Narain,[32] F.I. Olness,[6] A. Papa,[17, 18] R.D. Pisarski,[1] M. Pitt,[15]
S. Rappoccio,[33] L. Reina,[34] J. Reuter,[26] M.H. Reno,[35] G.P. Salam,[36, 37] M. Strikman,[38]
N. Tran,[2] A. Tricoli,[1] M. Ubiali,[39] A. van Hameren,[29] A. Vossen,[40] and K. Xie[41]

[1]*Physics Department, Brookhaven National Laboratory, Upton, NY 11973, USA*
[2]*Fermi National Accelerator Laboratory, Batavia, IL 60510, USA*
[3]*Department of Physics & Astronomy, Northwestern University, Evanston, IL 60208, USA*
[4]*Department of Physics & Astronomy, Michigan State University, MI 48824, USA*
[5]*Department of Computational Mathematics, Science and
Engineering, Michigan State University, East Lansing, MI 48824*
[6]*Department of Physics, Southern Methodist University, Dallas, TX 75275, USA*
[7]*Department of Physics & Astronomy, The University of Kansas, Lawrence, KS 66045, USA*
[8]*The Massachusetts Institute of Technology, Department of Physics, Cambridge, MA 02139, USA*
[9]*École Polytechnique, Laboratoire Leprince-Ringuet, Av. Chasles, 91120 Palaiseau, France*
[10]*Laboratório de Instrumenta cão e Física Experimental de Partículas,
Av. Prof. Gama Pinto, 2, P-1649-003 Lisboa, Portugal*
[11]*European Centre for Theoretical Studies in Nuclear Physics
and Related Areas (ECT*), I-38123 Villazzano, Trento, Italy*
[12]*Fondazione Bruno Kessler (FBK), I-38123 Povo, Trento, Italy*
[13]*INFN-TIFPA Trento Institute of Fundamental Physics and Applications, I-38123 Povo, Trento, Italy*
[14]*Department of Physics, University of Oxford, UK*
[15]*CERN, 1211 Geneva 23, Switzerland*
[16]*Thomas Jefferson National Accelerator Facility, Newport News, VA 23606, USA*
[17]*Dipartimento di Fisica, Universitá della Calabria, I-87036 Arcavacata di Rende, Cosenza, Italy*
[18]*Istituto Nazionale di Fisica Nucleare, Gruppo collegato
di Cosenza, I-87036 Arcavacata di Rende, Cosenza, Italy*
[19]*Université Paris-Saclay, CNRS, IJCLab, 91405 Orsay, France*
[20]*Universität Hamburg, II Institut für Theoretische Physik, 22761 Hamburg, Germany*
[21]*Department of Physics, Kennesaw State University, Kennesaw, GA 30144, USA*
[22]*Departamento de Actuaria, Física y Matemáticas,
Universidad de las Americas Puebla, San Andrés Cholula, 72820 Puebla, Mexico*
[23]*High Energy Physics Division, Argonne National Laboratory, Argonne, IL 60439, USA*
[24]*Department of Physics, Illinois Institute of Technology, Chicago, IL 60616, USA*
[25]*Lawrence Berkeley National Laboratory, Berkeley CA 94720 USA*
[26]*Deutsches Elektronen-Synchrotron DESY, Notkestr. 85, 22607 Hamburg, Germany*
[27]*AGH University of Science and Technology,
Physics Faculty, Mickiewicza 30, 30-059 Kraków, Poland*
[28]*Department of Physics, The Ohio State University, Columbus, OH 43210, USA*

[29] Institute of Nuclear Physics, Polish Academy of Sciences, ul. Radzikowskiego 152, 31-342,Kraków, Poland

[30] SLAC National Accelerator Laboratory, Stanford University, Stanford, CA 94039, USA

[31] Department of Physics, Yale University, New Haven, CT 06511, USA

[32] Physics Department, Brown University, Providence, RI, 02912, USA

[33] University at Buffalo, State University of New York, Amherst, NY 14221 USA

[34] Department of Physics, Florida State University, Tallahassee, FL 32306-4350, USA

[35] Department of Physics & Astronomy, University of Iowa, Iowa City, IA 52242-1479, USA

[36] Rudolf Peierls Centre for Theoretical Physics, University of Oxford, Oxford, OX1 3PU, UK

[37] All Souls College, University of Oxford, Oxford OX1 4AL, United Kingdom

[38] Department of Physics, Pennsylvania State University, University Park, PA 16802, USA

[39] DAMTP, University of Cambridge, Cambridge, CB3 0WA, UK

[40] Department of Physics, Duke University, Durham, North Carolina 27708, USA

[41] Pittsburgh Particle Physics, Astrophysics, and Cosmology Center,

Department of Physics and Astronomy, University of Pittsburgh, Pittsburgh, PA 15260, USA

(Dated: November 22, 2022)

---

[*] Convener, EF05 topical group

[†] Convener, EF06 topical group

[‡] Convener, EF07 topical group

ABSTRACT

This report was prepared on behalf of three Energy Frontier Topical Groups of the Snowmass 2021 Community Planning Exercise. It summarizes the status and implications of studies of strong interactions in high-energy experiments and QCD theory. We emphasize the rich landscape and broad impact of these studies in the decade ahead. Hadronic interactions play a central role in the high-luminosity Large Hadron Collider (LHC) physics program, and strong synergies exist between the (HL-)LHC and planned or proposed experiments at the U.S. Electron-Ion Collider, CERN forward physics experiments, high-intensity facilities, and future TeV-range lepton and hadron colliders. Prospects for precision determinations of the strong coupling and a variety of nonperturbative distribution and fragmentation functions are examined. We also review the potential of envisioned tests of new dynamical regimes of QCD in high-energy and high-density scattering processes with nucleon, ion, and photon initial states. The important role of the high-energy heavy-ion program in studies of nuclear structure and the nuclear medium, and its connections with QCD involving nucleons are summarized. We address ongoing and future theoretical advancements in multi-loop QCD computations, lattice QCD, jet substructure, and event generators. Cross-cutting connections between experimental measurements, theoretical predictions, large-scale data analysis, and high-performance computing are emphasized.

The report is based on many contributions to the EF05, EF06, and EF07 Topical Groups that were presented at the topical group meetings, in feedback on the white papers and the report, and through other communications. We express our gratitude to all Snowmass participants whose strong involvement in the groups' activities guided the vision expressed here. The following Snowmass white papers were instrumental in developing the report:

- Physics with the Phase-2 ATLAS and CMS Detectors [1]
- The Forward Physics Facility: Sites, Experiments, and Physics Potential [2]
- The Forward Physics Facility at the High-Luminosity LHC [3]
- Electron Ion Collider for High Energy Physics [4]
- Some aspects of the impact of the Electron Ion Collider on particle physics at the Energy Frontier [5]
- Heavy Neutral Lepton Searches at the Electron-Ion Collider [6]
- Opportunities for precision QCD physics in hadronization at Belle II – a Snowmass whitepaper [7]
- The Future Circular Collider: a Summary for the US 2021 Snowmass Process [8]
- The International Linear Collider [9]
- The Potential of a TeV-Scale Muon-Ion Collider [10]
- Event Generators for High-Energy Physics Experiments [11]
- The strong coupling constant: State of the art and the decade ahead [12]
- Proton structure at the precision frontier [13]
- Lattice QCD Calculations of Parton Physics [14]
- Impact of lattice $s(x) - \bar{s}(x)$ data in the CTEQ-TEA global analysis [15]
- Forward Physics, BFKL, Saturation Physics and Diffraction [16]
- Prompt electron and tau neutrinos and antineutrinos in the forward region at the LHC [17]
- Jets and Jet Substructure at Future Colliders [18]
- `xFitter`: An Open Source QCD Analysis Framework [19]
- Opportunities for new physics searches with heavy ions at colliders [20]

EXECUTIVE SUMMARY

Quantum Chromodynamics (QCD), the fundamental theory of strong interactions, plays a unique role in the Standard Model. Being a confining gauge theory, it is an interesting quantum field theory to study in its own right. It is also a crucial tool to enable discovery at virtually every high-energy collider. QCD predicts a rich panoply of phenomena associated with both perturbative and nonperturbative dynamics of the strong interactions. Continued success of the high-energy and nuclear physics research program hinges on an improved understanding of both regimes, as well as the dynamical transition between them.

Future SM measurements and new physics searches will allow the exploration of new kinematic regions, such as very high transverse momentum and very forward rapidities, where large scale hierarchies may induce hitherto unseen QCD effects. The upcoming era — featuring the HL-LHC, Belle II, the EIC, new advances in theory including in lattice QCD, and potentially a Higgs factory — will be a new golden age for QCD easily rivaling the 1990's when the Tevatron, HERA, and LEP were all operating.

To fully exploit the wealth of expected data, precision calculations in QCD perturbation theory are required at one- and two-loop accuracy for many processes at hadron colliders, and in some cases at even higher accuracy. Monte-Carlo event generators serve as the backbone of the majority of collider simulations and must be able to reach similar precision. The advancement of QCD theory is therefore critically important to the physics program at the energy frontier.

Many QCD effects are universal and can be understood through factorization and perturbation theory. The related systematic uncertainties are often a limiting factor in Standard Model measurements and searches for new phenomena. A major goal of the QCD research program has therefore been to increase the precision of both the experimental measurements and the theoretical predictions.

The strong coupling is the least well measured coupling of the Standard Model, and substantial progress in its determination is expected from both lattice QCD and future colliders, particularly e^+e^- facilities, with a projected reduction in uncertainty of almost an order of magnitude, leading to a precision on α_s in the permille range. The RG evolution of the strong coupling will be testable at high precision over a large dynamic range with the help of lepton-hadron or hadron-hadron colliders. Measurements of charm, bottom, and top quark masses at various energy scales test both the QCD dynamics and the mass parameters of the Standard Model, with subpercent precision for bottom quark mass expected at future Higgs factories.

Parton distribution functions (PDFs) and fragmentation functions (FFs) will play a prominent role in future precision experiments and new physics searches. New opportunities emerge for precise determination of these functions in many observations and to predict their behavior in lattice QCD. Taking advantage of these opportunities requires implementation of two- and three-loop computations of radiative contributions and methodological advances in large-scale phenomenological analyses of QCD data.

Detection of the decay products of far-forward hadrons at the proposed Forward Physics Facility (FPF) at the HL-LHC would offer an unprecedented opportunity for deeper tests of QCD in a novel high-energy regime. Neutrino production of all flavors as well as new particle production could be explored both by the FPF detectors alone and perhaps even in coincidence with ATLAS, leading to improved understanding of small-x dynamics, forward heavy flavor — particularly charm — production, neutrino scattering in the TeV range, and hadronization inside nuclear matter.

Jet substructure has emerged as a powerful framework and tool set for probing the highest energy scales to explore the structure of the strong force in final-state radiation on small angular scales, and to identify Lorentz-boosted massive particles including W, Z, & H bosons, top quarks, and exotica. Increased precision is expected to emerge from improved detector capabilities and from

the theoretical understanding of particle flow observables, as well as from grooming techniques and other methods to reduce the impact of universal soft gluon and hadronization effects on observables. Better theoretical understanding of energy correlation functions may enable new opportunities for measurements of fundamental properties of QCD.

Various domains of QCD are strongly interconnected. Progress in one area depends on the other domains. Going forward, the dialogue between experimentalists, theorists and tool developers will become ever more important to achieve precision measurements with reliable systematic uncertainty estimates.

CONTENTS

I. EXPERIMENTAL CONTEXT

Quantum Chromodynamics (QCD) predicts a rich panoply of phenomena associated with both perturbative and nonperturbative dynamics of the strong interactions. QCD affects every analysis at current and future experimental facilities operating with nucleons, heavy nuclei, and hadrons in general. While measurements of QCD parameters and studies of hadron structure are not always the primary goal at these facilities, related systematic uncertainties are often a limiting factor in the extraction of Standard Model (SM) parameters and the reach of new physics searches. QCD effects must therefore be known as precisely as possible. Predictions for QCD phenomena at the modern precision level stimulate developments in quantum field theory and computational methods. They are needed to identify phenomena beyond the Standard Model (BSM) and to understand the dynamics of the BSM physics once it is discovered.

This contribution to the Snowmass Community Study will discuss various aspects of QCD in the context of experimental facilities of interest to the domestic and international high-energy physics research program. We emphasize that the dialogue between QCD experimentalists, theorists and tool developers will become ever more important to achieve precision measurements with reliable systematic uncertainty estimates. We start with an overview of the QCD role at future Energy Frontier facilities.

I.1. The high-luminosity LHC (HL-LHC)

In the coming decade, experiments at the Large Hadron Collider (LHC) will make precise measurements of SM parameters, such as the W mass and Higgs boson couplings. Both the extraction of these parameters and their interpretation will be limited primarily by the precision of perturbative QCD calculations and their faithful implementation in Monte-Carlo simulations. Measurements of jet, photon, and heavy-quark cross-sections (including top quarks) will test perturbative QCD at higher orders and constrain parton distribution and fragmentation functions as well as the running of the strong coupling α_s. These analyses are also needed for understanding backgrounds for many other interesting processes.

The HL-LHC provides an opportunity to test QCD with improved precision, particularly at high energies where uncertainties are dominated by statistics. A prime example are angular correlation measurements, such as the one described in Sec. IV.4. The average pileup at the LHC is around 25 events, and it is expected to reach values of around 150–200 during the HL-LHC operation. This will result in significant degradation in the physics object reconstruction performance and hence on the physics outcome without dedicated mitigations. While not an experimental or theoretical consideration of the LHC experiments' original designs, jet substructure is now being widely used to minimize the impact of pileup, to probe fundamental and emergent properties of the strong force, to enhance the precision of measurements of highly-Lorentz-boosted SM particles, and to extend the sensitivity of searches for new particles. Novel types of event shape observables also provide new opportunities for precision tests of QCD.

A detailed description of the opportunities for QCD measurements at the HL-LHC is given in Ref. [1].

I.2. Forward QCD experiments at the HL-LHC

Detection of the far-forward decay products of hadrons at the Forward Physics Facility (FPF) at the HL-LHC offers an unprecedented opportunity for deeper tests of QCD in the high-energy regime [2, 3]. The FPF program would expand the physics reach of the ongoing FASERν and

SND@LHC experiments. One class of reactions that can be investigated at the FPF are single-inclusive forward emissions, where a neutrino with rapidity $y \gtrsim 6$ is identified. Both inclusive and exclusive processes can be measured and tested by considering several kinds of final states, such as charged light hadrons, vector mesons (extensively studied at HERA [21–28]), and mesons with open charm or beauty, accompanied by their decay producing at least a forward neutrino.

These kinds of studies can be performed by the FPF detectors alone. Requiring coincidence with the ATLAS detector may allow identification of states with large invariant masses, whose decay products are not entirely captured by the FPF, but fall partly into the FPF's and partly into ATLAS's coverage areas. These measurements will lead to an improved understanding of forward heavy flavor—particularly charm production, neutrino scattering in the TeV range, and hadronization inside nuclear matter. The possibility of combining information from the ATLAS detector and a forward detector at the FPF relies on the ability to use an FPF event to trigger ATLAS. This requires very precise timing and has consequences for the design of the forward detector. An additional issue is the extreme pileup expected at the HL-LHC as events with multiple hard-scattering processes within the same bunch crossing. Section VI.4 continues the discussion of the FPF.

I.3. The Electron Ion Collider

It is vital to understand how the properties of nucleons and nuclei emerge from their constituents: quarks and gluons. To advance this goal, a high-energy and high-luminosity polarized electron-ion collider (EIC) is being designed and constructed by Brookhaven National Laboratory and Jefferson Lab over the course of the next decade [29] as a high priority on the agenda by the US nuclear physics community. The versatile EIC physics program [30] dedicated to exploration of hadronic matter over a wide-range of center-of-mass energies has significant synergies with exploration of QCD at the HL-LHC (Sec. I.1), Forward Physics Facility (Sec. I.2) and other HEP experiments. Throughout this document, we provide many examples of the positive impact that the EIC program will have on high-energy QCD. The Snowmass EIC whitepapers [4–6] include many more examples.

Indeed, in addition to performing spin-dependent three-dimensional tomography of nucleons and various ion species, the EIC is capable of obtaining new precise measurements of hadronic structure in deep inelastic electron-proton and electron-nucleus scattering (DIS) over a wide range of CM energies, $\sqrt{s} = 20 - 140$ GeV, and with high instantaneous luminosity of up to $\mathcal{L} = 10^{34}$ cm$^{-2} \cdot$ s^{-1}. With its variable CM energy and excellent detection of final hadronic states, the EIC can precisely probe the unpolarized proton PDFs and their flavor composition at momentum fractions $x > 0.1$, in the kinematic region of relevance for BSM searches at the HL-LHC, but at QCD scales of only a few (tens of) GeV where no deviations from the Standard Model are expected. The EIC can therefore elevate the accuracy of DIS experiments to a new level in the large-x region that is currently covered by fixed-target experiments from more than 20 years ago.

Furthermore, in addition to neutral-current DIS, parity-violating charged-current (CC) reactions can be employed to study nucleon and nuclear structure with highly-polarized beams for electrons and light ions, as well as unpolarized beams for heavy ions. Charge-current DIS on heavy-nucleus targets has large uncertainties, and this in turn is an issue for accelerator-based neutrino oscillation experiments, particularly those at DUNE, that have a significant share of events from neutrino CC DIS. Studies of CC DIS at the higher energies typical to the EIC, possibly complemented by studies at the FPF, will benefit HEP objectives in neutrino-nuclear scattering measurements at lower energies. These advancements will depend on new QCD-based theory ingredients for CC DIS simulations, as discussed in Sec. IX.2.

The EIC will establish a new QCD frontier to address key open questions, such as the origin

of nucleon spin, mass, and the emergence of QCD many-body phenomena at extreme parton densities. There will be ample cross-pollination between studies of the hadron structure in the EIC experiments and using lattice QCD (cf. Sec. V) and other *ab initio* approaches. Precise measurements of most accessible combinations of phenomenological PDFs at the EIC will provide useful benchmarks for lattice QCD calculations, and the latter in turn can make predictions for nonperturbative QCD functions that are not readily accessible in experiments.

As the EIC will push the DIS experiments into an entirely novel territory, its success will critically depend on accurate and precise theoretical modeling, including theoretical advances in multiloop perturbative QCD+EW calculations, implementation of spin-dependent and transverse momentum dependent QCD evolution, development of new event generators for lepton-hadron scattering, and, just as importantly, the infrastructure for all-out accuracy control in phenomenological analyses of the EIC large data samples.

I.4. The Belle II Experiment

The theory uncertainty on the SM prediction for the anomalous magnetic moment of the muon is dominated by the leading-order hadronic contribution, which can be calculated from the cross section for $e^+e^- \to$ hadrons, measured in e^+e^- experiments. The corresponding experimental result is dominated by BABAR and KLOE measurements of two pion production, but the two differ notably [7]. Belle II will perform these measurements with larger data sets, and at least comparable systematic uncertainty, aiming to resolve the discrepancy. Furthermore, Belle II's multi-ab^{-1} data set will facilitate new approaches to suppress systematic uncertainties. The low-background environment of e^+e^- annihilation exploited at unprecedented statistical precision will also enable highly impactful tests of transverse-momentum-dependent QCD evolution and factorization in jet and hadron production. Measurements of multidimensional correlations of momenta and polarizations of final-state hadrons during hadronization will further our understanding of soft QCD and will enable refinement and tuning of Monte-Carlo event generators at levels that may be instrumental to reach the precision needed to accomplish the LHC program. The lever arm in collision energy with respect to Large Electron-Positron Collider (LEP) data offers a robust basis for extrapolation to LHC energies. The Belle II data set size will enable unique fully multidimensional measurements that capture the fuller picture of hadronization dynamics.

A detailed description of the opportunities of QCD measurements at Belle II is given in Ref. [7].

I.5. Future Electron-Positron Colliders

Due to their QCD neutral initial state, e^+e^- colliders are the simplest setting in which to study dynamics in QCD, enabling precision measurements well beyond what is possible at hadron colliders. At high luminosity, the clean environment will also provide enormous (multi)jet data samples to improve our understanding of parton showers, higher-order logarithmic resummations, as well as hadronization and nonperturbative phenomena. QCD final states at high-energy electron-positron colliders will generally be more complex compared to earlier experiments. This complexity is comparable to that already observed in the LHC experiments. For instance, the hadronic Higgs-strahlung analysis at a Higgs factory requires excellent jet clustering performance in four-jet final states [31, 32]. At higher energy, di-Higgs, top-quark pair, and $t\bar{t}H$ production lead to six-jet and even eight-jet final states; such that jet clustering becomes the dominant experimental limitation [33].

There has been much progress since LEP in understanding QCD final states, driven by a renewed interest in studying jet substructure at the LHC. The techniques developed have enabled

a variety of new ways of understanding QCD phenomena with increasing sophistication [34, 35]. Precision determinations of event shapes have also enabled precision extractions of the strong coupling, α_s [36, 37]. A wide variety of event shapes were measured at LEP in events that always contained two quark-initiated jets. With nonperturbative effects tuned against this rich data set, parton-shower Monte Carlo programs model quark-jet shapes extremely well. The MC programs are less confident in modeling gluon jets, which were not produced that often at LEP, but which are copiously produced at the LHC. A particular advantage of future lepton colliders is the availability of pure samples of gluon jets through the process $e^+e^- \to HZ$, with Z decaying to leptons, and the Higgs boson decaying to gg [38–40]. Understanding of b-quark showering and hadronization will also be improved; these are leading sources of systematic uncertainty in the measurement of the forward-backward asymmetry of b quarks in e^+e^- collisions at LEP [41].

The optimization of detector concepts is mainly driven by improving jet energy resolution using particle flow. The ILD [42] and SiD [43] experiments at the ILC, as well as the CLIC detector [44] and the CLD design [45] for the FCC-ee, are engineered to efficiently associate tracks and calorimeter energy deposits and, together with improvements in software [46], might reach jet energy resolutions around 5-20%. These concepts also offer excellent substructure performance [47]. Machine-induced backgrounds at e^+e^- colliders are generally benign compared to the pile-up levels encountered at the LHC, but can have a non-negligible impact on jet reconstruction, especially at higher energy [32, 33, 48, 49].

I.6. Future Muon-Muon Colliders

Jet algorithms developed for electron-positron colliders should also apply well to muon colliders. Proposed muon colliders offer a tremendous physics reach for discoveries, while maintaining appealing experimental aspects of lepton collider environments such as a lack of pileup and underlying event. Muon colliders will produce final states that are generally more complicated than e^+e^- machines due to the higher energies; boosted topologies will also tend to be more prevalent.

A critical difference between muon and electron accelerators is the presence of large beam-induced background (BIB) processes for muon machines [50–52], which arise due to muons in the beam decaying via $\mu \to e\nu\bar{\nu}$ before colliding. The resultant electrons interact with experimental elements along the beamline, creating electromagnetic showers of soft photons and neutral particles that can interact with detectors. Detectors at future muon colliders will need to incorporate specifically-designed shielding and subsystems to mitigate BIB processes. The exact characteristics of the BIB depend strongly on the machine centre-of-mass energy and accelerator lattice, and must be studied in-detail for different scenarios. Advanced pileup mitigation techniques studied at the LHC could provide versatile handles to remove beam-induced background contamination during reconstruction [53–55].

I.7. Future Lepton-Hadron Colliders

Lepton-hadron deep inelastic scattering (DIS) is a cornerstone process to determine nonperturbative QCD functions, such as PDFs, describing the hadron structure in high-energy collisions. Recent studies [30] demonstrate that the HL-LHC physics potential in electroweak precision studies and BSM searches can be greatly enhanced by concurrent DIS experiments providing complementary and competitive constraints on the PDFs. This is just one aspect of a versatile physics program, with a variety of QCD observables and final states, at any ℓh collider. One such DIS experiment is the planned EIC that is being designed and constructed by BNL and Jefferson Lab; it was already discussed in Sec. I.3. The EIC will provide valuable measurements of PDFs at

momentum fractions above 0.1 and relatively low Q. An Electron-Ion Collider in China (EIcC) accesses the hadron structure, including spin effects, at a lower energy ($\sqrt{s} = 15 - 20$ GeV), where nonperturbative effects are more pronounced [56]. The Large Hadron Electron Collider (LHeC) at CERN [57–60], on the other hand, would extend DIS into the TeV energy range that considerably overlaps with the LHC kinematic region. The LHeC would be able to explore the PDFs, and QCD dynamics in general, at x down to $\sim 10^{-6}$ at $Q \sim 1$ GeV and up to $0.5 - 0.8$ at $Q \sim 0.5 - 1$ TeV. It can therefore investigate QCD dynamics in the x regions relevant for forward production at the LHC and FPF and to perform unique electroweak measurements and BSM searches.

An appealing and highly innovative collider configuration for QCD studies is a muon-hadron collider with $\sqrt{s}$ up to 1-6.5 TeV and instantaneous luminosity of up to $\mathcal{L} = 10^{34}\, \mathrm{cm}^{-2} \cdot \mathrm{s}^{-1}$ [10]. It can be constructed through a staged program that involves development of the core muon beam technology followed by installation of *one* muon beam at an existing facility (Fermilab, CERN,...) that has a high-energy hadron beam. A muon-hadron collider therefore can have an energy reach in DIS comparable to the LHeC or even FCC-eh, while at the same time serving as a technology demonstrator for $\mu^+\mu^-$ colliders. A Muon-Ion Collider (MuIC) at the Brookhaven National Laboratory would be a natural successor of the EIC program in 2040's. Key merits of the MuIC proposal are the strong synergy with existing accelerator HEP and nuclear physics facilities in the US and expansion of QCD studies at the EIC into a new range of energies. On the one hand, the MuIC energy would be high enough to conclusively study small-x partonic saturation with multiple types of ions and even beam polarization. On the other hand, at such energies parity-violating processes with weak bosons can be incisively employed to probe the flavor and spin properties of various nucleon and nuclear targets. The MuIC would also be a discovery machine, as it would produce a variety of final states with Higgs bosons and top quarks and perform unique searches for compositeness, leptoquarks, parity-violating BSM interactions. Due to its unique kinematics stipulated by the initial beam energies, the MuIC would require development of a very forward muon spectrometer to operate at pseudorapidities $\eta \approx -7$ and muon energies up to 1 TeV [Appendix in Ref. 10].

Figure 1 in Ref. [10] compares the CM energies and instantaneous luminosities of the past and proposed future electron-hadron and muon-hadron colliders. Figure 4 of the same whitepaper shows possible timelines for the construction of muon-ion colliders at BNL and CERN.

I.8. Future Hadron Colliders

High-energy hadron colliders provide the best opportunity to make a wide range of precision measurements of perturbative and nonperturbative QCD. Measurements of jet, photon, and top-quark cross-sections test higher-order perturbative QCD, and constrain parton distribution and fragmentation functions, and the running of α_s. There are currently two major future hadron-hadron collider proposals, the FCC-hh at CERN and the SPPC in China, both targeting *pp* collisions at a center of mass (CM) energy of about 100 TeV. Each machine would deliver an integrated luminosity of around 25 ab^{-1} per experiment, reaching an instantaneous luminosity of 3×10^{35} cm^{-2} s^{-1}, almost an order of magnitude larger than the HL-LHC.

These are extremely ambitious projects requiring breakthroughs in accelerator technology, detector design, and physics object reconstruction, and a coherent effort in all aspects is required. The searches for the heaviest BSM objects in the unprecedented multi-TeV energy regime will observe QCD processes in which all particles of the Standard Model, including top quarks and electroweak bosons, are emitted within parton showers. If, in addition to reconstructing multi-TeV final states, detectors for a 100 TeV machine are to provide the necessary precision to measure the SM processes, the detector coverage should be extended with respect to the LHC detectors, since

many SM processes are expected to be extremely forward. The calorimetry systems must provide excellent energy resolution over a wide range of energies in the central and forward regions, and increased hermetic coverage with respect to the LHC ones (reaching $|\eta| < 6$).

Studies have shown [61] that the granularity of the detector is of particular importance. For instance, SM Higgs decays into ZZ pairs would produce two Z bosons with multi-TeV energies, each with p_T less than 100 GeV, and opening angles between the Z boson decay products of about 0.1 radian. Detector capabilities to reconstruct these objects are fairly challenging (for instance, an average Z boson would shower mostly within one LHC calorimeter cell). This challenge is accentuated by so-called "hyper-boosted" jets, whose decay products are collimated into areas the size of single calorimeter cells. Holistic detector designs that integrate tracking, timing, and energy measurements are needed to mitigate for these conditions [62–67]. The extreme levels of radiation present in a 100 TeV collider pose another challenge for the design. A factor-of-five larger pileup than at the HL-LHC is expected posing stringent criteria on the detector design. The energy calibration of calorimeter cells, composite clusters, single particles, and jets is a challenging task at a 100 TeV pp collider [68]. Detailed studies at higher energies will be needed to achieve the best possible precision at future colliders.

II. THE STRONG COUPLING AND TESTS OF RG EVOLUTION

The strong coupling, α_s, is a fundamental parameter of the SM, and it is also the least well known of its gauge couplings. The uncertainty on α_s will be one of the limiting factors in measurements at the High-Luminosity LHC and other experiments. Detailed summaries of the status of α_s determinations are given in the PDG review on Quantum Chromodynamics [69] and a dedicated Snowmass whitepaper [12]. Table I first shows the results of the seven extraction methods that contribute to the PDG world-average combination. The lattice QCD methods are described in more detail in Sec. II.3 and involve themselves a variety of techniques. Each category lists the dominant sources of theoretical and experimental uncertainty that propagate into $\alpha_s(m_Z)$ today, as well as feasible targets for reducing these sources within about 10 years and, in parentheses, in even longer future. The last row shows the relative uncertainty of the current world average (0.8%) and of the one expected within the next decade ($\approx 0.4\%$). Section II.4 briefly reviews the procedures to compute the world average.

The long-term prognoses in the parentheses show that, in principle, $\sim 0.1\%$ precision can be ultimately achieved in $\alpha_s(m_Z)$ determinations from at least one lattice QCD method and electroweak fits at a future high-luminosity e^+e^- facility. To translate these advances into the per mil precision of the world-average result in the final row, no large unexplained discrepancies should impact the individual extraction methods. Ruling out such discrepancies presents an emerging challenge for precise analyses of $\alpha_s(m_Z)$ and PDFs, as the number of contributing systematic factors grows rapidly when the targeted precision increases, and when multiple hard scales are present in the problem. In the latest precision analyses such as the latest PDG α_s combination (cf. Fig. 1), some experimental determinations show mutual tensions, and those may be further exacerbated when some measurements have a substantially smaller uncertainty than the others. The same complication may occur with theoretical predictions. A significant inconsistency among several α_s extractions hence may be much more likely due to unknown or underestimated systematic errors in experiment or theory than because of BSM physics. Since we will probably continue to face such issues in the future, exhaustive exploration of systematic effects will become critical for interpretation of precise α_s extractions. Agreed-upon protocols for resolution of conflicts among individual determinations could be helpful, as well as cross calibration of common sources of systematics.

TABLE I. Summary of current and expected future (within the decade ahead or, in parentheses, longer time scales) uncertainties in the $\alpha_s(m_Z)$ extractions used today to derive the world average of α_s. Acronyms and symbols: CIPT='contour-improved perturbation theory', FOPT='fixed-order perturbation theory', NP='nonperturbative QCD', SF='structure functions', PS='Monte Carlo parton shower'. Entries of the table are explained in Ref. [12], from which the table is taken. Category 7 is based on $\alpha_s(M_Z)$ determinations from ℓh and hh collider observables performed outside of global PDF fits (category 4)– see the discussion item (f) in Sec. 10.1 of Ref. [12].

Method	Relative $\alpha_s(m_Z)$ uncertainty	
	Current theory & exp. uncertainties sources	Near (long-term) future theory & experimental progress
(1) Lattice	0.7% Finite lattice spacing & stats. N^{2,3}LO pQCD truncation	$\approx 0.3\%$ (0.1%) Reduced latt. spacing. Add more observables Add N^{3,4}LO, active charm (QED effects) Higher renorm. scale via step-scaling to more observ.
(2) τ decays	1.6% N^{3}LO CIPT vs. FOPT diffs. Limited τ spectral data	$< 1.\%$ Add N^{4}LO terms. Solve CIPT–FOPT diffs. Improved τ spectral functions at Belle II
(3) $Q\bar{Q}$ bound states	3.3% N^{2,3}LO pQCD truncation $m_{\rm c,b}$ uncertainties	$\approx 1.5\%$ Add N^{3,4}LO & more $(c\bar{c})$, $(b\bar{b})$ bound states Combined $m_{\rm c,b} + \alpha_s$ fits
(4) DIS & global PDF fits	1.7% N$^{2,(3)}$LO PDF (SF) fits Span of PDF-based results	$\approx 1\%$ (0.2%) N^{3}LO fits. Add new SF fits: $F_2^{p,d}$, g_i (EIC) Better corr. matrices, sampling of PDF solutions. More PDF data (EIC/LHeC/FCC-eh)
(5) e^+e^- jets & evt shapes	2.6% NNLO +N$^{(1,2,3)}$LL truncation Different NP analytical & PS corrs. Limited datasets w/ old detectors	$\approx 1.5\%$ ($< 1\%$) Add N^{2,3}LO+N^{3}LL, power corrections Improved NP corrs. via: NNLL PS, grooming New improved data at B factories (FCC-ee)
(6) Electroweak fits	2.3% N^{3}LO truncation Small LEP+SLD datasets	($\approx 0.1\%$) N^{4}LO, reduced param. uncerts. ($m_{\rm W,Z}$, α, CKM) Add W boson. Tera-Z, Oku-W datasets (FCC-ee)
(7) Standalone hadron collider observables	2.4% NNLO (+NNLL) truncation, PDF uncerts. Limited data sets ($t\bar{t}$, W, Z,e-p jets)	$\approx 1.5\%$ N^{3}LO+NNLL (for color-singlets), improved PDFs Add more datasets: Z $p_{\rm T}$, p-p jets, σ_i/σ_j ratios,...
World average	0.8%	$\approx 0.4\%$ (0.1%)

TABLE II. Values of $\alpha_s(m_Z)$ determined at N^{3}LO accuracy from Z-boson pseudoobservables ($\Gamma_Z^{\rm tot}$, R_Z, and $\sigma_Z^{\rm had}$) individually, combined, as well as from a global SM fit, with propagated experimental, parametric, and theoretical uncertainties broken down [70]. The last two rows list the expected values at the FCC-ee from all Z pseudoobservables combined and from the corresponding SM fit.

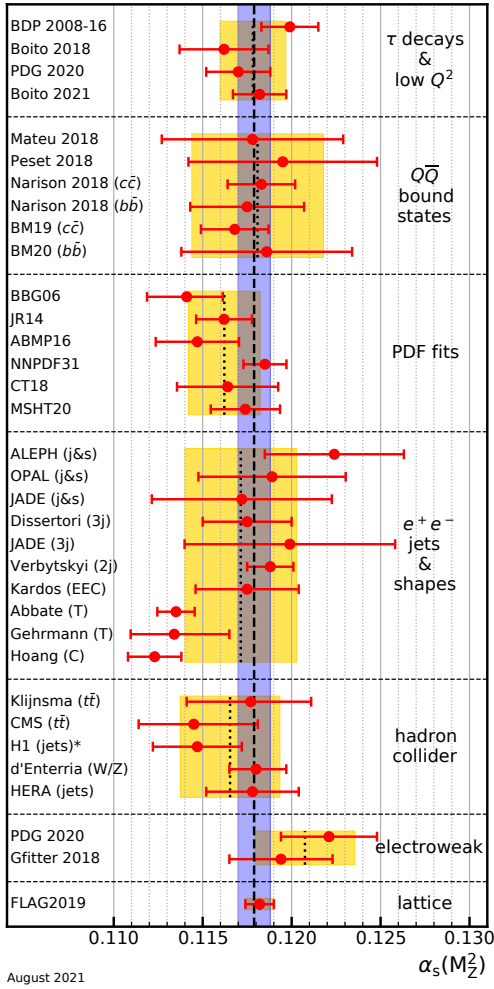| Observable	$\alpha_s(m_Z)$	uncertainties		
		exp.	param.	theor.
$\Gamma_Z^{\rm tot}$	0.1192 ± 0.0047	± 0.0046	± 0.0005	± 0.0008
R_Z	0.1207 ± 0.0041	± 0.0041	± 0.0001	± 0.0009
$\sigma_Z^{\rm had}$	0.1206 ± 0.0068	± 0.0067	± 0.0004	± 0.0012
All above combined	0.1203 ± 0.0029	± 0.0029	± 0.0002	± 0.0008
Global SM fit	0.1202 ± 0.0028	± 0.0028	± 0.0002	± 0.0008
All combined (FCC-ee)	0.12030 ± 0.00026	± 0.00013	± 0.00005	± 0.00022
Global SM fit (FCC-ee)	0.12020 ± 0.00026	± 0.00013	± 0.00005	± 0.00022

FIG. 1. Summary of latest determinations of $\alpha_s(m_Z)$ from seven subfields. The yellow (light shaded) bands and dotted lines indicate the pre-average values of each subfield. The dashed line and blue (dark shaded) band represent the final $\alpha_s(m_Z)$ world average [March'22 update of the PDG'21 results [71]].

FIG. 2. Lattice determinations of the strong coupling, pre-averages from different calculational methods and final averaging. Figures taken from [72].

II.1. Extraction of α_s from e^+e^- data

At the FCC-ee, combining the 3×10^{12} Z bosons decaying hadronically at the Z pole, and the $\sqrt{s}$ calibration to tens of keV accuracy obtained using resonant depolarization [73], will provide measurements with unparalleled precision. The statistical uncertainties in the Z mass and width, today of ± 1.2 MeV and ± 2 MeV (dominated by the LEP beam energy calibration), will be reduced to below ± 4 keV and ± 7 keV respectively. Similarly, the statistical uncertainty in measuring Z boson partial widths ($R_{\ell,Z}$) will be negligible, and the $Z \to \mu^+\mu^-$ decay channel alone, yielding an experimental precision of 0.001 from the knowledge of the detector acceptance, will suffice to reach an absolute (relative) uncertainty of 0.001 (5×10^{-5}) on the ratio of the hadronic-to-leptonic partial Z widths. Thus, accounting for the dominant experimental systematic uncertainties at the FCC-ee, one can expect $\delta m_Z = 0.025$–0.1 MeV, $\delta\Gamma_Z = 0.1$ MeV, $\delta\sigma_Z^{had} = 4.0$ pb, and $\delta R_{\ell,Z} = 10^{-3}$ [74]. In

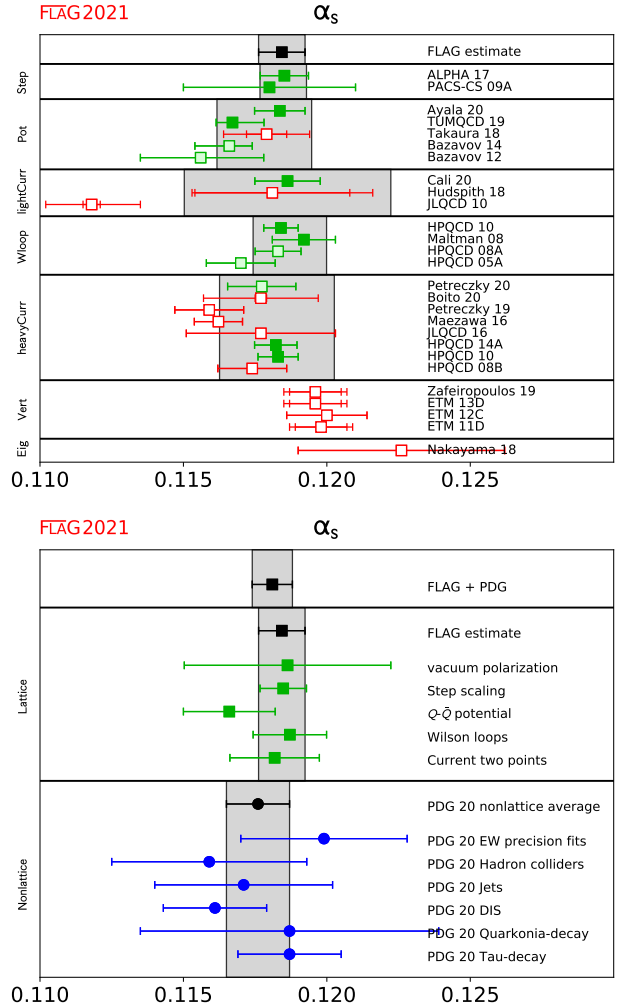addition, the QED coupling at the Z peak will be measured with a precision of $\delta\alpha = 3 \times 10^{-5}$ [75], thereby also reducing the corresponding propagated parametric uncertainties. Implementing the latter uncertainties into GFitter leads to the results listed in the last two rows of Table II, where the central $\alpha_s(m_Z)$ value is arbitrarily set at the current SM global fit extraction [70]. The final uncertainties in the QCD coupling constant are reduced to the $\sim$0.1% level, namely about three times smaller than the propagated theoretical uncertainties today. Theoretical developments in the years to come should further bring down the latter by a factor of four [76]. A final QCD coupling constant extraction at the FCC-ee with a 2-per mil total uncertainty is thereby reachable: $\alpha_s(m_Z) = 0.12030 \pm 0.00013_\text{exp} \pm 0.00005_\text{par} \pm 0.00022_\text{th}$ (Table II). The large improvement, by more than a factor of ten, in the FCC-ee extraction of $\alpha_s(m_Z)$ from the Z boson data (and its comparison to the similar extraction from the W boson pseudoobservables) will enable searches for small deviations from the SM predictions that could signal the presence of new physics contributions.

II.2.   Extraction of α_s from e$^\pm$p data

Future electron-proton collider experiments provide many opportunities for precision determinations of α_s. At lower center-of-mass energies, the EIC in the US [4, 30, 77] and the EicC in China [56] would provide new high-luminosity data. As an example, Fig. 3(a) suggests reduction in the α_s uncertainty extracted from the CT18 NNLO global PDF fit [78] by up to 40% after a high-statistics sample of the simulated inclusive ep DIS data for the EIC is included. In all ep measurements, the α_s value is correlated with the PDFs, especially the gluon PDF. Hence all provided projections assume that strong constraints on the PDFs will be simultaneously obtained. The EIC will provide also a novel possibility to extract α_s at N^{3}LO accuracy analyzing polarized PDFs, by exploiting the Bjorken sum rule [79], with a few percent precision [12]. Also, DIS global event shapes at the EIC on their own, such as 1-jettiness, can determine of $\alpha_s(m_Z)$ at a level of a few percent [30].

The proposed Large Hadron electron Collider at CERN (LHeC) [58, 59] would provide $e^\pm p$ collision data at a center-of-mass energy of 1.3 TeV, and hence its measurements of hadronic final-state observables would cover a considerably larger kinematic range than at the ep collider HERA. Inclusive neutral-current and charged-current DIS cross sections would be also measured with high precision both in the low-x and high-x regions, given an excellent detector acceptance and high luminosity. Inclusive DIS data alone would allow one to measure α_s very precisely, again assuming tightly constrained PDFs, and to the extent that was not fully possible with HERA data. An experimental uncertainty of

$$\delta\alpha_s(m_Z) = \pm 0.00022\,(\text{exp+PDF})\,, \tag{1}$$

could be possibly achieved in a combined determination of PDFs and $\alpha_s(m_Z)$ [59]. These and following estimates assume an idealized uncertainty on the PDFs ("given by $\Delta\chi^2 = 1$ at 68% probability"). More realistic PDF uncertainties tend to be larger because of such factors as some inconsistencies between experiments [80]. As an illustration, Fig. 3(b) compares the prospected uncertainties after the LHeC using the idealized prescription with recent determinations in global PDF fits.

A simulation of inclusive jet cross section data, using realistic models of systematic uncertainties, suggests that a determination of $\alpha_s(m_Z)$ with uncertainty of

$$\delta\alpha_s(m_Z) = \pm 0.00013\,(\text{exp})\ \pm 0.00010\,(\text{PDF}) \tag{2}$$

can be within reach in the HL-LHC + LHeC era. The right-hand side separately shows the experimental and PDF uncertainties (estimated with a disclaimer as above). Similarly as at HERA,
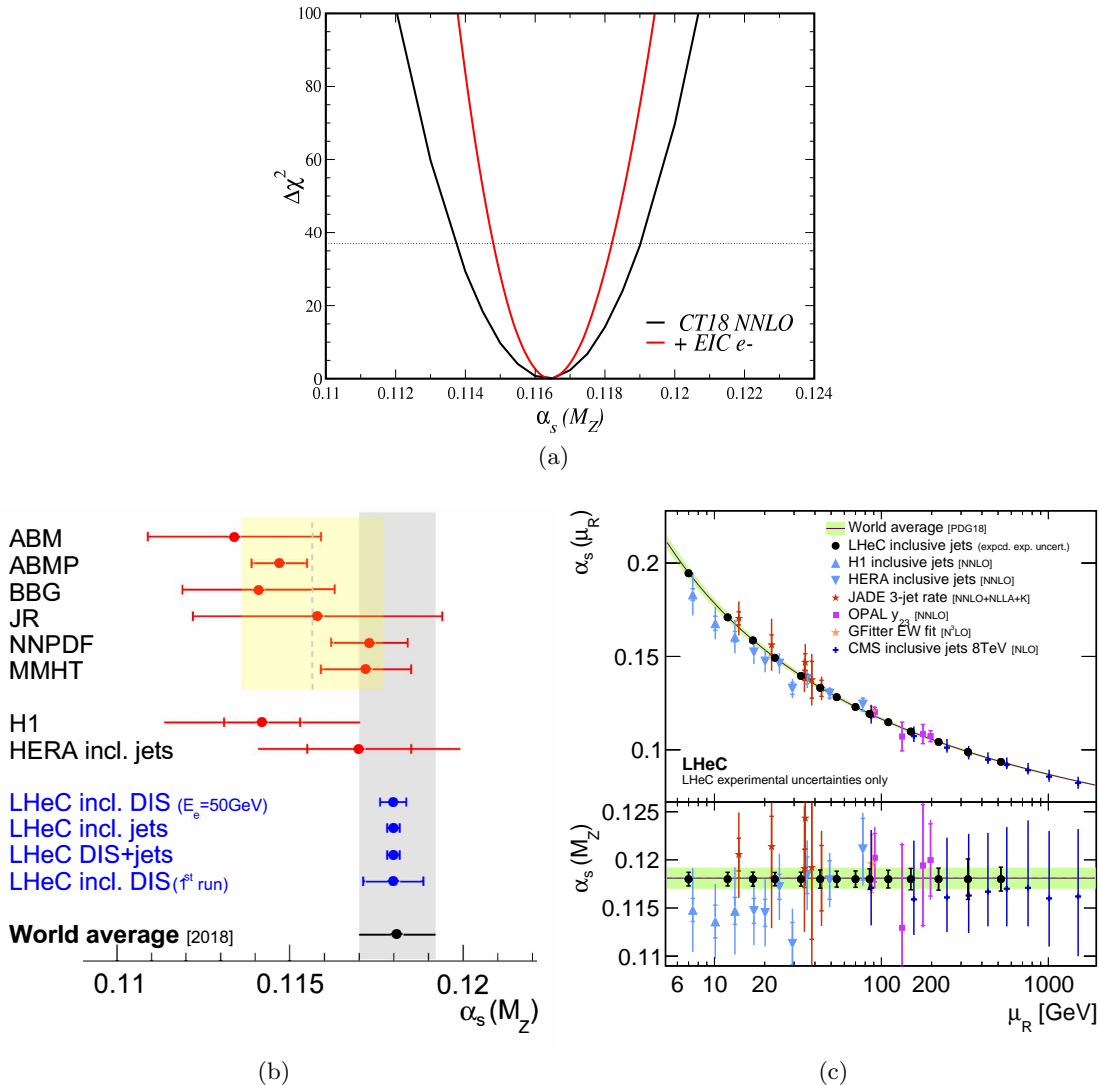
FIG. 3.   (a) An estimated precision improvement in the α_s determination in the CT18 NNLO fit [78], as quantified by the log-likelihood χ^2, following the inclusion of 100 fb^{-1} of EIC inclusive electron-proton scattering data. From Refs. [4, 30]. (b) Comparison of prospected determination of $\alpha_s(m_Z)$ from inclusive DIS data at the LHeC in comparison to determinations in (global) PDF fits. (c) An illustration of the prospected experimental uncertainties in a study of the running of α_s from inclusive jet cross sections at the proposed LHeC experiment. The LHeC figures are taken from Ref. [59].

the running of α_s could be investigated at the LHeC as a function of the renormalization scale using jet data. Figure 3(c) displays prospects for such scale-dependent determinations of $\alpha_s(m_Z)$ (and corresponding values of $\alpha_s(\mu)$). It is observed that, from LHeC inclusive jet cross sections, the running could be tested in the range from a few GeV up to about 600 GeV with per mil precision, resulting in an indispensable experimental confirmation of validity of renormalized QCD from the low-scale α_s determinations from τ-decays or lattice QCD to TeV scales.

II.3.   Extraction of α_s from lattice QCD

Multiple lattice QCD methods have been developed to extract the strong coupling constant: the step-scaling [81–90], small Wilson loops [91–94], QCD static energy [72, 95–104], heavy-quark

two-point correlators [94, 105–112], hadronic vacuum polarization [113–117], QCD vertex functions [118–124], decoupling method [12, 125], eigenvalues of the Dirac operator [126, 127] methods. See recent reviews of the lattice methods for α_s in Ref. [12, 104, 128, 129]. The Flavor Lattice Averaging Group (FLAG) report [72, 130–132] attempts a global lattice average (cf. Fig. 2)

$$\alpha_s(m_Z) = 0.1184(8) \qquad \qquad \text{(FLAG global average) [72].} \qquad (3)$$

FLAG uses a set of quality criteria to decide which determinations to include in the average. This procedure is similar to that adopted by the PDG. Reference [12] suggested that the FLAG and PDG procedures should be harmonized as much as possible. Unlike the procedure used for FLAG averages of other quantities, for α_s FLAG applies its own view of the perturbative-truncation uncertainty and inflates the error of some subaverages. Note that there have been updates to individual analyses since the current FLAG 2021 report [72] was published.

The current $\pm 0.7\%$ precision of the lattice-QCD extraction of $\alpha_s(m_Z)$ can be reduced by about a factor of two within the next ~ 10 years. In order to improve the lattice-QCD–based determinations of α_s, it would be important to reach higher renormalization scales by both advancing the lattice simulations and incorporating improved (higher-order) pQCD counterpart calculations. Lattice simulations should be run with smaller lattice spacings, allowing even better continuum extrapolations, and they should include charm-quark effects (2+1+1-flavor calculations). Perturbative expansions will require calculating N^{3}LO, N^{4}LO, and/or N^{3}LL contributions, depending on the process under study. In addition, treatment of QED and isospin-breaking effects in both the scale setting and running of α_s may be needed in some cases (in particular, when aiming at longer-term 0.1% uncertainties).

To further reduce the error from lattice calculations, sufficient dedicated computing resources are needed to generate state-of-the-art samples for lattice-QCD analyses. Enough person-power will be necessary to develop perturbation theory for selected observables in a finite spacetime volume and to compute identified higher-order pQCD corrections to match improved lattice-QCD samples.

II.4.   The world-average combination of α_s

The lower Fig. 2 illustrates the 2021 method to obtain the world-average value of α_s [69]. Separate weighted averages of lattice and non-lattice determinations are first computed. Then the final world-average combination of $\alpha_s(m_Z) = 0.1179 \pm 0.0009$ (labeled as "FLAG+PDG" in the figure) is computed as the average of non-lattice and lattice values, with the relative accuracy of 0.8% shown in Table I. The future projection of the α_s combination in the rightmost column of Table I is based on a weighted average of the seven categories on equal footing, which would give $\alpha_s(m_Z) = 0.1180 \pm 0.0006$ (i.e., a smaller uncertainty of 0.5%) in the case of the current world average.

The world-average combination prescription may evolve as groups of experiments get more precise, possibly revealing currently unseen disagreements. In the future, lattice determinations may be combined with the experimental ones that are affected by systematics of similar origin, such as τ decays [129]. Alternatively, if one group of determinations becomes much more precise than the others, it could be used as a reference. Correlations between different groups of determinations in Table I deserve further scrutiny. For example, the extractions from the hadron collider category 7 are PDF-dependent and, therefore, must share some degree of correlation with the extraction from the DIS+global-PDF fits category 4.

II.5.   The running bottom quark mass

Within the Standard Model of particle physics, the masses of quarks are free parameters whose values must be determined experimentally, while their scale dependence is predicted by scheme dependent Renormalization Group Evolution (RGE). These calculations have reached 5-loop accuracy [133–135] and have been implemented in public software packages [136, 137].

The most precise extractions of the bottom quark mass [138–148] rely on the measurement of the mass of bottomonium bound states and the $e^+e^- \to$ hadrons cross section as experimental input, in combination with QCD sum rules and perturbative QCD calculations. Several lattice QCD groups have also published results, the most recent of which reaches a precision of approximately 0.3% [149–153] (see also the FLAG report [154]). The world average provided by the Particle Data Group (PDG) [71] also includes inputs from HERA [155] and the BaBar and Belle experiments at the B-factories [156, 157]. Extractions from Z-pole data were performed at LEP [158–162] and SLD [163, 164]. Measurements of the bottom quark mass at the scale of the Higgs boson mass were performed in [165], based on ATLAS [166] and CMS [167] experimental data.

In the next decade the study of the "running" of the bottom quark mass is expected to turn into a precision test of QCD [168]. These investigations will complement analogous studies for the running charm mass, such as in [169]. Measurements at several energy scales in bottomonium, Z, and Higgs production can be used, in a general way, to sense the presence of massive new colored states that may contribute to the quark mass evolution. A dedicated high-luminosity e^+e^- run at the Z-pole, i.e. the "GigaZ" program of a linear collider or the "TeraZ" run at the circular colliders, yields a sample of Z-bosons that exceeds that of the LEP experiments and SLD by orders of magnitude. Ref. [170] provides an extrapolation under the assumption that the extraction of $m_b(m_Z)$ from the three-jet rates will be limited by the theory uncertainty and hadronization uncertainties. This requires fixed-order calculations at NNLO accuracy, with full consideration of mass effects. The Higgs factory program, with several inverse attobarn at a center-of-mass energy of 240-250 GeV can take advantage of radiative-return events. The Lorentz-boost of the Z-bosons complicates the selection, reconstruction and interpretation. A dedicated full-simulation study is therefore required to provide a reliable, quantitative projection. However, it is clear that the radiative-return data has the potential to significantly improve the precision of existing LEP/SLC analyses. Finally, a high-energy electron-positron collider operated at a center-of-mass energy of 250 GeV or above can extend the analysis to higher energies and thus probe the effect of coloured states with masses heavier than that the Higgs boson on the running of the bottom quark mass. The potential of the three-jet rate measurement to determine $m_b(\mu)$ for $\mu = 250$ GeV has been studied in Ref. [170]. A measurement with a precision of 1 GeV was found to be feasible for $\mu = 250$ GeV

The measurement of $m_b(m_H)$ from the Higgs decay width to a bottom-antibottom quark pair is expected to increase rapidly in precision as the precision of Higgs coupling measurement improves [165]. The current theory uncertainty from missing higher orders and parametric uncertainties from α_s and m_H is estimated to be 60 MeV [165], well below the current experimental precision. The theory uncertainty is dominated by the parametric uncertainty from the Higgs boson mass. The current uncertainty on the Higgs mass of 240 MeV leads to an uncertainty of ∼40 MeV on $m_b(m_H)$ and is expected to come down considerably as more precise determinations of m_H appear. Future prospects for Higgs mass measurements are summarized in Ref. [171]. Both the HL-LHC [172] and the Higgs factory [173] are expected to provide a measurement of the Higgs boson mass to 10-20 MeV precision, which is sufficient to reduce the impact of this source of uncertainty on $m_b(m_H)$ to below 10 MeV. The determination of $m_b(m_H)$ in $H \to b\bar{b}$ decay is expected to become the "golden" measurement among the high-energy determinations [168].

Ref. [172] provides the projections for the LHC and its luminosity upgrade, extrapolating the partial run 2 results under the following assumptions: both statistical and systematic uncertainties
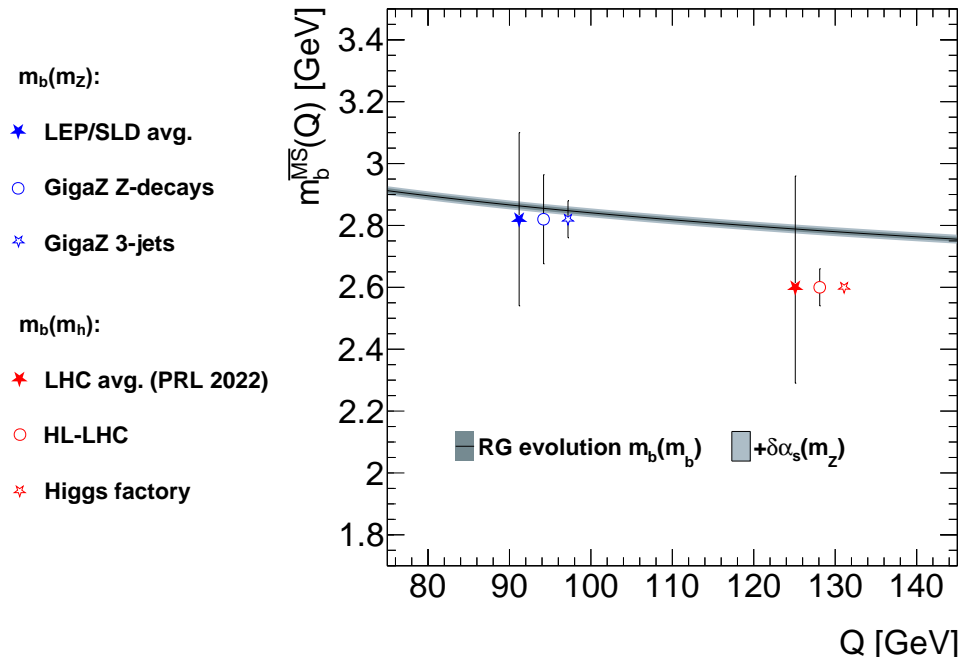
FIG. 4.   Prospects for measurements of the scale evolution of the bottom quark $\overline{\text{MS}}$ mass at future colliders. The markers are projections for $m_\text{b}(m_Z)$ from three-jet rates at the Z-pole and for $m_\text{b}(m_H)$ from Higgs boson branching fractions. The RGE evolution of the mass is calculated at five-loop precision with REvolver [137].

are envisaged to scale with integrated luminosity L as $1/\sqrt{L}$ up to certain limits, while theory uncertainties are expected to improve by a factor two. This "S2 scenario" leads to a projected uncertainty on the Higgs branching ratio to bottom quarks of 4.4% (1.5% stat., 1.3% exp., 4.0% theo.) and on $\lambda_{bz} = \mu^{bb}/\mu^{ZZ}$ of 3.1% (1.3% stat., 1.3% syst., 2.6% theo.), an improvement by nearly a factor of ten with respect to the first measurement in Ref. [165]

In the next decades, with the completion of the high luminosity program of the LHC and the construction of a new "Higgs factory" electron-positron collider, rapid progress is envisaged in the measurement of Higgs coupling measurement. These precise measurements will enable an extraction of the $\overline{\text{MS}}$ bottom quark mass $m_\text{b}(\mu)$ at the scale given by the Higgs boson mass, $m_\text{b}(m_\text{H})$, with a precision of the order of 10 MeV. With a relative precision of 2 per mil, the high-scale measurement can reach a similar precision as $m_\text{b}(m_\text{b})$ based on low-energy measurements.

The projections and extrapolations discussed above are summarized in Fig. 4. The markers are centered on the current central values for $m_\text{b}(m_Z)$ and $m_\text{b}(m_H)$ and the error bars indicate the projected precision. The solid line indicates the evolution of the PDG world average from $m_\text{b}(m_\text{b})$ to a higher scale using the RGE calculation included in the REvolver code [137] at five-loop precision. The uncertainty band includes the projected uncertainty of 10 MeV on $m_\text{b}(m_\text{b})$ (dark grey) and an 0.5% uncertainty on $\alpha_s(m_Z)$.

TOPIC	STATUS, Snowmass'2013	STATUS, Snowmass'2021
Achieved accuracy of PDFs	N^{2}LO for evolution, DIS and vector boson production	N^{2}LO for all key processes; N^{3}LO for some processes
PDFs with NLO EW contributions	MSTW'04 QED, NNPDF2.3 QED	LuXQED and other photon PDFs from several groups; PDFs with leptons and massive bosons
PDFs with resummations	Small x (in progress)	Small-x and threshold resummations implemented in several PDF sets
Available LHC processes to determine nucleon PDFs	W/Z, single-incl. jet, high-p_T Z, $t\bar{t}$, $W + c$ production at 7 and 8 TeV	+ $t\bar{t}$, single-top, dijet, $\gamma/W/Z$+jet, low-Q Drell Yan pairs, . . . at 7, 8, 13 TeV
Current, planned & proposed experiments to probe PDFs	LHC Run-2 DIS: LHeC	LHC Run-3, HL-LHC DIS: EIC, LHeC, MuIC, . . .
Benchmarking of PDFs for the LHC	PDF4LHC'2015 recommendation in preparation	PDF4LHC'21 recommendation issued
Precision analysis of specialized PDFs		Transverse-momentum dependent PDFs, nuclear, meson PDFs
NEW TASKS in the HL-LHC ERA		
Obtain complete N^{2}LO and N^{3}LO predictions for PDF-sensitive processes	Improve models for correlated systematic errors	Find ways to constrain large-x PDFs without relying on nuclear targets
Develop and benchmark fast N^{2}LO interfaces	Estimate N^{2}LO/N^{3}LO theory uncertainties	New methods to combine PDF ensembles, estimate PDF uncertainties, deliver PDFs for applications

TABLE III. Top part: Some of the PDF-focused topics explored in Snowmass'2013 [176] and '2021 studies. Bottom part: a selection of new critical tasks for the development of a new generation of PDFs that achieve the objectives of the physics program at the high-luminosity LHC.

III. PARTON DISTRIBUTION FUNCTIONS IN GLOBAL QCD ANALYSES

III.1. Proton parton distributions

III.1.1. Overview

The Snowmass whitepaper "Proton structure at the precision frontier" [13] summarizes the ubiquitous role of parton distributions functions (PDFs) in future precision measurements. A revolution in computing hard-scattering cross sections in perturbative QCD up to the second and third order in α_s (N^{2}LO and N^{3}LO, respectively) opens appealing opportunities for precision applications of the PDFs. By knowing the PDFs for the gluon and other quark flavors approximately to 1–2% accuracy, one greatly reduces the total uncertainties on the Higgs couplings in gluon-gluon fusion and electroweak boson fusion [172]. The energy reach in searches for very heavy new particles at the HL-LHC can be extended to higher masses by better knowing the PDFs at the largest momentum fractions, $x > 0.1$, and by pinning down the flavor composition of the partonic sea [174]. As interest grows in hadron scattering at very small partonic momentum fractions, $x < 10^{-5}$, at hadron colliders (HL-LHC, LHeC, FCC-hh) as well as in the astrophysics experiments, one must include effects of small-x resummation and saturation the PDFs when warranted [175].

PDFs for unpolarized protons — the cornerstone nonperturbative QCD functions — are traditionally determined from global analyses of fixed-target and collider data on DIS, production of lepton pairs, jets, top quarks, and increasingly in other processes [78, 177–185]. Table III illus-

trates the progress that has been made since the 2013 Snowmass Summer Study [176]. The bottom part of the table lists new tasks for the PDF analysis that emerge in the HL-LHC era. While the most precise N^2LO or even N^3LO theoretical cross sections should be preferably used in the fit when possible, accuracy of the PDFs also depends on the other commensurate factors that must be properly estimated. Given the complexity of N^2LO/N^3LO calculations, their fast approximate implementations (such as fast NNLO interfaces) must be developed to allow efficient observable computations in the PDF analyses. Control of experimental and theoretical uncertainties requires, in particular, to either fit the experiments that are minimally affected by the unknown factors (for example, to include cross sections only on proton, rather than on nuclear targets to minimize the associated uncertainties in the most precise determinations), or to estimate the associated uncertainty of these unknown factors in the fit. The PDFs are provided with uncertainties that must account for acceptable variations in methodology, including the choice of the functional forms to parametrize PDFs at an initial energy scale and the method for propagation of experimental uncertainties, as well as implementation of physical constraints on the PDFs, such as sum rules, positivity of physical observables, and integrability of relevant PDF combinations. The PDF uncertainties must representatively reflect these factors [186]. Methodological advances should also include development of practical standards for the delivery of PDFs to a wide range of users. The format of the PDF delivery must optimize for accuracy, versatility, and speed across a broad range of applications—a highly non-trivial task, given the ubiquity of the PDF uses. The PDF4LHC working group [187] leads the development of such standards and delivery formats for the LHC community, in particular, by publishing a comprehensive recommendation (PDF4LHC21 [188]) on the usage of PDFs and computation of PDF uncertainties at the LHC. The PDF4LHC working group also distributes combined N^2LO PDF4LHC21 error sets to streamline computations with PDFs across typical LHC studies, such as searches for new physics or theoretical simulations.

New experimental measurements are essential for constraining the PDFs to the needed accuracy in the HL-LHC era. The large volume of the pre-LHC data, combined with the rapidly growing LHC data, offers a wealth of information about the hadron structure. Yet, the uncertainties on PDFs do not decrease as the square root of the number of data points because of some disagreements among the data sets and systematic uncertainties in many experiments. Constraints on the PDFs can be strengthened by fitting high-luminosity data sets under elevated accuracy control at all stages of the measurements and their analysis.

Recent studies [30, 190] provide projections using various techniques for the reduction of PDF uncertainties under anticipated near-future theoretical and experimental developments. As an illustration, the left panel of Fig. 5 compares the current PDF uncertainty for $gg \to H_{\mathrm{SM}}$ production and its reduction when simulated HL-LHC measurements are included in the conservative (scen A) and optimistic (scen C) scenarios, using PDF4LHC15 NNLO PDFs [189] as the baseline.

The right panel shows an analogous projection for the reduction of the PDF uncertainty on the SM Higgs and $t\bar{t}$ cross sections at the LHC upon including the simulated measurements in DIS at the EIC, this time using the CT18 NNLO framework [78]. The ability of the LHC measurements to reduce the PDF uncertainty critically depends on the control of systematic effects. A lepton-hadron collider such as an EIC (see [4] and below), EIcC, MuIC, or LHeC [13, Sec. 3.C] that runs roughly concurrently with the HL-LHC phase would elevate the precision of PDFs in key HL-LHC measurements in a synergistic way that would be unattainable via HL-LHC measurements alone. Section III.1.3 includes some examples. A precision QCD program at the EIC is therefore a promising opportunity to obtain PDF measurements in the kinematic region of large x and small Q that is currently accessed only in fixed-target DIS and Drell-Yan experiments. This region is of high relevance to the LHC, as the currently large uncertainties in the PDFs at $x > 0.5$ directly affect the LHC high-mass BSM searches. These uncertainties at the largest x (outside of the reach of current experiments) and $Q = 1 - 10$ GeV propagate to smaller x at $Q = 100 - 1000$ GeV via
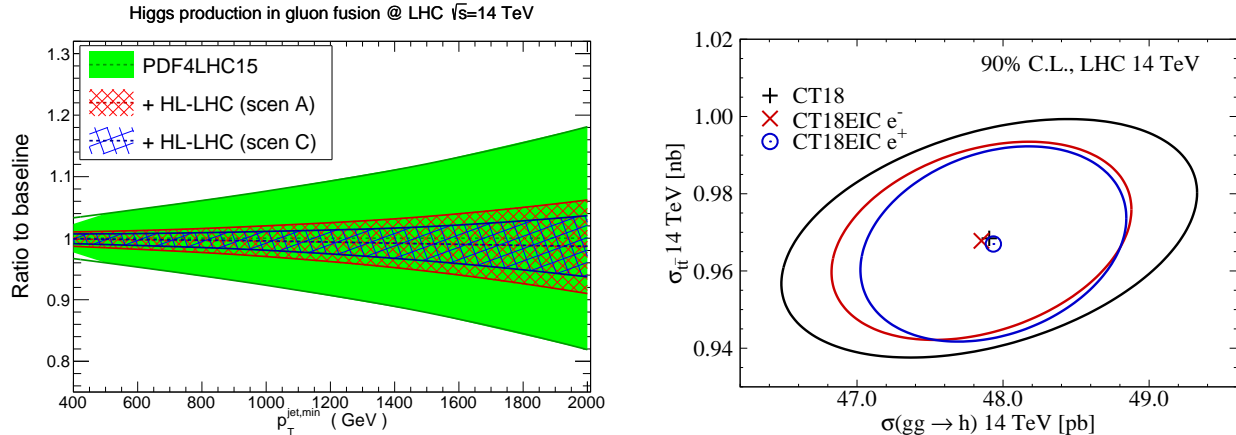
FIG. 5. Examples of projections for PDF uncertainties in the HL-LHC era. **Left:** Uncertainties for NNLO Higgs production via gluon fusion at $\sqrt{s} = 14$ TeV obtained with published PDF4LHC15 NNLO PDFs [189] (green band) and after additional constraints are imposed on these PDFs using simulated HL-LHC data in two scenarios (red and blue bands) [190]. **Right:** 90% C.L. uncertainty ellipses for NNLO predictions for $gg \to H_{\rm SM}$ and $t\bar{t}$ production at the LHC 14 TeV obtained using CT18 NNLO PDFs [78] and after imposing simulated constraints from inclusive DIS at the EIC [30].

QCD evolution and affect the LHC precision measurements.

III.1.2. HL-LHC experiments to probe PDFs

At the HL-LHC, a large range of experiments can either constrain the PDFs or depends on the PDFs [191, Sec. 3.A]. There are significant opportunities for constraining the PDFs and general appreciation of their importance. Even so, available estimates of the projected impact on the PDFs may vary considerably even for the same experimental data set, reflecting the methodology of the analysis and adopted definitions of the PDF uncertainties. These uncertainty estimates generally account for a combination of experimental, theoretical, parametrization, and methodological sources. Just as in the case of world-average QCD coupling determinations discussed in Sec. II, the reduction of the PDF uncertainty due to a combination of experiments reflects both the accuracy of individual experiments and mutual consistency of experiments.

Taking production of hadronic jets as an example, large differences exist between predictions using different PDF sets at the highest jet transverse momenta, $p_{\rm T,j}$ and dijet invariant masses $m_{\rm jj}$. These differences are due to sensitivity of the jet cross sections to the gluon density in the proton. As an illustration, Fig. 6(a) [1] shows the ratio of several PDF sets as a function of $p_{\rm T,j}$. An LHC data set with a large number of events has high statistical precision in these regions. However, since the shown PDFs already include significant constraints from various jet data sets, the achievable reduction even more depends on the LHC systematic uncertainties, which are insufficiently known. Progress in understanding of the systematic uncertainties is critical for taking full advantage of these promising measurements. This issue is explored in Sec. 5.A of Ref. [13].

Figure 6(b) estimates the impact that inclusion of the HL-LHC measurements into a PDF fit could have on the HL-LHC dijet production cross section [190]. Under various HL-LHC running scenarios, the uncertainty estimated with the PDF4LHC15 error PDF ensemble [189] decreases upon adding simulated data in (di)jet, gauge boson, and top quark production. The degree of reduction depends on the various factors mentioned above. In the shown "optimistic" scenario, the reduction of the PDF uncertainty on jet cross sections (and, by extension, on Higgs and other
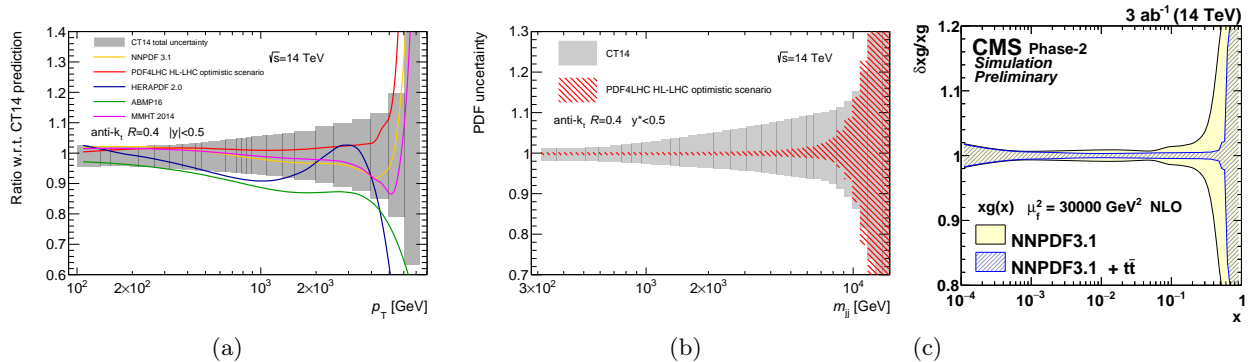
FIG. 6. (a) Ratio of cross-sections predictions for several PDF sets to the CT14 PDF prediction and CT14 uncertainty (gray band) for inclusive jet cross-section at $\sqrt{s} = 14$ TeV [192]. (b) Comparison of the PDF uncertainty in the dijet cross-section calculated using the CT14 PDF [178] and PDF4LHC HL-LHC sets at $\sqrt{s} = 14$ TeV with 3000 fb^{-1} [192]. (c) An estimated reduction of the relative uncertainty on the gluon PDF by profiling NNPDF3.1 PDFs [182] using simulated $t\bar{t}$ measurements at the HL-LHC [193]. The reduction of the uncertainties depends on the estimation methodology, see the main text.

cross sections dominated by gluon scattering) is quite dramatic.

Figure 6(c) shows the possible impact on NNPDF3.1 PDFs [182] upon adding $t\bar{t}$ cross section measurements at the HL-LHC, also sensitive to the gluon PDF, using the profiling method in the `xFitter` program [19]. The plot is based on estimations of differential $t\bar{t}$ cross-section measurements in the e/μ+jets channels at the HL-LHC with an integrated luminosity of 3000 fb^{-1} at $\sqrt{s} = 14$ TeV by CMS [193]. This final uncertainty can be below 5%, also reflecting an optimistic projection, as the default profiling in `xFitter` emphasizes the selected experiment more than the other experiments placing relevant constraints in the fit [Appendix F in 78]. The most significant increase in accuracy is expected to come from an improved jet energy calibration and a reduced uncertainty in the b-jet identification—the dominant systematic uncertainties. The precision will profit from the enormous amount of data and the extended η-coverage of the Phase-2 CMS detector, which enables fine-binned measurements at high rapidity that are not possible with the current detector.

Many other LHC processes over a wide kinematic region—production of direct photons, massive bosons with jets or heavy quarks, heavy quarks of all three generations—can provide valuable insights about proton PDFs. We refer the reader to the Snowmass PDF whitepaper [13] and recent reviews and textbooks [190, 194, 195]. It is critical to determine the same (combinations of) PDFs in multiple accurate measurements to pin down systematic uncertainties both in experiment and theory. For example, to further reduce the uncertainty on the critical gluon PDF, one must reconcile occasionally inconsistent pulls on the gluon in the relevant x regions imposed by fixed-target DIS, HERA DIS, jet, and $t\bar{t}$ production measurements.[1] New measurement channels therefore can provide desired independent information. As an illustration, direct photon production studied differentially in E_T^γ and η^γ is sensitive to the gluon PDF over a large x range [192]. The photon+jets measurements can be insightful when performed differentially in E_T^γ, $p_{T,\text{jet}}$, $\cos\theta^*$, and $m_{\gamma j}$. With the full 3000 fb^{-1} dataset, the reach of these measurements will increase, from 3 TeV to 7 TeV in $m_{\gamma j}$, and from 2.5 TeV to 3.5 TeV for E_T^γ and p_T^{jet}. The projected impact of these and other precision measurements at the HL-LHC is shown in Fig. 7, which compares the PDF uncertainties from the MMHT2014 PDF set to PDF sets derived using projections of measurements from the HL-LHC [190]. Better control of photon isolation is needed to take full advantage of this channel.

---

[1] The pulls on the PDFs can be examined by adding individual experiments into a PDF fit or removing them, or directly in a fit to many experiments using a fast sensitivity technique like in [196], with examples in [78, 197].
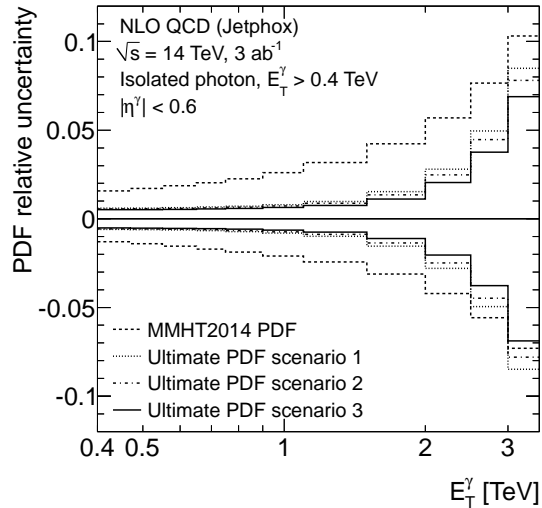
FIG. 7. Relative uncertainty in the predicted number of inclusive isolated photon events due to the uncertainties in the PDFs as a function of E_T^γ. [192]

III.1.3.   PDFs at the EIC

An EIC can significantly reduce PDF uncertainties both in HL-LHC EW precision measurements and, as importantly, searches for the heaviest final states, by measuring a range of interactions up to $\sqrt{s} = 140\,\text{GeV}$ in comparatively clean ep DIS processes. Spin-averaged EIC data on inclusive DIS, production of heavy quarks and QCD jets using neutral- and charged-current exchanges will allow for comprehensive flavor separation of (un)polarized PDFs and enhanced-precision determinations of QCD and EW couplings and quark masses.
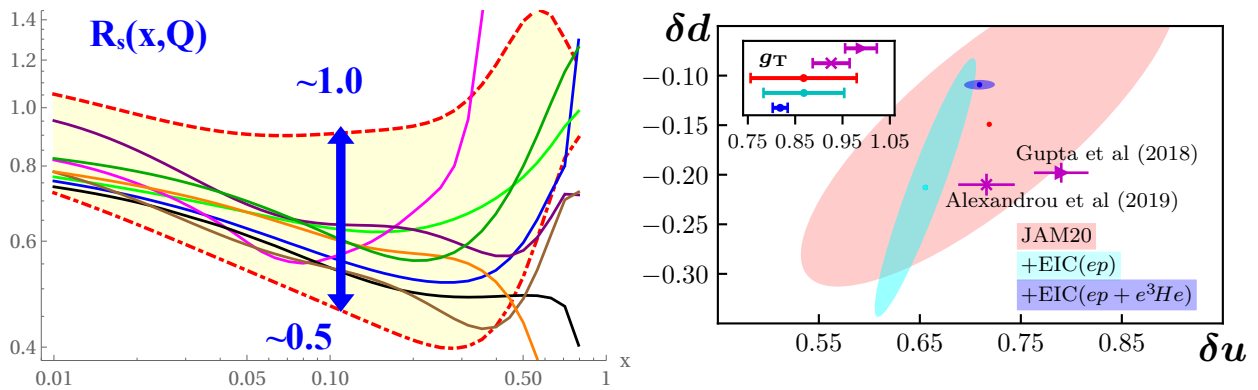

FIG. 8.   (a) The strange quark ratio $R_s(x,Q) = (s + \bar{s})/(\bar{u} + \bar{d})$ at Q=10 GeV for a selection of PDFs at partonic momentum fractions accesible at the EIC. (b) Flavor tensor charges δu, δd as well as the isovector charge g_T from the JAM'20 PDF analysis [198] as well as a re-fit that includes EIC Collins effect pion production pseudodata for a proton beam only and for both proton and ^{3}He beams together. Also shown are the results from two recent lattice-QCD calculations [199, 200] (purple). All results are at $Q^2 = 4\,\text{GeV}^2$ with error bands at 1σ CL. From [4].

The EIC can resolve long-standing questions regarding the precise balance of quark flavors contributing to the proton's structure, in particular the strangeness content of the proton. As

Fig. 8(a) illustrates, the ratio $R_s(x, Q) = (s + \bar{s})/(\bar{u} + \bar{d})$ has significant uncertainty in the EIC's kinematical region due to the insufficiently known strangeness PDF. As explored in Ref. [201], these uncertainties translate into large event-level shifts in CC DIS charm-jet production at the EIC, implying considerable potential to constrain the strangeness PDF.

Lattice QCD is making impressive advances in computations of nonperturbative QCD functions at $x > 0.1$ and factorization scales Q of a few GeV (Sec. V). This is precisely the region covered by the EIC kinematics, which creates ample opportunities for comparing lattice QCD predictions against the EIC data on 3-dimensional hadron structure. Lattice QCD can be compared against precisely known spin-averaged PDFs and make predictions for various spin-dependent PDFs. Not only the x dependence of PDFs can be compared, but also various Mellin moments integrated over the whole x range, as illustrated in Fig. 8(b) on an example of isovector tensor charges predicted based on the current JAM'20 PDFs, upon adding the EIC data on the proton and helium beams, or using two lattice QCD calculations. Section V.2 reviews lattice calculations of collinear PDFs in more depth.

III.2. Nuclear parton distributions

The structure of nucleons and nuclei are both key to understanding heavy-ion collisions as well as fundamental features of the nucleus. Much less is known about the nuclear PDFs than about the nucleon ones, especially for heavy nuclei at momentum fractions x below 0.1 and above 0.5, where modifications in a nuclear medium rapidly increase. In particular, particle production at small x of the nucleus and the possible QCD effects that may be revealed in it, such as the Color Glass Condensate [202] regime, are poorly known. Measurements made during the LHC Run 1 and Run 2 in Pb-Pb and especially p-Pb collisions have favored the inclusion of nuclear modification to the parton distribution functions (PDF) extracted for free protons. The p-Pb collision system is an excellent tool to study and constrain these nuclear parton distribution functions (nPDFs), since the asymmetric system allows one to select low-x regions of the nucleus by looking at forward rapidity, namely, the proton-going direction.
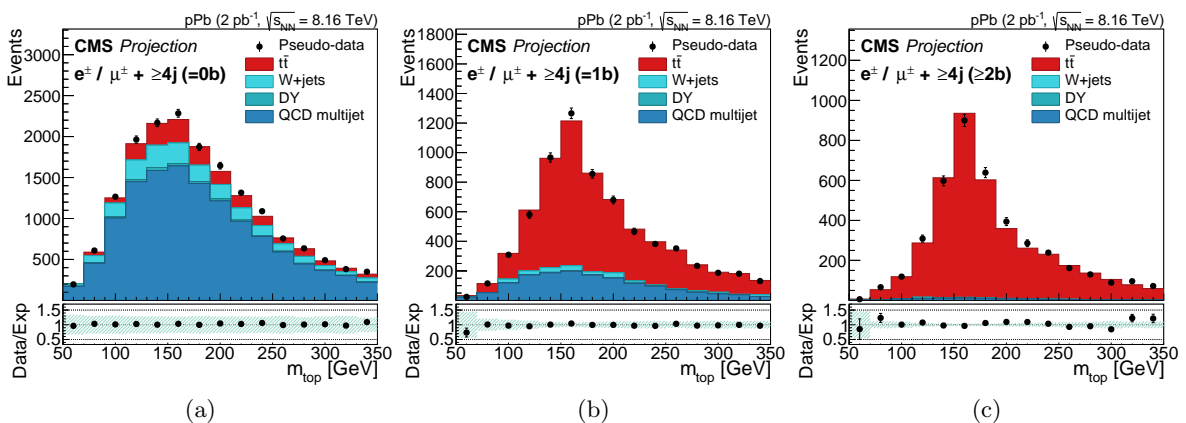

(a)   (b)   (c)

FIG. 9. Distributions of m_{top} in the (a) 0, (b) 1, and (c) 2 b-tagged jet categories. The sum of the predictions for the $t\bar{t}$ signal and background is compared to pseudodata (sampled randomly from the total of the predictions in each category). The bottom panels show the ratio between the pseudodata and the sum of the predictions. The shaded band represents the relative uncertainty due to the limited event count in the simulated samples and the estimate of the normalization of the QCD multijet background [203].

To this end, ATLAS and CMS both intend to measure W and Z boson production from p-Pb

collisions to constrain the quark nPDFs [203, 204], especially differentially in rapidity of the Z boson or charged lepton pseudorapidity of the W boson. Complementing these measurements, CMS has projected the measurement of dijet pseudorapidity which is sensitive to the gluon nPDF [203]. The measurement of differential $t\bar{t}$ cross sections in p-Pb collisions is a novel and potentially precise probe of the nuclear gluon density [38]. Figure 9 shows the mass distributions of the top quark and relevant backgrounds projected for p-Pb collisions for three different selections on the number of b-tagged jets [203]. Additional experimental leverage of the event-by-event sensitivity to Q^2 and nuclear x may be obtained by EW boson (W and Z) plus jet events, as projected by ATLAS [204].
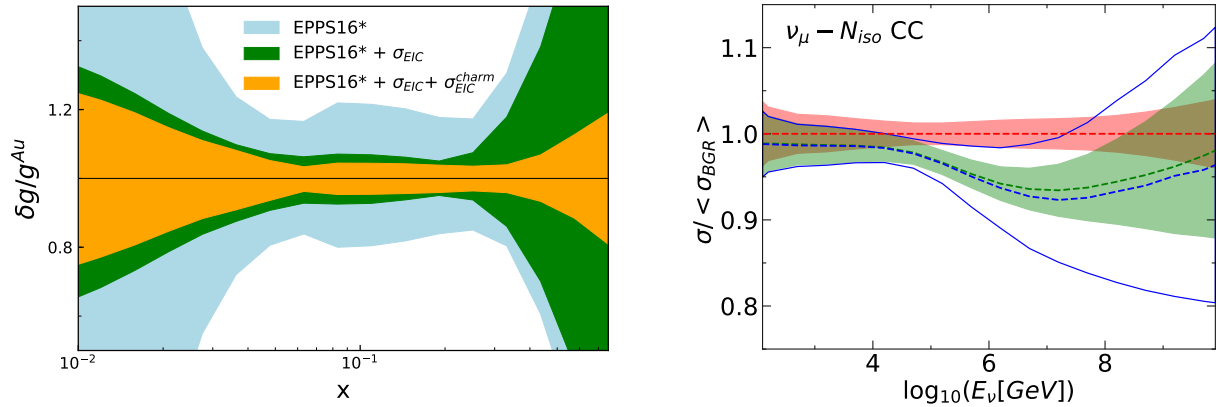

FIG. 10. Left: Estimated reduction in the EPPS16* [205] uncertainty for the gluon distribution in gold upon inclusion of EIC inclusive and charm production data [30]. Right: Nuclear PDF uncertainties based on nNNPDF2.0 [206, 207] for CC neutrino-nucleus DIS cross sections, without and with the EIC pseudodata included. Cross sections are plotted as a ratio to predictions for the proton as a function of the neutrino energy E_ν. See details in [4, Sec. 3.2.3].

The EIC can revolutionize understanding of nuclear PDFs for a large span of nuclear mass and charge quantum numbers, A and Z. As in the case of nucleon PDFs, studies of nuclear scattering at the EIC and HL-LHC are highly complementary. They will result in the reduction in nuclear PDF uncertainties and flavor separation at previously unaccessible x down to 10^{-2}, where modifications due to partonic saturation may kick in. As an illustration, the left Fig. 10 shows the reduction the relative uncertainty on the gluon PDF in gold after fitting inclusive DIS and semi-inclusive charm production pseudodata for the EIC, using the present EPPS16* nuclear PDFs as the baseline. In turn, better knowledge of nuclear PDFs will improve theoretical predictions for neutrino-nucleus scattering at future facilities like DUNE/LBNF. The right Fig. 10 shows the estimated reduction in the PDF uncertainty for CC neutrino scattering on an isoscalar heavy nucleus with $A = 31$ after including the EIC simulated data.

At $x < 10^{-2}$, ratios of cross sections of vector meson photoproduction in ultraperipheral collisions (discussed in Sec. VIII) of ions or protons offer a method to probe the small-x nuclear gluon PDF by tying it to the better known gluon PDF in the nucleon. First LHC measurements of this kind [208–210] all show moderate suppression in lead compared to a proton-target reference, consistently with models predicting moderate shadowing such as [211]. However, this method currently has large uncertainties and feels contamination from quarks [212]. Photoproduction of dijets [213] and heavy quarks will open additional avenues to test universality of nuclear PDFs at small x and look for evidence of partonic saturation.

Interpretation of many pA and AA collision experiments will require to know nuclear PDFs as a function of the initial parton's impact parameter b, in addition to the parton's momentum fraction

x. Various models predict the A and x dependence of the nuclear modification to the b-dependent PDFs and can be tested in the LHC and EIC experiments. At small x, a natural assumption is that the nuclear modification primarily depends on the parton thickness at a given b. One could try to determine b dependence of nuclear PDFs in a model in which hard and soft collisions are not correlated [214] or using the leading-twist shadowing theory [215].

III.3. Meson parton distributions

Global fits of PDFs for pions and kaons can clarify mechanisms of formation of hadronic bound states and hadron mass generation – the central topics in nonperturbative QCD [216, 217]. New measurements sensitive to meson PDFs are expected to be performed at fixed-target energies, the EIC [30] and the EIcC [56], then confronted against predictions from nonperturbative approaches and lattice QCD. As an example of what may be feasible in the near future, Fig. 11 shows a phenomenological PDF for a valence quark in the pion extracted from pion-nucleus Drell-Yan and tagged-neutron DIS data in NLO QCD with threshold resummation, and complemented with constraints from lattice QCD [218]. Such studies can be extended to other processes at NNLO and include more accurate lattice QCD predictions. They offer a window to elucidate the bound-state dynamics and transition to the perturbative QCD regime.
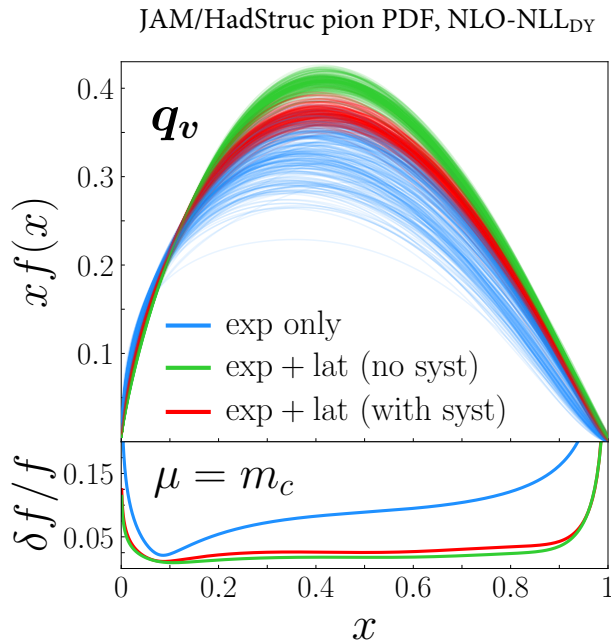

FIG. 11. Determination of a valence quark PDF in a pion using a combination of experimental and lattice QCD data, and including resummation of threshold radiative contributions [218].

IV. HADRONIZATION AND FRAGMENTATION FUNCTIONS

The process of hadronization describes how detected final-state hadrons are formed from partons. Since hadronization is governed by nonperturbative dynamics, it cannot be calculated analytically and, in contrast to the partonic structure of hadrons, is elusive in lattice calculations [219].

Having an accurate description of hadronization is, however, important for many measurements in high-energy physics and crucial for all measurements at hadron colliders.

IV.1.   Hadronization measurements at Belle II

A fragmentation function (FF) quantifies the probability for a parton to hadronize into a detected final-state particle of a known momentum. Precision measurements of FFs are instrumental for extracting the spin-averaged and spin-dependent nucleon structure [220] in the planned experiments at the EIC and Belle II. The emphasis of the Belle II program will be on investigation of full multidimensional dependency of FFs with complex final states, such as dihadrons or polarized hyperons. These final states are sensitive to spin-orbit correlations in hadronization. Their factorization universality properties and kinematic dependencies are still to be fully mapped out. However, they are important, as tagging on such final-state degrees of freedom allows more targeted access to the hadron structure in semi-inclusive deep inelastic scattering (SIDIS) experiments, e.g., at JLab and the EIC. One recent example of this is the extraction of the twist-3 PDF $e(x)$ via dihadron correlations, which is sensitive to the force that the gluons exert on a fragmenting quark as it traverses the nucleon remnant [221–224].

Detailed understanding of hadronization is necessary to model background and signal processes for new physics discoveries at B-factories themselves, but also at the LHC. Currently, modeling of backgrounds originating from light-quark fragmentation is mainly performed by Monte-Carlo Event Generators (MCEGs), such as Pythia [225], HERWIG [226] or Sherpa [227]. Tuning those generators to a precision needed for discovery science requires a model for correlated production of multiple hadrons that can only be verified with clean semi-inclusive e^+e^- annihilation data. Experimental data for this purpose are mostly available from LEP, but, to confidently extrapolate the model to LHC energies, input measurements are also necessary at CM energies an order of magnitude below LEP. The relatively low CM energy at Belle II, paired with extremely high luminosity, provides a large lever arm when combining Belle II and LEP/SLD data to probe hadronization effects over a wide energy range.

A comprehensive program with the high-statistics Belle II data is also needed to reach the precision necessary for the Belle II analyses themselves. MCEGs are also crucial for inference-based models, e.g. [228], which will be applied in the future to extract physical quantities. A recent development has been the extension of MCEGs to include spin-orbit correlations. Belle II measurements can inform the development of these novel MCEGs by benchmarking against spin dependent di-hadron correlations.

Where MCEGs describe full events, and the most common single-hadron FFs integrate over the whole event with the exception of the hadron in question, intermediate representations accounting for more correlations in hadronization gain more recognition in the field. The fragmentation functions for production of hadron pairs mentioned above are such an example. Beyond the current factorization theorems, there have been significant recent efforts to define correlation measurements that are sensitive to hadronization dynamics, can be interpreted within hadronization models (e.g., a QCD string model), and, while not yet realized, might be describable in a full QCD calculation with future, extended factorization theorems. These kind of correlation measurements have already been a focus at the LHC (see *e.g.*, Ref. [229]). At Belle II, correlations between leading particles can be precisely measured. Accurate knowledge of parton (in particular gluon [230]) FFs into hadrons (both inclusively and for individual hadron species) in e^+e^- collisions is also of utmost importance to have an accurate "QCD vacuum" baseline to compare with the same objects measured in proton-nucleus and nucleus-nucleus collisions and thereby quantitatively understand final-state ("QCD medium") modifications of the FFs [231, 232].

IV.2.   Measurements at the Electron Ion Collider

To capitalize on a new era of experiments like the EIC and HL-LHC, sound predictions for parton dynamics beyond collinear evolution are necessary. Transverse-momentum-dependent (TMD) PDFs and FFs will become the primary means to investigate the mechanism of hadronization in a 3D-picture [4]. Historically, they have been accessed through Semi-Inclusive DIS (SIDIS) and e^+e^- annihilation with observation of two final-state hadrons. However, phenomenological extractions based on such processes are complicated by the fact that, in the cross section, the TMD FF does not appear on its own, but it is always convoluted with another TMD (two TMD FFs in e^+e^- annihilations, one TMD PDF and one TMD FF in SIDIS). Disentangling these functions is usually difficult. The problem can be bypassed if one can extend the TMD factorization scheme to cross sections that involve only one TMD FF. In this sense, the cleanest process that accesses one TMD FF is single hadron production in e^+e^- annihilations, $e^+e^- \to h\,X$.

A factorization theorem was recently derived in Ref. [233] for $e^+e^- \to h\,X$, where the transverse momentum P_T of the detected hadron is measured with respect to the thrust axis. Under certain approximations, this cross section can be written as a convolution of a TMD FF with a coefficient that is totally predicted by perturbative QCD and can be interpreted as a partonic cross section [234, 235]. Since this process is more inclusive than SIDIS and e^+e^- annihilation into two hadrons, the role of the soft gluons is different. The soft nonperturbative part of the TMD can be disentangled, and it becomes possible to define a phenomenology work plan that involves a much larger number of different processes by dealing with one single unknown at a time. Within this framework, the future EIC, which will explore a very broad kinematical region, could provide informative measurements for both TMD PDFs and FFs.

IV.3.   Measurements at future e^+e^- colliders

The reaction of e^+e^- annihilation has always been a method of choice to access hadronization in a clean environment. Much of the predictivity of QCD at colliders in fact stems from factorization theorems paired with measurements at PETRA, PEP, LEP and SLD. There is a class of universal nonperturbative inputs that were not yet defined at the time of LEP and SLD, which could be measured precisely at the ILC and other future e^+e^- machines, and would have a significant impact on the LHC physics program. Modern measurements rely strongly on the use of particle flow and tracking information. However, only observables that are completely inclusive over the spectrum of final states can be computed purely from perturbation theory. The nonperturbative input needed for theoretical predictions of track-based observables is universal and can be parametrized by so-called "track functions" [63, 236], which describe the fraction of energy carried by charged particles from a fragmenting quark or gluon. Recently it has been shown how to compute jet substructure observables by incorporating track functions [237, 238] as a step toward precision jet substructure measurements at the HL-LHC and future colliders.

IV.4.   Hadronization and color reconnection at the HL-LHC and FCC-ee

Nonperturbative uncertainties from final-state hadronic effects linked to power-suppressed infrared phenomena, such as color reconnection (CR), hadronization, and multiparticle correlations (in spin, color, space, momenta)—which cannot be currently computed from first-principles QCD and often rely on phenomenological Monte Carlo modeling– may limit the ultimate accuracy at hadron-hadron colliders. Whereas the perturbative radiation in the process can be in principle theoretically controlled, there is a CR "cross talk" among the produced hadronic strings that can only

be modelled phenomenologically [239]. In the *pp* case, CR can limit precision in the extraction of the top mass, contributing 20–40% of the net uncertainty [240]. In contrast, the FCC-ee would offer a relatively clean radiation environment for systematic study of such effects [241]. In $e^+e^- \to t\bar{t}$, as the top quarks decay and hadronize closely to one another, their mutual interactions, decays into bottom quarks, and/or gluon radiation rearrange the color flow and thereby the kinematic distributions of the final hadronic state. To understand CR dynamics that limits the reach of CP-violation searches in $H \to W^+W^-$ hadronic decays [242], one can optimally study the process $e^+e^- \to W^+W^- \to q_1\bar{q}_2q_3\bar{q}_4$ [242], where CR can lead to the formation of alternative "flipped" singlets $q_1\bar{q}_4$ and $q_3\bar{q}_2$, and correspondingly more complicated string topologies [243]. The combination of results from all four LEP collaborations excluded the no-CR null hypothesis at 99.5% CL [244], but the size of the WW data sample was too small for any quantitative studies. At the FCC-ee, if the W mass is determined to better than 1 MeV by a threshold scan, the semileptonic WW measurements (unaffected by CR) can be used to probe the impact of CR in hadronic WW events [241, 245].

Ultimately, enormous data sets collected at the FCC-ee would lead to negligible statistical and small systematic uncertainties on such observables sensitive to the geometric pattern of soft QCD interference. Even at the HL-LHC, these issues can be put under better control in spite of its typically larger uncertainties on particle production due to the underlying event, multiple parton scattering, and dense particle tracks. For example, in production of top-quark pairs, t jets are defined when the top quark decays hadronically, and the decay products are clustered as a single jet. Figure 12 shows $t\bar{t}$ cross-section as a function of the azimuthal angle separation $\Delta(\phi)$ between the two leading $t\bar{t}$ jets. In this analysis by the CMS Collaboration [246], kinematic distributions of jets in inclusive jet production, top quark jets and jets arising out of the hadronic decay of W-bosons have been studied, following previous $\sqrt{s} = 7$ TeV analyses [247–250]. The azimuthal correlation between the two jets is indicative of the interference effects arising out of the color connection of the jets.
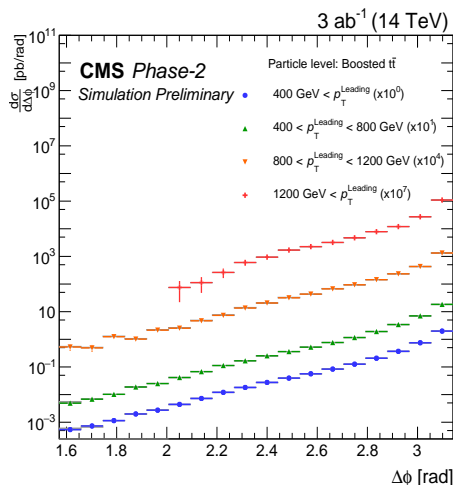

FIG. 12. The particle level cross-section of the $t\bar{t}$ process as a function of the $\Delta(\phi)$ between the two leading $t\bar{t}$ jets. [246]

At the HL-LHC, hadronization uncertainties can also be studied and reduced by taking advantage of better event generators and GEANT detector simulation code, reduced material in trackers, higher reconstruction efficiency, wider angular and momentum acceptance [251]. During the LHC measurements themselves, hadronization uncertainties can be further reduced thanks to detec-

tors with advanced hadron identification capabilities (e.g., via timing, dE/dx, and/or dN/dx) and modern data analysis methods, such as those exploiting the jet substructure and the Lund plane approaches [35, 252]. Better models for hadronization will lead to more accurate experimental measurements and deeper understanding of strong interactions to all orders.

V. PARTON DISTRIBUTION FUNCTIONS IN LATTICE QCD

Lattice QCD (LQCD) is a theoretical tool that allows us to study the nonperturbative regime of QCD directly with full systematic control. The approach is based on regularizing QCD on a finite four-dimensional Euclidean spacetime lattice and is often studied using numerical computations of QCD correlation functions in the path-integral formalism using national-scale supercomputers. To make contact with experimental data, the numerical results are extrapolated to the continuum (with lattice spacing $a \to 0$) and infinite-volume ($L \to \infty$) limits. When the calculation is done using heavier-than-physical quark masses (to save computational time), one also has to take the $m_q \to m_q^{\text{phys}}$ limit. Lattice QCD has been known for great precision in providing flavor-physics inputs, CKM matrix elements, quark masses and more (See Snowmass Rare Precision and Lattice Gauge Theory reports). The progress of lattice PDF calculations has long been limited by computational resources, but recent advances in both algorithms and worldwide investment in pursuing exascale computing have led to exciting progress in LQCD calculations. Many collaborations have performed hadronic structure calculations directly at physical pion mass with multiple lattice spacings to control lattice artifacts. Some LQCD calculations have reached a level where they not only complement, but also guide current and forthcoming experimental programs, such as on nucleon tensor charges and the strange-quark contribution to proton spin [253, 254].

There has been rapid progress in new methodology for calculating the momentum fraction (x) dependence of PDFs on the lattice. Here, we will mention a few select examples of this progress; for recent reviews, see Refs. [253–256].

- Extensive calculations have been carried out for isovector PDFs and distribution amplitudes (DAs). Precision calculations require control over systematics from renormalization, the continuum limit, the inverse problem in short-distance factorization (SDF) and extrapolation to large lightcone distance in large-momentum effective theory (LaMET). Calibrations can be made against lattice moments and high-precision experimental data. Closure tests with artificial data can be used to assess the robustness of the current procedures. To make an impact on high-energy collider phenomenology, developing calculations at the 5% level (total systematics) for isovector collinear PDFs and improving the precision of the current PDF calculations including sea-quark distributions (as well as large-x quarks and gluons) will require significant increases in computational resources.

- Methods for calculating collinear PDFs, generalized parton distributions (GPDs), TMD distributions and evolution kernels have undergone extensive development. While one-loop matching kernels are widely available, high-precision calculations require two-loop (only available for isovector PDFs) or higher-order matching, as well as quantitative understanding of renormalon uncertainties and higher-twist effects. The key systematic uncertainties that need to be understood arise from inverse problems and coordinate-space extrapolations at large distances.

- While many lattice exploratory studies have been undertaken, extensive high-statistics lattice-QCD data spanning different hadron momenta, quark masses, lattice spacing, volumes, valence and sea quarks, are needed to understand systematic effects. New methods

are needed to increase the signal-to-noise ratio for hadronic matrix elements, particularly for large hadron momentum and large spatial correlations. Criteria need to be established for reducing the excited-state contamination, finite-volume effects, and the effects of nonzero lattice spacing.

- Lattice computations are complementary to phenomenological PDF analyses, and in certain cases they can be used together to obtain hybrid parton distribution sets [257–260]. This is particularly important for three-dimensional nuclear femtography, because extracting the GPDs from experimental data alone can be extremely challenging. The connected-sea and disconnected-sea partons are innately coded in lattice calculations of the PDFs, GPDs and TMDs via the respective insertions. Lattice calculations and phenomenological analyses of the PDFs and their moments can go hand-in-hand in discriminating between the connected-sea and disconnected-sea components of the PDFs. This separation will help to understand the partonic composition of the proton's spin, for example.

- Besides the collinear PDFs, exploratory calculations have been undertaken for other salient QCD functions, including GPDs, higher-twist distributions, as well as the Collins-Soper rapidity evolution kernel and soft functions introduced by TMD factorization. As some of these functions are not easy to assess in experiment, their controlled lattice calculations can play a prominent role in future studies.

V.1. New methodologies for PDF computations

Mellin moments of the collinear PDFs are the simplest quantities to calculate on the lattice. Moments provide "global" momentum-space information about partons. It is, however, not easy to connect them directly to a particular experiment in which particles of definite momentum are measured. A more desirable theoretical approach is to directly access dependence of PDFs on the partonic momentum fraction x, i.e., "local" information in momentum space. Toward this goal, two approaches have been developed by lattice QCD in recent years. The first focuses on the SDF in coordinate space, and the other is based on an expansion in terms of a large hadron momentum, LaMET. Both methods require calculating coordinate-space correlation functions in large-momentum hadron states.

Multiple SDF methods have been developed by the lattice community, based on hadronic tensors [261–264], Compton amplitudes or "OPE without OPE" [265–269], current-current correlators [270–276] and pseudo-PDFs [277]. All these approaches provide constraints on collinear PDFs beyond individual moments. To determine the PDFs from the discrete lattice data on a range of coordinate-space correlations (a "Ioffe-time distribution"), one solves the inverse problem, which may take the form of a fit with either a fixed parametrization or a neural network. The lattice data can be fitted on their own or included into a global analysis of PDFs together with experimental hard-scattering data, as described in Secs. III.1.3 and III.3.

An alternative approach to parton physics on the lattice follows from Feynman's original conception of partons as constituents of hadrons traveling closely to the speed of light [278]. In this formulation, PDFs quantify distributions of quarks and gluons in hadrons with large longitudinal momentum, $P_\infty = P_z \to \infty$. This approach can compute the collinear PDFs, TMD PDFs and light-front wave functions using standard twist-2 operator definitions in Euclidean space [279]. The UV behavior of these functions is usually renormalized by (modified) minimal subtraction in $n < 4$ dimensions. A finite large momentum P_z is used to approximate P_∞, and a large-momentum expansion is carried out, with systematic power corrections characterized by the expansion parameter $\Lambda_{\rm QCD}^2/(xP_z)^2$. This follows from the physical picture of partons, which lose their meaning if their
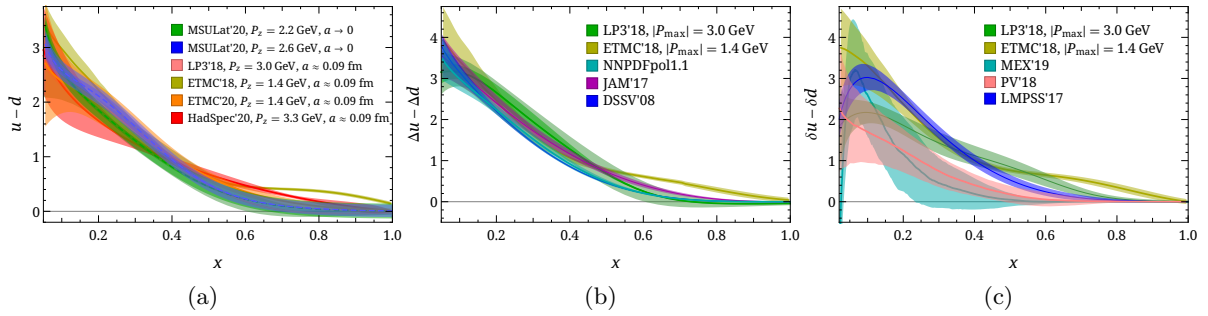
FIG. 13. Comparisons of lattice calculations of the nucleon isovector PDFs. (a) Unpolarized PDFs from the physical-continuum limit, "MSULat'20" [281], a single lattice spacing calculation at (or extrapolated to) physical pion mass using LaMET methods, "LP3'18" [282] and "ETMC'18" [283], and pseudo-PDF method, "ETMC'20" [284] and "HadSpec'20"[274]. (b) Helicity PDFs from LP318 [285, 286] and ETMC18 [287, 288] lattice computations, and global fits NNPDFpol1.1 [289], JAM17 [290], DSSV08 [291]. (c) Transversity PDFs MEX19 [292], PV18 [293], LMPSS17[257].

longitudinal momentum reaches the soft nonperturbative scale $\Lambda_{\rm QCD}$, corresponding to zero or soft modes instead of collinear ones. More importantly, the UV cut-off $\Lambda_{\rm UV}$ is always taken to be much larger than P_z, and the lattice matrix elements must be matched on the standard lightcone parton distributions to account for different UV behavior. This approach to partons is similar to heavy-quark effective theory, in which heavy-quark masses are taken to infinity, and has been called large-momentum effective theory or LaMET [255, 280].

V.2. Examples of computations

V.2.1. Nucleon isovector PDFs

The most studied x-dependent structure is the nucleon unpolarized isovector PDF $u(x) - d(x)$. Multiple collaborations have reported either direct lattice calculations at physical pion mass or extrapolations to physical pion mass using quasi-PDF [281–283, 294] and pseudo-PDF methods [274, 284]. Figure 13(a) shows the results of lattice calculations using at least one near-physical pion mass, with systematic effects taken into account to varied degrees. Overall, there is a reasonable agreement at $x = 0.1 - 0.6$ after scaling up the systematic uncertainties where they may be underestimated. The $SU(2)_f$ antiquark asymmetry, $\bar{d}(x) - \bar{u}(x)$, can be also computed, albeit with a lower accuracy unless an increased value of P_z is used [282, 285, 294]. Increasing the boost momentum of the lattice calculations will be critical for computing these PDF combinations at smaller or larger x.

When predicting spin-dependent PDFs, lattice calculations already may provide comparable predictions than phenomenological global analyses. Figures 13(b) and (c) summarize lattice predictions for helicity and transversity nucleon isovector PDFs at physical pion mass for the helicity and transversity PDFs [283, 285–287].The helicity lattice results are compared to two phenomenological fits, NNPDFpol1.1 [289] and JAM17 [290], exhibiting nice agreement. The lattice results for the transversity PDFs have better nominal precision than the global analyses by PV18 and LMPSS17 [257]. As none of these polarized lattice calculations have taken the continuum limit $(a \to 0)$, and they have remaining lattice artifacts (such as finite-volume effects), further studies will be warranted with more computational resources and multiple lattice spacings and volumes.
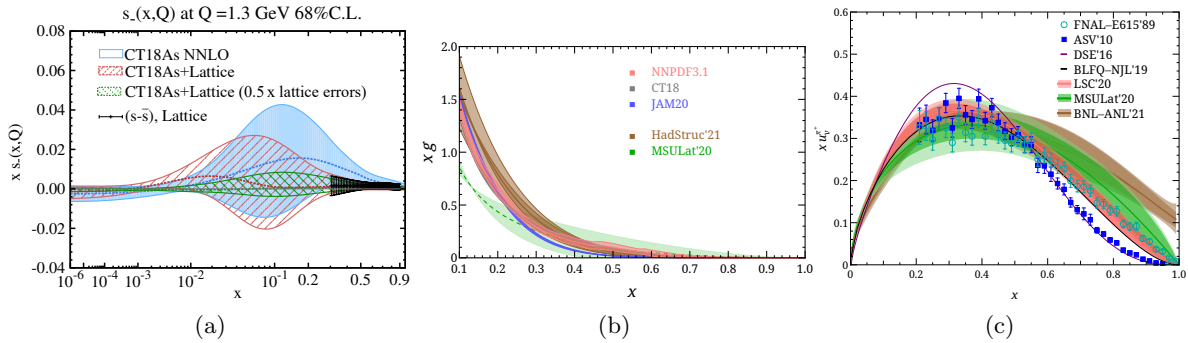
FIG. 14. (a) Impact of constraints from lattice QCD (black dashed area) on the difference between strange quark and antiquark PDFs in a recent CT18As NNLO fit [15]. The red (green) error bands are obtained with the current (reduced by 50%) lattice-QCD errors. (b) The unpolarized gluon PDF $xg(x, \mu)$ in $\overline{\text{MS}}$ at $\mu = 2$ GeV, obtained from the fit to the lattice data at pion masses $m_\pi = 135$ (extrapolated), 310 and 690 MeV by MSULat [295] and at pion mass $m_\pi = 380$ MeV by HadStruc21 [296], compared with the NNLO CT18 and NNPDF3.1 gluon PDFs. (c) Lattice results on the valence-quark distribution of the pion, BNL [297] and MSULat [298] lattice groups using LaMET method, JLab and W&M group [276], using LCS method.

V.2.2. Strange and anti-strange PDFs

The experimental uncertainty on the strange quark and antiquark PDFs remains large: in the global fits they contribute in subleading channels or in neutrino-nucleus DIS experiments with substantial uncertainties. DIS and LHC experiments, while not in a certain disagreement on the amount of strangeness in the proton, may exert contradicting pulls on it that depend on the type of the global analysis [78, 183, 299–302]. Some of these tensions are relieved by allowing $s(x) \neq \bar{s}(x)$ at the Q_0 scale, as is done in some [183, 184] but not all analyses. The strangeness contributes a large part of PDF uncertainty in precision W and Z boson measurements at the LHC [303], so understanding its behavior is important. Lattice QCD can already provide competitive constraints on the strangeness asymmetry $s_-(x) \equiv s(x) - \bar{s}(x)$ and reduce some of the uncertainties that are not constrained in the experiment [15]. Figure 14(a) shows that the uncertainty on $s_-(x)$ in the CT18As NNLO fit is tangibly reduced upon adding the first lattice-QCD constraints on $s_-(x)$ at $x \in [0.3, 0.8]$. In the figure, the uncertainty in the lattice data points at $x > 0.3$ is quite small compared to the error band of CT18As determined from the global fit, so that including the lattice data in the CT18As_Lat fit greatly reduces the s_--PDF error band size in the large-x region. The reduction of the CT18As_Lat error band at $x < 0.3$ depends on the chosen parametrization form of $s_-(x)$ at $Q_0 = 1.3$ GeV. Hence, it is important to have more precise lattice data, extended to smaller x values. The figure also illustrates the projected reduction in the CT18As_Lat uncertainty on $s_-(x)$ if the current uncertainties on lattice data are reduced by half.

V.2.3. Gluon PDF

There have been attempts in lattice QCD to constrain the notorious gluon PDFs, which usually require orders-of-magnitude higher statistics than their quark counterparts to get a nonzero result within the statistical uncertainty. The first exploratory study of this kind was done by the MSULat group [304], using $m_\pi^{\text{sea}} = 330$ MeV. Up to perturbative matching and power corrections at $O(1/P_z^2)$, the lattice results are compatible with global fits within the statistical uncertainty at large z. Since then, there have been improvements in the operators for the gluon-PDF lattice

calculations [305–307], which will allow us to take the continuum limit for the gluon PDFs in the future. The followup work using the "pseudo-PDF" method by MSULat group [295] attempts an extrapolation of the gluon PDF to the physical pion mass at a single lattice spacing. HadStruc collaboration [296] used a different numerical technique in extracting the gluon PDF with a 360-MeV pion. These results are shown in Fig. 14(b). While currently these calculations are done at x of order 0.1, the future lattice calculations may be valuable in predicting the gluon PDF at $x > 0.5$, where the experimental constraints on the gluon weaken considerably.

V.2.4. *Pion and kaon PDFs*

Lattice QCD predictions are already included in some global fits of pion PDFs [218], as reviewed in Sec. III.3. Future experiments, such as COMPASS++ and AMBER, will greatly improve our knowledge of both the pion and kaon PDFs. Since 2018, there have been several LQCD calculations of the valence-quark dependence of PDFs for pseudoscalar mesons [275, 276, 297, 298, 308–312]. Reference [298] was the first study of lattice pion and kaon PDFs to take the continuum-physical limit of the matrix elements with a sufficient number of lattice spacings and light pion masses. There has also been a first next-to-next-to-leading order (N^{2}LO) matching [313, 314] lattice calculation of the pion valence-quark PDF [297] with 300-MeV pion mass. Both works take important steps toward precision PDFs from lattice QCD. Figure 14(c) illustrates selected lattice PDF predictions for the valence-quark PDF at $x \to 1$, where it can be compared against various nonperturbative approaches [218, 275, 308, 315–321].

Gluon PDFs of mesons suffer from significant signal-to-noise issues, so it is harder to get precise signals than for their valence-quark counterparts. Recently, attempts were made to study the gluon PDFs of the pion [295] and kaon [322] with lightest pion masses of 220 and 310 MeV, respectively. These studies show mild dependence of the pion gluon parton distribution on lattice spacing and pion mass. The lattice results can be used to improve the large-x region of the global fits with more computational resources and implementation of mixing with the quark PDFs.

V.2.5. *Other lightcone quantities*

There has been also recent progress made in determining the x-dependent meson distribution amplitudes (DAs) [273, 323–332]. DAs are important universal quantities to describe exclusive processes at large momentum transfers $Q^2 \gg \Lambda_{\mathrm{QCD}}^2$ using factorization theorems. Some well-known examples of such processes, which are relevant to measuring fundamental parameters of the Standard Model, include $B \to \pi l \nu$, $\eta l \nu$ giving the CKM matrix element $|V_{ub}|$, $B \to D\pi$ used for tagging, and $B \to \pi\pi$, $K\pi$, $K\bar{K}$, $\pi\eta$, etc., which are important channels for measuring CP violation (see e.g. Ref. [333]). The lattice studies also help us to understand the flavor SU(3) symmetry breaking among light flavors before attributing the effects to enhancement of higher-order amplitudes or even new physics.

New experiments and facilities will explore the three-dimensional structure of hadrons described by the GPDs and TMDs. GPDs are hybrid momentum and coordinate-space distributions of partons that bridge the standard nucleon structure observables, form factors and inelastic cross sections. Only recently have there been a few lattice calculations made for the pion GPDs with the pion mass of 310 MeV [334], and for nucleon GPDs with the pion masses of 260 MeV [335] and 139 MeV [336, 337]. These calculations require an increase in computational resources by at least an order of magnitude relatively to PDF calculations due to the additional boost momenta required. For the best determinations of GPDs, the lattice results can be combined with experimental measurements in a global analysis.

TMDs depend on the parton's transverse momentum k_T, in addition to the longitudinal momentum fraction x. They are nonperturbative inputs for processes that follow TMD factorization, such as Drell-Yan process and SIDIS. Early lattice studies computed selected TMD functions at heavier-than-physical pion masses ranging down to about 300 MeV [338–342]. Recently, there were first extraction of the Collins-Soper kernel, soft function and wavefunctions for TMDs [343–348]. Like for the PDF calculations, lattice precision calculations of TMDs will require large hadron momentum to suppress the power corrections at $\mathcal{O}(1/(P_z b_T)^2)$.

V.3.   Outlook and challenges

A Snowmass whitepaper [14] provides more details on the rapid advances in LQCD calculations of PDFs and other QCD functions and has more complete references to relevant work. Experimental exploration of the three-dimensional structure at the Jefferson Lab, EIC, other facilities will match the ongoing theoretical advancements that open doors to many previously unattainable predictions, from the x dependence of collinear nucleon PDFs to TMDs [338–340, 342, 349] and related functions [343, 345–348], GPDs [334–337], and higher-twist terms, progress that was not envisioned as possible during the 2013 Snowmass study.

There remain challenges to be overcome in the lattice calculations, such as reducing the noise-to-signal ratio, extrapolating to the physical pion mass, and increasing hadronic boosts to suppress systematic uncertainties. Computational resources place significant limitations on the achievable precision, as sufficiently large and fine lattices are necessary to suppress finite-size and higher-twist contaminating contributions. New ideas can bypass these limitations. With sufficient support, lattice QCD can fill in the gaps where the experiments are difficult or not yet available, improve the precision of global fits, and provide better SM inputs to aid new-physics searches across several HEP frontiers.

VI.   FORWARD SCATTERING AND SATURATION

Studies of forward and diffractive scattering processes provide rich opportunities to probe QCD dynamics. In this section, we review select examples of ongoing studies and future experiments in this important area.

VI.1.   Low-x physics and BFKL resummation

In hadron-hadron collisions, final states produced at large rapidities, small partonic momentum fractions x, as well as those with the absence of energy in the forward region (with the so-called rapidity gap) in elastic, diffractive, and central exclusive processes offer multiple avenues to learn about QCD dynamics. In these processes, the standard collinear QCD factorization discussed in Secs. III and IX is generally not applicable. Some of these configurations originate from purely non-perturbative reactions, while others can be explained in terms of multi-parton chains or other extensions of the perturbative QCD parton picture such as the Balitsky-Fadin-Kuraev-Lipatov (BFKL) formalism [350–353].

When scattering contributions are evaluated in the high-energy or *Regge* limit, the convergence of the perturbative series is spoiled by large logarithms, and an all-order resummation of these large logarithms must be carried out. The BFKL approach performs this resummation by factorizing QCD cross sections into a convolution of two process-dependent impact factors and a

process-independent Green's function. This factorization has been proven up to the next-to-leading logarithmic accuracy (NLA).

The BFKL Pomeron predicts a fast powerlike rise of the gluon distribution in the proton in the kinematic regions where $x \to 0$. While such a rise is seen in data, unitarity bounds prohibit such a rise to continue forever: at a certain value of x, this rise must slow down to a logarithmic growth. The latter is strongly related with the formation of an over-occupied system of gluons, known as the Color Glass Condensate, whose exploration is one of the central physics goals of the EIC. While at the EIC a dense QCD state will be achieved through scattering of electrons on heavy ions, forward-rapidity experiments at the LHC, including the FPF, allow for a complementary exploration, since high-gluon densities are produced through the low x evolution of the gluon distribution in the proton.

Closely related to diffractive events are photon-induced reactions at the LHC and other colliders. These reactions are reviewed in the dedicated Section VIII. In such events, either one or both initial-state protons or ions act as a photon source. The first configuration results in exclusive photon-hadron interaction at highest CM energies and therefore yields another tool to study the highest gluon densities with high precision. Such exclusive reactions are complementary to ion scattering at the EIC, since at the LHC high parton densities are predominately generated by high-energy evolution, while the EIC at its lower CM energy relies on the nuclear enhancement. A dedicated Snowmass whitepaper [16] elaborates in detail on BFKL and low-x physics, especially Mueller-Navelet jets, jet-gap-jet events, very forward jets, and vector meson production as a possible sign of BFKL resummation and saturation phenomena.

VI.2. Hard diffraction and sensitivity to the Pomeron

Hard diffraction corresponds to events when at least one proton is intact after interaction and corresponds to the exchange of a colorless object called the Pomeron. Measurements at the LHC can constrain the Pomeron structure in terms of quarks and gluons that has been previously derived from QCD fits at HERA and at the Tevatron [354, 355]. One can probe if the Pomeron is universal between ep and pp colliders. Tagging both diffractive protons in allows to probe the QCD evolution of the gluon and quark densities in the Pomeron and to compare with earlier measurements. In addition, it is possible to assess the gluon and quark densities using the dijet and γ+jet productions [356–359]. The measurement of the dijet cross section is directly sensitive to the gluon density in the Pomeron and the γ+jet and W asymmetry measurements [359] are sensitive to the quark densities in the Pomeron. However, diffractive measurements are also sensitive to the survival probability which needs to be disentangled from PDF effects, and many different measurements will be needed to distinguish between them. It is clear that understanding better diffraction and probing different models will be one of the key studies to be performed at the high luminosity LHC, the EIC, and any future hadron collider.

VI.3. Soft diffraction and the Odderon

Soft diffraction and elastic interactions have been studied for the last 50 years at different colliders. Elastic pp and $p\bar{p}$ scattering at the high energies of the Tevatron and LHC corresponds to the $pp \to pp$ and $p\bar{p} \to p\bar{p}$ interactions, where the protons and antiprotons are intact after interaction and scattered at very small angle, and nothing else is produced. Many experiments have been looking for evidence of the existence of the Odderon, a C-odd counterpart of the Pomeron associated with colorless gluon exchanges [360, 361]. At ISR energies [362–366], there was indication of a possible 3σ difference between pp and $p\bar{p}$ interactions. This was not considered a clean Odderon

signal, as elastic scattering at low energies can be due to exchanges of additional particles such as ρ, ω, ϕ mesons and Reggeons. Distinguishing between all these possible exchanges is not simple and becomes model-dependent. The advantage of using higher energies such as at the Tevatron or LHC [367–371] is that meson and Reggeon exchanges can be neglected. Recently, a combination of measurements of elastic cross sections for $p\bar{p}$ at D0 and for pp by TOTEM was interpreted as a discovery of an Odderon exchange with a significance that ranges from 5.3 to 5.7σ (depending on the model) [372]. Further measurements of elastic pp cross sections will happen at higher LHC energies, and search for Odderon exchanges will be performed in additional channels, such as production of ω mesons. It is also clear that the discovery of the Odderon is likely related to the existence of glueballs, and the search for their production will happen at the LHC, RHIC, and the EIC.
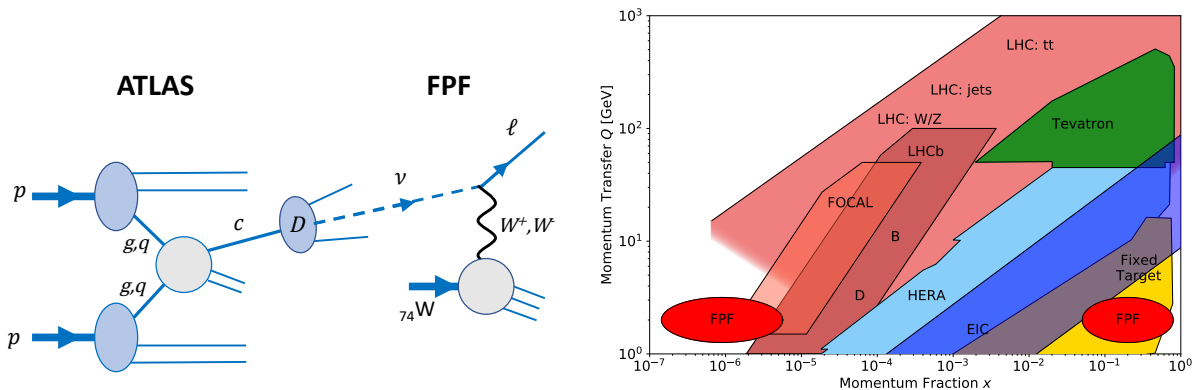

FIG. 15. (a) The production and detection processes for forward D-meson production at the HL-LHC, followed by their decay into neutrinos falling within the FPF acceptance. (b) The (x, Q) regions (red ovals) that can be accessed at the FPF via this process.

VI.4. Forward Physics Facility

VI.4.1. Overview

Experiments at the Forward Physics Facility (FPF) [2, 3] introduced in Sec. I.2 offer a unique opportunity to test and study QCD in a new regime. Three FPF experiments, with tungsten or liquid argon targets, will detect far-forward neutrinos that come from decays of hadrons produced in collisions at the LHC ATLAS interaction point, including from decays of charm mesons illustrated in Fig. 15(a). With its capability of distinguishing neutrinos and antineutrinos of different flavors, the FPF will provide versatile experimental data on both light- and heavy-flavor production at the LHC.

The kinematic reach of the FPF in pp collisions is illustrated in Fig. 15(b). The figure also indicates the approximate kinematic coverage for other experiments that provide inputs for global PDF analyses, including future facilities such as the EIC [30] and the ALICE Forward Calorimeter (FOCAL) upgrade [373]. The FPF will extend the coverage of the low-x region by almost two orders of magnitude at low-Q, reaching down to $x \simeq 10^{-7}$. The FPF will be sensitive to very high-x kinematics as well.

These kinematic ranges open a wide range of opportunities for QCD studies, such as charting the gluon at very low x, revealing BFKL and saturation dynamics, and testing Monte Carlo models for forward hadron production. Understanding small-x dynamics in pp collisions, already important at

the LHC and HL-LHC [172, 374], is crucial for any future higher-energy pp collider such as FCC-hh [375–378], where even standard electroweak processes such as W and Z production become dominated by low–x dynamics, and an accurate calculation of the Higgs production cross section requires accounting for BFKL resummation effects. Therefore, FPF measurements would provide a bridge between the physics program at the HL-LHC and that of an eventual higher-energy pp collider. On the top of that, they will provide improved predictions for DIS in key astroparticle physics processes, such as improving the extrapolations of the neutrino-nucleus cross section to ultra-high energies and the modeling of showers in cosmic ray interactions in the atmosphere.

By going more differential, e.g., by covering a wide rapidity range either by placing the FPF detectors at different radial distances from the beam collision axis or by making the FPF detectors work in coincidence with the ATLAS detector, the FPF may clarify the transition from collinear to BFKL factorization. Azimuthal-angle distributions, should they be accessible, may allow studies of transverse momentum dependence of production and decay, as well as enhanced searches for BSM signals. As multiple QCD phenomena would contribute at the FPF, disentangling them will strongly benefit from a coordinated program with other facilities, including forward production at LHCb, large-x CC DIS at the EIC [30], and small-x particle production at the HL-LHC and in future DIS experiments such as the MuIC [10] or LHeC [59].

Heavy-ion collisions at the HL-LHC will produce a large number of hadrons, creating a neutrino flux that can be observed at the FPF. These data could be used to study hadron propagation through nuclear matter or the quark-gluon plasma in different kinematic regimes. In addition, charm production in heavy-ion collisions may potentially probe nuclear PDFs for initial-state gluons and test gluon saturation, which is expected to be present at higher x compared to the proton case. For these studies to be feasible, the detection process of neutrino DIS on a nuclear target must be well understood. Again, this makes concurrent studies of CC DIS on heavy ions at the EIC highly beneficial for the success of the FPF program, see Sec. VI.4.3.

VI.4.2. Forward charm production

Forward charm production at the LHCb is an emerging process to probe the small-x gluon PDF [379–382]. Figure 16(a) illustrates the impact of the LHCb forward charm production data on the gluon PDF in the nucleon and lead at $x < 10^{-2}$ in the recent NNPDF analyses. [The figure does not include large theoretical uncertainties, which will be reduced in upcoming NNLO and resummation calculations.] The FPF measurements will probe this PDF at $x < 10^{-5}$, where the current uncertainty is even bigger, and the PDF is reconstructed by extrapolation from large x.

The large-x kinematic region is of interest due to the sensitivity of the FPF experiments to an intrinsic charm component of the proton [383]. The nonperturbative charm component, known as intrinsic charm, may arise due to long-distance interactions of the charm quark with one of the beam remnants. Intrinsic charm results in a characteristic enhancement of the charm PDF at $x > 0.1$, as illustrated in Fig. 16(b) on the example of the ratio of charm-to-light flavor PDFs as a function of x for $Q = 2$ GeV. While charm production in pp collisions is dominated by gluon-gluon scattering, in the presence of the intrinsic charm, the charm-gluon initial state enters and may even be dominant for forward D-meson production. Several studies have investigated the possible existence of this intrinsic charm, including measurements by LHCb [384–387]. FPF measurements would provide a complementary handle on intrinsic charm, which in turn could enhance the expected flux of prompt neutrinos arising from the decays of charm mesons produced in cosmic-ray collisions in the atmosphere [388–391]. These represent an important background for astrophysical neutrinos at neutrino telescopes such as IceCube [392] and KM3NeT [393]. See the Snowmass white paper on high-energy and ultra-high-energy neutrinos [394].
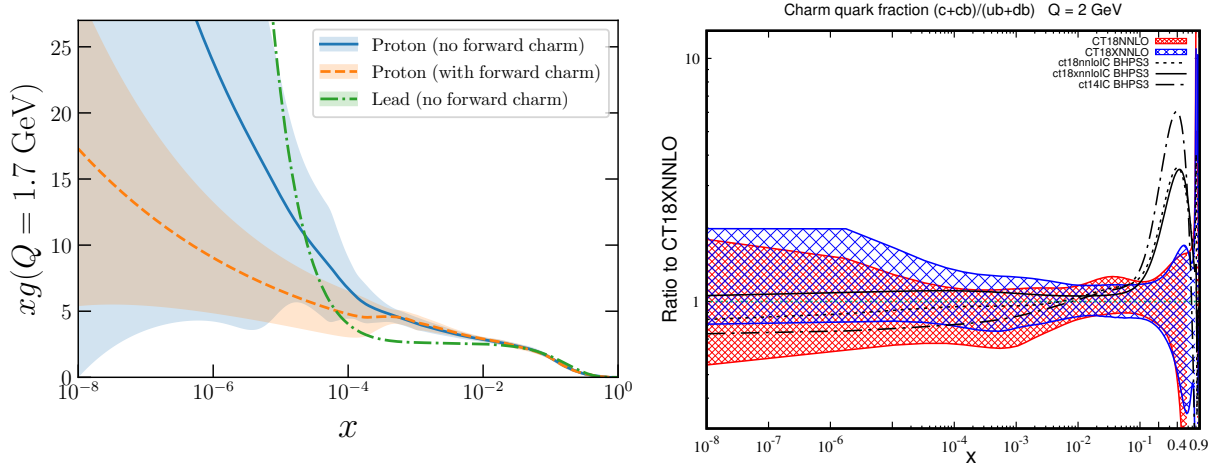
FIG. 16. (a) The small-x gluon PDF at $Q = 1.7$ GeV in the NNPDF3.1 proton fits without and with forward D meson data from LHCb, together with the lead nuclear PDF in the nNNPDF2.0 analysis. (b) The charm-quark fraction ratio $(c(x,Q) + \bar{c}(x,Q))/(\bar{u}(x,Q) + \bar{d}(x,Q))$ for $Q = 2$ GeV. The error bands represent the CT18 NNLO (red) and CT18X NNLO (blue) PDF uncertainties at 90% C.L. [78]. From Ref. [3].

VI.4.3. Neutrino-induced deep inelastic scattering

Among the various detectors proposed for the FPF, the principal detection modes will effectively realize an experiment on high-energy neutrino-induced deep-inelastic scattering (DIS), with event properties being reconstructed from the kinematics of the outgoing charged lepton and hadrons. The ability of neutrino DIS measurements to probe specific quark flavours via the weak current significantly improves global determinations of proton and nuclear PDFs [194]. Neutrino–induced CC DIS structure functions provide access to different quark flavour combinations compared to charged lepton DIS, and hence FPF data can complement other planned experiments such as the EIC. The FPF potential can be further enhanced by using a range of nuclear targets. The coverage for CC nuclear structure functions at the FPF broadly overlaps with that for NC charged-lepton expected at the EIC [30, 395]. Analogous information from previous neutrino-induced DIS measurements on nuclear targets, such as NuTeV [396], NOMAD [397], CCFR [398], and CHORUS [399], plays a prominent role in many global PDF fits of nucleon and nuclear PDFs (with the two related via nuclear corrections).

Inclusive CC DIS and especially semi-inclusive charm production in CC DIS are the primary channels to probe the PDFs for strange quarks and antiquarks. Strangeness PDFs offer insights about the nonperturbative proton structure [400], while they are also responsible for a large part of the PDF uncertainty in weak boson mass measurements at the LHC [303]. On the experimental side, determination of the (anti-)strangeness PDF has been a hot topic for the PDF community as the fits prefer somewhat different shapes for the strangeness PDFs [78, 301, 302, 401]. The elevated PDF uncertainty from fitting such inconsistent experiments propagates into various pQCD predictions (see e.g. those recently presented in Ref. [402]).

VI.5. Probing the multidimensional structure of hadrons

Extensions of collinear PDFs can be defined based on alternative factorization theorems to describe strong interactions in special kinematical regions. These include transverse-momentum-

dependent PDFs (TMDs) introduced in the context of TMD factorization (see e.g. [403]) and the related unintegrated PDFs (uPDFs) in the context of high-energy factorization at small momentum fraction x. The connection between the two has been investigated in several papers (see e.g. [24, 404, 405]). There is an extended literature on the theory and phenomenology of TMDs, for quarks and gluons, with or without polarization. Most recent global fits of quark TMDs [406–409] are based on data from semi-inclusive DIS, Drell-Yan, and Z-boson production processes. Studying these and other processes in the low-x and high-x regions opens a window on detailed behavior of QCD radiation.

Among the TMDs, the gluon unpolarized TMD correlator operator is the least known and has non-trivial spin dependence [410]. Besides the unpolarized gluon TMD, the counterpart distribution of linearly polarized gluons in an unpolarized nucleon, $h_1^{\perp g}$, gives rise to spin effects even in collisions of unpolarized hadrons [411–418]. Golden channels for the study and extraction of the gluon TMD and uPDF in hadron-hadron collisions correspond to the inclusive emission of a single particle over forward ranges of rapidity as well as over more central regions in gluon-induced hard scatterings [24, 419–422].

TMD factorization is violated at high orders in processes with multiple identified hadronic states [423]. These violations are likely more pronounced in forward regions and should be experimentally investigated for interpretation of various applications.

The gluon and quark GPDs characterize the three-dimensional nucleon structure in terms of longitudinal momentum fraction x and momentum transfer to the nucleon, t. The GPDs play an important role in many processes. For instance, the amplitude of onium hard diffractive production in the scaling limit is proportional to the gluon GPD. There are indications, based on HERA data, that the universality limit for J/ψ production is reached already for photoproduction, while in ρ production it is reached only at $Q^2 \gtrsim 15$ GeV^2 [424]. Investigation of universality of t dependence in Υ and J/ψ production, as well as of connections of GPDs to collinear PDFs [425, 426], would be insightful tests of the current GPD models.

Vector meson photoproduction in UPCs (see Ch. VIII) is also an effective way to measure GPDs in ions [427], with proof-of-principle measurements of these kinds already available [428]. Multi-dimensional distributions that go beyond TMDs – the so-called generalized transverse-momentum distributions (GTMDs) [429–431] – can be measured in forward processes, for instance exclusive double Drell–Yan [432], ultraperipheral pA collisions [433], and diffractive forward production of two quarkonia [434]. High-energy studies of TMD's, GPDs, and GTMDs complement the program of three-dimensional femtography at the EIC and JLab.

VII. HEAVY ION PHYSICS

The heavy-ion (HI) program at the LHC has been a successful and important part of the LHC physics program in Runs 1 and 2. The LHC experiments including ALICE, the dedicated detector focuses on HI physics, general purpose detectors CMS, ATLAS and LHCb, have been participated in the data-taking. Its chief aim was the identification and characterization of a Quark Gluon Plasma (QGP) in lead-lead (Pb-Pb) collisions. In addition to QGP studies, the program has included many advances in the understanding of the partonic nuclear structure, collectivity in small collision systems [435–439], and electromagnetic (EM) interactions [440, 441]. A detailed plan for the goals and expected measurements at the HL-LHC is presented in Ref. [442]. These are summarized below covering results on jet modification and heavy-flavor (HF) hadrons, primarily in Pb-Pb collisions, bulk particle collectivity in both Pb-Pb as well as smaller collision systems, nuclear parton density in proton-lead (p-Pb) and photonuclear collisions, and finally EM interactions from ultraperipheral Pb-Pb collisions. The latter topic is discussed in the next chapter.

The nominal expectations for the LHC Run 3 and Run 4 are for: 13 nb^{-1} of Pb-Pb collisions at $\sqrt{s_{\mathrm{NN}}} = 5.5$ TeV and 1.2 pb^{-1} of p-Pb collisions at $\sqrt{s_{\mathrm{NN}}} = 8.8$ TeV. In addition to the larger available luminosity, detector upgrades planned for both ATLAS and CMS experiments will benefit the HI program. In particular, the increased charged particle tracking pseudo-rapidity acceptance will be a boon to bulk particle measurements, the upgraded Zero Degree Calorimeters (ZDC) [443, 444] will improve triggering and identification for ultraperipheral collisions (UPC), and the addition of time-of-flight particle identification capability enabled by the MIP Timing Detector [445] will allow to differentiate among low momentum charged hadrons, such as pions, kaons, or protons, improving the HF measurements. The ALICE ITS3 upgrade that is planned for installation before Run 4 will significantly improve the heavy flavor meaurements down to very low transverse momentum. For data-taking in LHC Run 5, the ALICE collaboration planned a major upgrade of its detector referred to as ALICE 3 [446] which will enable an extensive program to fully exploit the LHC for the study of the properties of the QGP.

At RHIC, the construction of sPHENIX detector [447], equipped with calorimeters as well as high precision inner trackers, will be finished and start the heavy-ion data-taking in 2023. The electromagnetic and hadron calorimeter will enable full jet analyses in pp and heavy ion collisions at RHIC energies for the first time. Together with the high precision tracking systems, the collaboration aims to provide high precision heavy flavor meson and quarkonium data in Au-Au collisions.

VII.1.   Jet Quenching

High momentum-transfer interactions between partons in the nuclei produce hard probes of the QGP. One can study the impact of QGP on color charges with fast-moving partons. In QGP, medium-induced gluon radiations and elastic scatterings could transfer the parton energy to a large angle from the original mother parton momentum vector. The partons inside the jets could excite a QGP wake. The effect of QGP on color charges can therefore be observed as the attenuation of the jets [448–461], and the modification of their substructure [462–474], often referred to as jet quenching.

The large data samples and the improved jet reconstruction due to the upgrade of the tracking system of the CMS and ATLAS detectors will provide significantly reduced statistical and systematic uncertainties for key measurements of medium modification of light (heavy) quark jets using photon/Z (D^0-meson) tagged samples [475, 476]. Moreover, the sPHENIX detector with large acceptance calorimeters [477] will enable the high precision full jet measurements for the first time at RHIC. Since electroweak bosons don't participate in the strong interaction, by measuring the jets tagged against recoiling isolated photons or Z bosons, one can access the energy loss of a parton by using the boson energy as the reference for that of the parton before quenching. In particular, the jet fragmentation functions and the jet shapes will be measured precisely for high-z region where the difference between pp and Pb-Pb collisions is not resolved yet [475, 476], as shown in Fig. 17a, thus providing information on the medium-modified structure of quark-initiated jets. The azimuth and transverse momentum correlations between bosons and jets, measured in γ+jets and Z+jets events presented in Fig. 17b, are valuable observables to study parton energy loss in the QGP [475]. By comparing the LHC and RHIC data, we aim to constrain the temperature dependence of the transport coefficients of QGP.

Another significant improvement expected at the HL-LHC is the measurement of radial distribution of D^0 mesons in jets [475]. By studying the modification of this observable in Pb-Pb compared to pp, one can gain insights into the dynamics of heavy quarks in the QGP. In addition, the large low-PU pp data samples at $\sqrt{s} =14$ TeV can be a great opportunity for precision measurements of

the system-size dependence of the jet quenching phenomena. In this regard, high multiplicity pp events provide the reference results in small systems, thus completing the system-size dependence of the jet quenching phenomena.
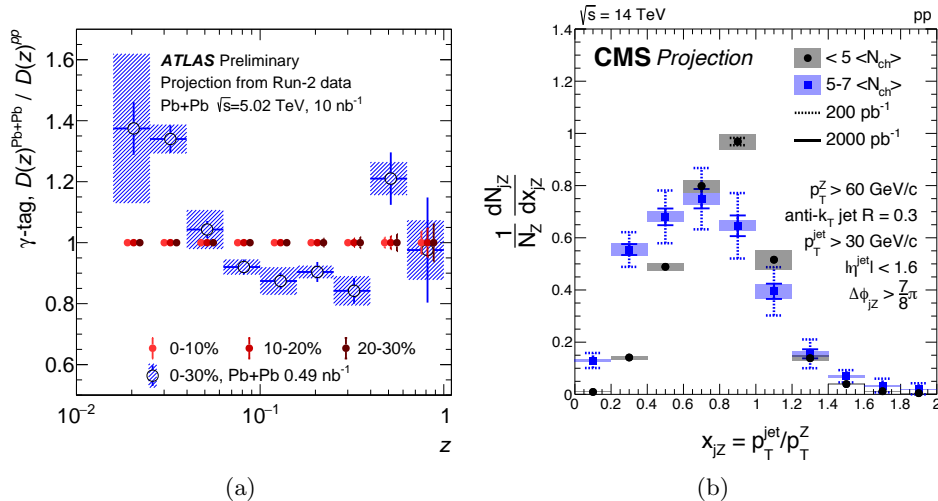

FIG. 17. (a) The statistical precision of the ratio of jet fragmentation functions in Pb–Pb and pp collisions at $\sqrt{s_{NN}} = 5.02$ TeV in ATLAS for jets recoiling from a photon [476]. The error bars at unity for $0-10\%$, $10-20\%$, and $20-30\%$ centrality classes show the expected statistical uncertainties at the HL-LHC. (b) Prospects of Z boson-jet transverse momentum balance distribution in low pileup pp collisions at $\sqrt{s} = 14$ TeV in CMS [475].

VII.2. Heavy Quarks

Heavy quarks provide a unique opportunity to probe the QGP with slow-moving probes. Charm and beauty quarks, as a consequence of their large masses ($m_{c,b} > \lambda_{QCD}$), are mostly produced during the early stages of the collision in hard scattering processes. As HF quarks propagate through the medium, they are expected to lose less energy than light flavor through radiation due to the dead-cone effect, i.e., the suppression of small-angle gluon radiation induced by the lower heavy quark velocity at the same kinetic energy as light quarks. These interactions may lead to the thermalization of low-momentum HF quarks, which would then take part in the expansion and hadronization of the medium. In addition, HF mesons, such as quarkonia, can be dissociated in the medium due to Debye color screening or recombined from individual heavy quarks and anti-quarks diffusing through the medium [478–480]. Therefore, the measurement of HF hadrons can provide crucial information on the full evolution of the system and allows us to get information on the quark-mass dependence of the medium-induced radiations.

The larger experimental data samples at the HL-LHC, combined with improved detector performance and measurement techniques, will allow the ALICE, CMS, and ATLAS experiments to significantly improve over the current HF hadron [481–489], and quarkonia [490–497] measurements. The new ALICE ITS2 inner tracking system will give ALICE greatly improved capabilities for charm and bottom [498]. Looking further ahead, the ALICE ITS3, planned for installation before the start of Run 4 will push this even further [499]. Those upgrade projects aim to measure charm hadrons down to $p_T = 0$. The p_T dependence of the quarkonium nuclear modification factor (R_{AA}) will be measured with high precision up to about 80 GeV for prompt J/ψ and 50 GeV for $\Upsilon(1S)$ [500] (compared to 50 and 30 GeV respectively, with the present data), allowing to discern

whether quarkonium formation at high p_T is determined by the Debye screening mechanism, or by energy loss of the heavy quark or the quarkonium in the medium. The elliptic flow measurements of charm mesons in p-Pb collisions [501] and of HF decay muons [502] and $\Upsilon(1S)$ mesons [500] in Pb-Pb collisions will be significantly improved as observed in Fig. 18, providing insights on the collective expansion and degree of thermalization of HF quarks in the medium at low p_T, and on the presence of recombination of bottomonia from deconfined beauty quarks in the QGP. The production of strange B mesons and charm baryons in pp and Pb-Pb collisions [500] will also be measured with sufficient precision to further investigate the interplay between the predicted enhancement of strange quark production and the quenching mechanism of beauty quarks, and the contribution of recombination of HF quarks with lighter quarks to the hadronization process in HI collisions. Finally, the precise measurements of beauty mesons in p-Pb collisions [500] will help to elucidate the relative contribution of hadronization and nuclear-matter effects (e.g. nuclear PDF, gluon saturation, and coherent energy loss), as well as serve as a baseline for the understanding of beauty-quark energy loss in Pb-Pb collisions.

At RHIC, the sPHENIX detector with enhanced capability for the studies of heavy flavor mesons and baryons could provide high precision data at lower collision energy. Together with data from HL-LHC, the measurements of HF hadron spectra, HF particle ratio, and azimuthal anisotropy will provide strong constraints on the heavy quark diffusion coefficient and its temperature dependence.
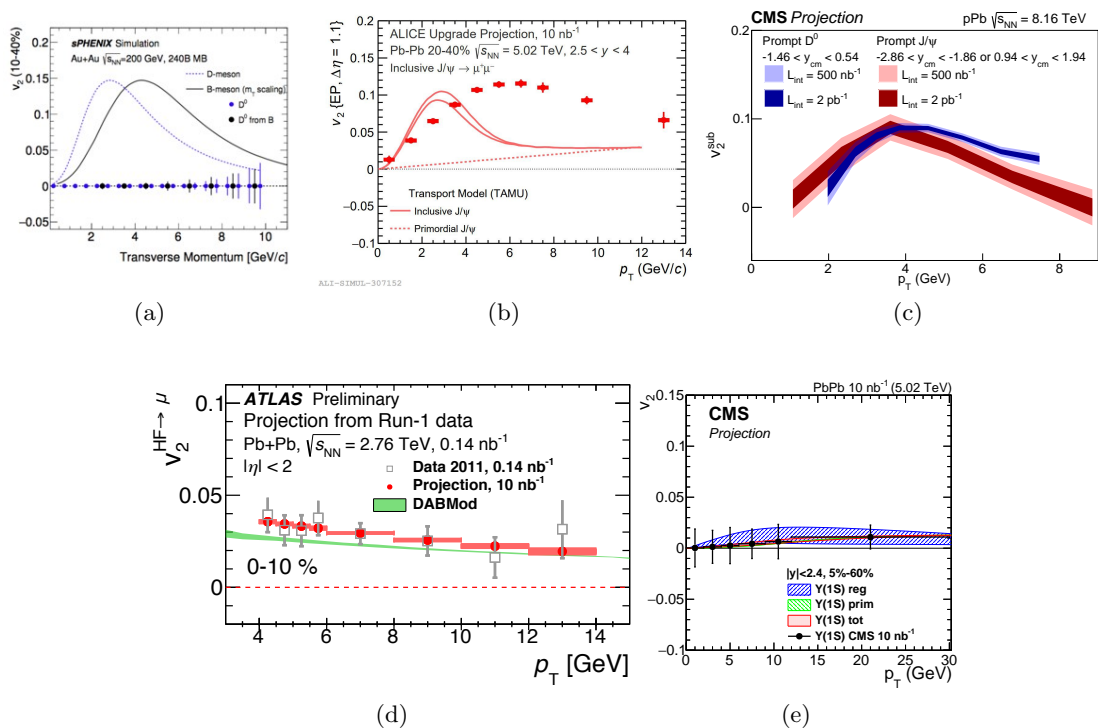

FIG. 18. Elliptic flow projections as a function of p_T of: (a) sPHENIX performance on D and B mesons at $\sqrt{s_{NN}} = 0.2$ TeV (b) J/ψ mesons in ALICE in Pb-Pb collisions at $\sqrt{s_{NN}} = 5.02$ TeV (c) prompt D and J/ψ mesons in CMS in high-multiplicity p-Pb collisions at $\sqrt{s_{NN}} = 8.16$ TeV [501], (d) HF decay muons in ATLAS in Pb-Pb collisions at $\sqrt{s_{NN}} = 2.76$ TeV [502] and (e) $\Upsilon(1S)$ mesons in CMS in Pb-Pb collisions at $\sqrt{s_{NN}} = 5.02$ TeV [500].

VII.3.   Hadronization and Exotic Hadrons

Insight into the hadronization process in QGP is provided by the comparison of the p_T distributions of various hadrons in Pb+Pb collision and in pp collisions. In particular, mechanisms such as recombination, involving soft partons close in phase space, could be important for the description of hadron production in high-density environments.

The abundant production of light nuclei and antinuclei measured by ALICE can be greatly improved in HL-LHC. In analogy with the case of light nuclei and of charmonium, the statistical hadronization or coalescence ansatz can be used to gain unique insight into the structure (e.g. tetraquark or molecular state) of exotic hadrons, such as the $X(3872)$ studied by LHCb in high-multiplicity pp collisions [503] and by CMS in Pb+Pb collisions [504]. Those initial measurements will be followed up with the high statistics data in LHC Run 3 and 4.

In LHC Run 5, the ALICE 3 detector would provide high precision measurement of multi-charm baryons, expanding the studies of hadronization performed in Run 3 and 4. ALICE 3 would also be the perfect tool for the study of the formation of light nuclei, hyper-nuclei, super-nuclei, and the experimental investigation of exotic states such as $X(3872)$ and the newly discovered T_{cc}^+.

VII.4.   Particle collectivity in small and large systems

With the large minimum bias samples of pp, pPb, and PbPb datasets of HL-LHC, it will be possible to reach an unprecedented experimental precision that will help us to understand the collectivity of small and large systems. The pivotal upgrades of trackers in CMS and ATLAS will enable the measurement of charged particles in the wide pseudo-rapidity range ($|\eta| < 4$). In small systems, a significant statistical improvement is expected for the elaborate flow variables. In particular, the symmetric cumulant observables, $\mathrm{SC}(m,n)$ which are the correlations between Fourier coefficients based on 4-particle correlations will be assessed [505]. Since those are very sensitive to the initial state and its fluctuation, precision measurements of them will constrain the current interpretation of the ridge phenomenon in small systems [438, 506–508], as well as catching hold of non-flow effects in early stages [501]. In addition, we expect a crucial improvement in our understanding of the system size of collisions by measuring the Hanbury Brown and Twiss (HBT) radii in small systems [502]. With azimuthally sensitive femtoscopy, the spatial ellipticity of the medium at freeze-out can be measured. In particular, the HL-LHC p-Pb data will allow us to unambiguously investigate the normalized second-order Fourier component of the transverse HBT radius as a function of the magnitude of flow. In Pb-Pb collisions, an interesting observable which can be highly enriched by HL-LHC data is the flow decorrelation [509]. The extended η acceptance in Run 4 will lead to significant improvement in characterizing the rapidity dependence of the factorization breaking. A significant improvement of the forward-backward multiplicity correlation and multi-particle cumulants will bring a better understanding of the fluctuations of the medium in early stages [502].

VIII.   PHOTONUCLEAR AND PHOTON-PHOTON INTERACTIONS AT COLLIDERS

Ultraperipheral ion collisions (UPCs) are electromagnetic interactions of relativistic heavy ions. They occur when the nuclei pass by with impact parameter $b > 2R_A$, where R_A is the nuclear radius [510, 511]. These photon fields may interact with the opposing nucleus, in a photonuclear interaction, or with each other, in a $\gamma\gamma$ collision. At a lepton-lepton collider, hadroproduction in photon-photon fusion offers complementary ways to study QCD dynamics. Photonuclear interactions at the LHC (Sec. VIII.1) can probe target nuclei down to very small x values, $x \lesssim 10^{-6}$. Meanwhile,

photon-photon collisions both at the (HL-)LHC (Sec. VIII.2) or an e^+e^- collider (Sec. VIII.3) can probe high-energy QCD resummations, diffractive interactions, and BSM phenomena.

In the UPCs, the strongly Lorentz-contracted electromagnetic fields of relativistic nuclei act as nearly-real photon fields that extend up to high energies. The maximum photon energy is $\gamma\hbar c/b$, where b is the transverse distance from the interaction point to the center of the emitting nucleus. The LHC can reach γA center-of-mass energies up to 1.5 and 5.4 TeV for proton and lead targets, respectively [512]. For $\gamma\gamma$ interactions, the maximum collision energies are 170 GeV and 4.2 TeV in Pb-Pb and pp collisions, respectively.

These opportunities were recognized early [513], and all four LHC experiments have studied UPCs, along with STAR and PHENIX at RHIC. There are extensive plans for UPC studies at the LHC during Runs 3 and 4 [514]. These studies will benefit from the extensive detector upgrades that were implemented during the second long shutdown, such a new streaming DAQ readout in ALICE, which will remove a bottleneck when triggering on low-multiplicity UPC events [515].

VIII.1. Photonuclear interactions

Photonuclear collisions are an effective tool for the study of the nuclear structure, and several collision observables may be used to constrain the nPDF (similar to the p-Pb studies discussed in Section III.2). So far, most UPC studies of photonuclear interactions have involved vector mesons, which are experimentally very clean, but are subject to significant theoretical uncertainty [516]. These uncertainties can be alleviated by going beyond the NLO perturbative approximation that is currently used e.g. in [212], or by taking the ratio of the cross-sections on proton and ion targets to measure shadowing.

The HL-LHC will allow ALICE and CMS to extend such measurements to the $\psi(2S)$ and potentially the $\Upsilon(1S)$ meson [203]. They will also allow for a substantially expanded set of measurements, including photoproduction of dijets (already pursued by ATLAS [213]) and of open charm, likely bottom and possibly even top quark pairs [514, 517–521]. As was discussed in Sec. VI.5, in the limit of high virtualities, exclusive photoproduction of vector mesons provides direct information about the transverse distribution of partons for a given x. In the scaling limit, the transverse spread is given by a Fourier transform of photoproduction amplitude $A(x,t)$, which should exhibit universal t dependence. Testing this universality with data will be informative.

Inelastic hard diffraction at small t provides a unique information on fluctuations of the gluon field. The ratio of differential cross sections for incoherent and coherent onium production at $t = 0$ reflects event-by-event fluctuations of the square of the gluon density [522], while at $t > 0$, competition between the fluctuations and parton knockouts takes place [424, 427].

Production of multiple vector mesons in UPCs can be also studied, as illustrated in Fig. 19 showing projections for the nuclear correction in PbPb scattering at ALICE and CMS, including expected uncertainties. For estimated rates for vector meson production in the different LHC experiments during Run 3 and Run 4, refer to [514].

VIII.2. Photon-photon scattering

This section considers ultraperipheral events in pp scattering at the LHC, during which the protons remain intact and are measured in special units called roman pots. In these photon-exchange events, quasi-real photons are emitted by the incoming interacting protons. Both the ATLAS and CMS-TOTEM collaborations have installed roman pot detectors at about 220 meters from the interaction points, the so-called ATLAS Forward Proton (AFP) and CMS-TOTEM Precision Proton Spectrometer (PPS). In standard runs at high luminosity, the ATLAS or CMS detectors with intact
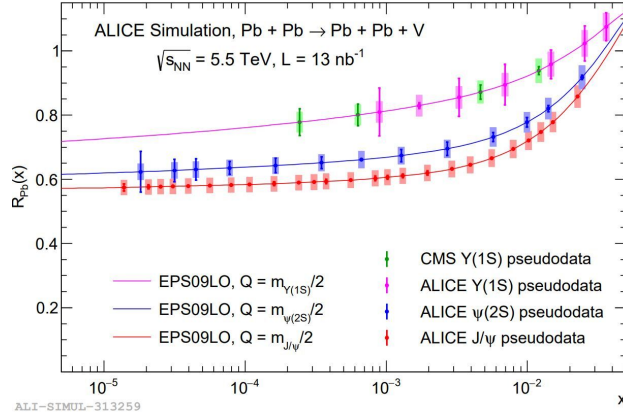
FIG. 19. Pseudodata projections for nuclear suppression factor by ALICE and CMS measured with the photoproduction of three heavy vector mesons in PbPb UPCs are shown. From Ref. [514].

protons tagged in the roman pots can detect final states with typical invariant mass 400-2300 GeV, enabling sensitivity to a wide range of new physics effects. The events are especially clean. As an example, one may observe exclusive pairs of photons or W bosons in the central region. In the same way, one can look for exclusive production of ZZ, γZ, $t\bar{t}$ events via photon induced processes. The UPCs will be also sensitive to a variety of BSM scenarios, such as those that contain loops of virtual heavy particles coupling to photons that introduce an effective photon quartic compling ζ_1 at a low energy [523, 524].

VIII.2.1. *Photon-photon collisions at the LHC without tagging intact protons*

The ATLAS and CMS measurements of exclusive dimuons from $\gamma\gamma \rightarrow \mu^+\mu^-$ will reach a precision that can be used to calibrate the photon flux and reduce the uncertainty on the nuclear charge distribution [525]. The rare light-by-light (LbyL) scattering process [526], measured by both ATLAS and CMS, is statistics limited and will greatly benefit from the increased luminosity as well as improvements in triggering capabilities [525]. Of particular note is the search for BSM axion-like particles, which may be detectable via $\gamma\gamma \rightarrow a \rightarrow \gamma\gamma$ [527], and where LbyL interactions from Pb-Pb measured by both ATLAS and CMS already set the most stringent limits for axion masses between $\sim 5-100$ GeV and will improve with the new data as shown in Fig. 20 where we show the sensitivities in pp, p-Pb, Pb-Pb and Ar-Ar collisions. We clearly see the complementarity between heavy ion and proton collisions. Fig. 20, left, does not assume the tagging of intact protons whereas Fig. 20, right, does, as described in the next section. These analyses will benefit from upgrades to forward detectors, see for example [528] and [529].

The $\gamma\gamma \rightarrow WW$ process is unique because it occurs at leading-order only via electroweak gauge boson couplings, and is thus an ideal probe for searching for new physics via anomalous gauge boson couplings [535–537]. The rare electroweak process $\gamma\gamma \rightarrow W^\pm W^\mp \rightarrow e^\pm \nu_e \mu^\mp \nu_\mu$ was first observed (rejecting the background-only hypothesis with a significance of 8.4σ) in proton-proton collisions at the LHC by the ATLAS Collaboration in 2020 using 139 fb^{-1} of data collected in Run 2 [538]. The increased luminosity at the HL-LHC will allow differential measurements and a large improvement in the statistical precision of this measurement, provided pile-up mitigation and track reconstruction challenges are addressed. The impact of the HL-LHC environment and planned ATLAS detector upgrade is studied in [539].

An example is given in Figs. 21a and 21b for a differential measurement in the dilepton invariant
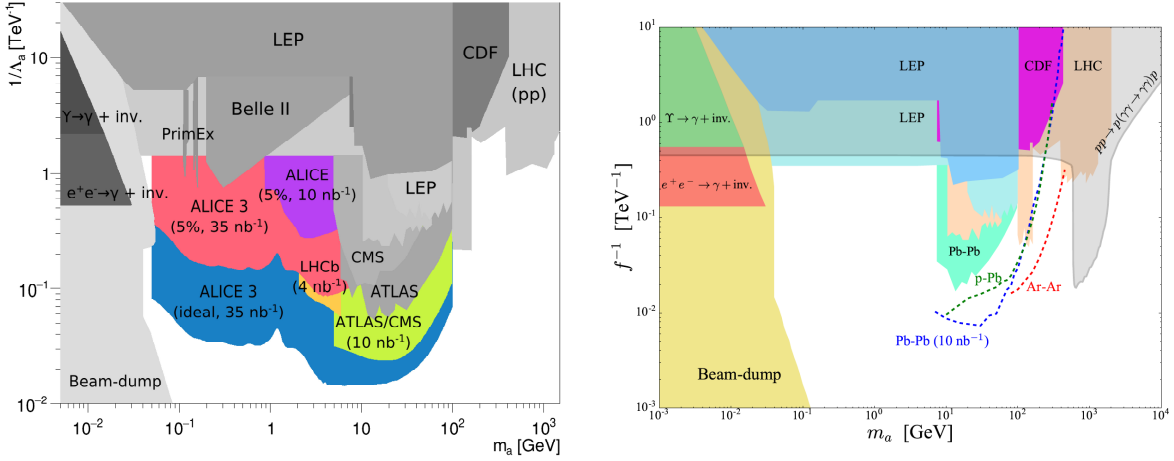
FIG. 20. Left: Compilation of exclusion ALPs sensitivities obtained by different studies [20, 442, 530]. In light green, the ATLAS $\gamma\gamma \to \gamma\gamma$ from 10 nb^{-1} limit at $\sqrt{s_{\mathrm{NN}}} = 5.52$ TeV is presented. The ATLAS $\gamma\gamma \to \gamma\gamma$ represents the exclusion limit derived from the LbyL cross section measured in Pb-Pb collisions by ATLAS [525], the CMS $\gamma\gamma \to \gamma\gamma$ limit comes from the recent analysis described in Ref. [531] and the projected performance with ALICE 3 detector [532]. Right: Sensitivity predictions on ALPs using pp, p-Pb, Pb-Pb and Ar-Ar interactions at the LHC [533, 534].

mass, $m_{\ell\ell}$, with the aim to probe the sensitivity in the high-$m_{\ell\ell}$ region most sensitive to dimension-8 EFT operators [537]. Figure 21a shows the expected signal and background yields at the HL-LHC stacked and as a function of $m_{\ell\ell}$, illustrating the improvements at high dilepton mass compared to the Run 2 analysis. Figure 21b compares the main sources of the uncertainty for the HL-LHC and the Run 2 analyses. While the Run 2 analysis is mainly limited by statistical uncertainties, the background systematic uncertainty will be dominant for most of the dilepton mass spectrum at the HL-LHC. It demonstrates the impact of the background modeling uncertainty by considering a reduction in this uncertainty by a factor of 2 and 4 compared to the Run 2 relative uncertainties.

VIII.2.2. Photon-photon collisions at the LHC with proton tagging

Turning now to photon-induced processes at ATLAS and CMS-TOTEM in which scattered protons are detected intact in the roman pots, we will first concentrate on diphoton exclusive production as an example. The conclusions can be generalized to exclusive WW, ZZ, γZ, and $t\bar{t}$ production via photon exchanges. Diphotons can be produced exclusively either via QCD or QED processes, with the cross sections as a function of a diphoton mass available in [537, 540–542]. Observing two photons in ATLAS/CMS and two tagged protons means a photon-induced process, with the acceptance of the roman pot detectors starting at about 400 GeV.

The number of exclusive diphoton production events for a luminosity of 300 fb^{-1} at the LHC is shown in Fig 22. SM exclusive diphotons (red dashed dotted line) and exclusive dileptons with leptons misidentified as photons (blue dotted line) can be neglected. The only background that matters is shown in red dashed lines and corresponds to inclusive diphoton production that coincides with detection of intact protons from the pileup. The BSM signal (black lines) is shown for an effective photon quartic complings ζ_1 of order 10^{-12} and 10^{-13} GeV^{-4} that are common in BSM models [523, 524].

Measuring intact protons is crucial for suppressing the pileup and other background. The method matches the kinematical information, as measured by the two photons, with the one using
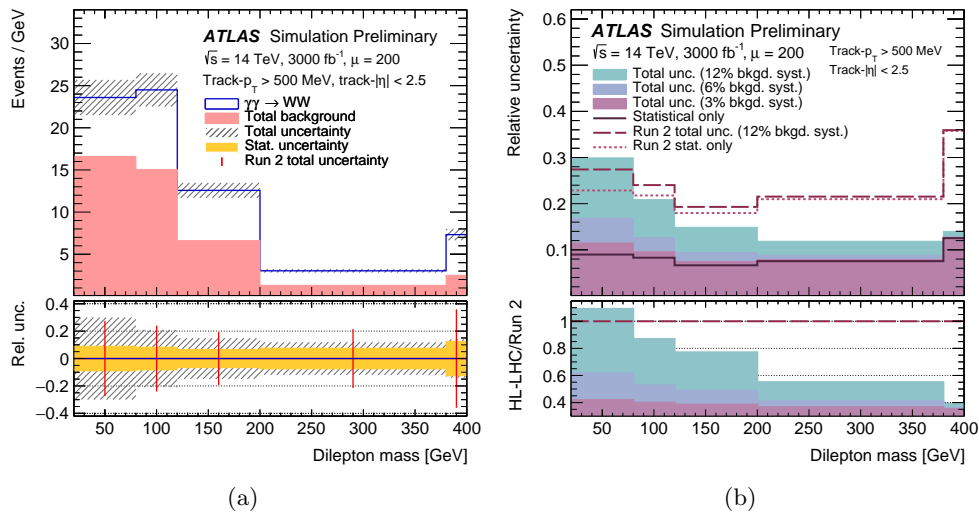
FIG. 21. (a) The expected signal and background yields at the HL-LHC shown stacked and as a function of the dilepton mass, with the relative statistical and total uncertainty on the signal shown in the bottom panel assuming the same background systematic as in Run 2 of 12%. (b) A comparison of the total uncertainty when considering a reduction in the nominal background systematic by a factor of 2 and 4 and compared to the Run 2 relative uncertainties, with the ratio of the total relative uncertainty on the signal yield at the HL-LHC as a ratio to the Run 2 uncertainty shown in the bottom panel. The average pileup in Run 2 was $\langle\mu\rangle=33.7$. [539]

the two protons. The results are shown in Fig. 23 for the mass ratio (left) and the rapidity separation (right) between the pp and $\gamma\gamma$ systems. With these exclusivity cuts, one can reduce the background from 80.2 to less than 0.1 events for 300 fb^{-1}, lifting the sensitivity to ζ_1 to a few 10^{-15} GeV^{-4} – better by more than two orders of magnitude compared to "standard" methods [537, 540–542]. This is now becoming a reality, with both CMS-TOTEM and ATLAS reporting observations of QED exclusive dilepton production, and CMS-TOTEM reporting the first limits on ζ_1 with about 9.4 fb^{-1} of data.

This method can be applied directly to search for axion-like particles (ALPs). For example, if an ALP interacts with the photons, the exclusive $pp \to p(\gamma\gamma \to \gamma\gamma)p$ process at the LHC with 300 fb^{-1} significantly extends the reach of the ALPs search at masses of order 1-2.3 TeV, see the sensitivity plot (coupling vs mass) in Fig. 20, right [533, 534]. In the 1 TeV ALP mass range, about two orders of sensitivity are gained by tagging on the protons, as compared to the standard methods. This is complementary with the strong sensitivity of Pb-Pb runs in the region of lower masses in Fig. 20, $\sim 10 - 500$ GeV, where the cross section for Pb-Pb runs is enhanced by the fourth power of the large nucleus charge [20, 527].

In addition to $\gamma\gamma$ final states, tagged $Z\gamma$ and WW states can be also observed. In $Z\gamma$ production, both leptonic and hadronic decays can be studied using the same kinematic techniques as above, which may achieve sensitivities to the $\gamma\gamma\gamma Z$ anomalous coupling up to 10^{-13} GeV^{-4}, better by three orders of magnitude [543] than with the standard untagged method based on the $Z \to \gamma\gamma\gamma$ decay.

In the WW exclusive channel, quartic $\gamma\gamma WW$ anomalous couplings can be tested [544]. Figure 24 shows that the SM and anomalous (BSM) contributions can be observed at low and high invariant masses of WW pair, respectively. The best sensitivity to the SM exclusive WW production originates from the leptonic decays of the Ws, with fast timing detectors desirable to suppress the neutrino background. One strategy to assess the $\gamma\gamma WW$ quartic anomalous couplings is to
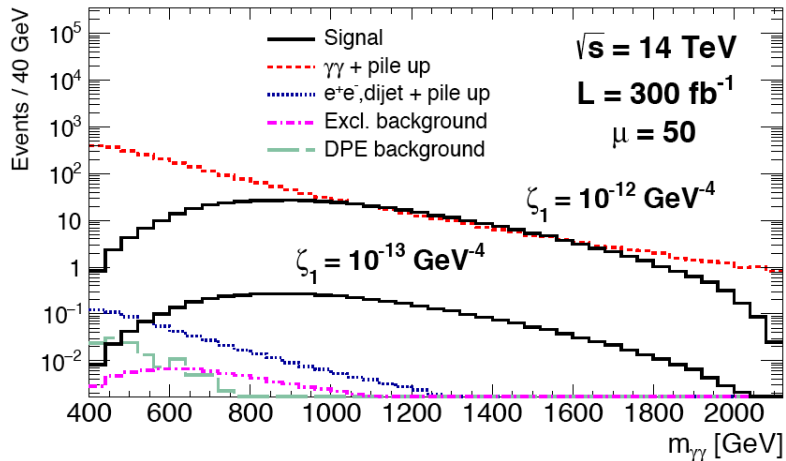
FIG. 22. Number of events as a function of the diphoton mass for signal and background for exclusive $\gamma\gamma$ production.
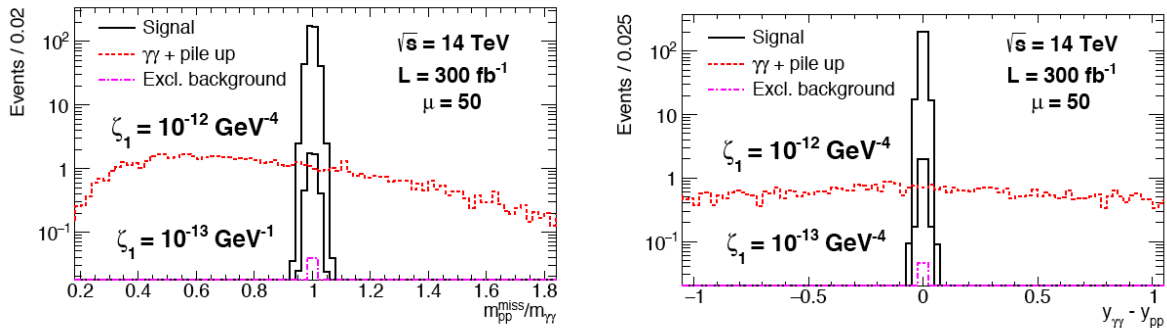

FIG. 23. Mass ratio and rapidity difference between the pp and $\gamma\gamma$ information for signal (in full line) and pile up background (dashed line).

look for hadronic decays of W bosons at large m_{WW}, even if the dijet background is quite high. Advanced jet variables such as subjettiness can help to reject the dijet background.

Following the same ideas, one can also look for exclusive production of ZZ and $t\bar{t}$ [545], as it was recently performed by the CMS and TOTEM collaborations.

VIII.3. Photon-photon scattering at e^+e^- colliders

An e^+e^- collider can function as a photon-photon collider when the two initial-state leptons are detected at small angles to the beam pipe. Since the virtual photons scatter as small transverse-size objects with no hadronic activity in the initial state, they offer interesting opportunities to test QCD in the Regge regime. In this $\gamma^*\gamma^*$ reaction, a future measurement combined with the available LEP2 data would constrain the growth of the total cross section with energy that is predicted by BFKL theory [546–551]. Diffractive production of two vector mesons (V), $\gamma^*\gamma^* \to VV$, can test NLA predictions for ρ [552–554] and J/ψ [555] mesons. Also, heavy-quark pair production can be observed [25, 556]. The BFKL resummation – an important formalism of QCD theory described in Sec. VI.1 – has been difficult to confirm in hadronic collisions. In $\gamma^*\gamma^*$ scattering, dependence on the initial photons' virtualities gives an additional powerful lever.
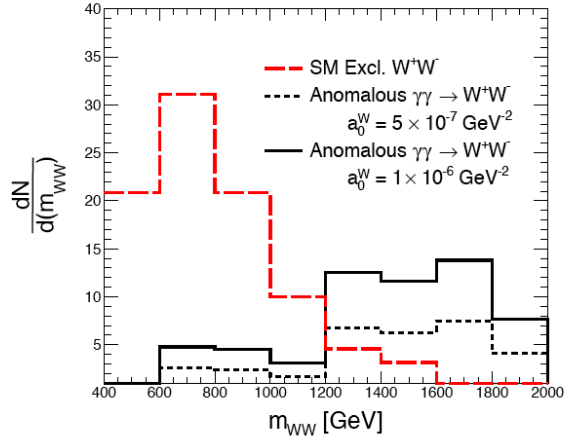
FIG. 24. *WW* mass distribution for exclusive *WW* production (SM is red dashed line and anomalous couplings in full ball line).

IX. PERTURBATIVE PRECISION CALCULATIONS FOR EXPERIMENTS

Perturbative precision calculations are crucial for measurements of SM parameters and a key ingredient for the reliable estimation of SM backgrounds to new physics searches [557]. They also serve as an input to precision simulations in modern MC event generators for collider physics.

IX.1. Fixed-order techniques

There has been significant recent progress in the computation of QCD radiative corrections [191, 558–560]. Several groups have used different approaches to achieve the first $2 \to 3$ NNLO calculations of hadron collider process. There have also been significant steps forward in the development of improved infrared subtraction schemes including methods to deal with higher-multiplicity processes at NNLO. There has also been remarkable progress in the area of differential N³LO calculations, with first results obtained for $2 \to 1$ benchmark processes. A summary of the state of the art and targets for future measurements is shown in Tab. IV. This Les Houches precision wishlist has served as a summary and repository for the higher-order QCD and EW calculations relevant for high-energy colliders, providing a crucial link between theory and experiment.

Computing fixed-order amplitudes for scattering processes remains one of the key challenges and obstacles to producing precise predictions for the LHC. Broadly speaking, one can divide the computation into two categories: Obtaining and reducing the amplitudes, and calculating the integrals which appear. A thorough review of recent formal developments can be found in [561]. The standard approach is the *projector method*, where the amplitude is expressed as a linear combination of all potential D-dimensional tensor structures each multiplied by a scalar coefficient containing scalar integrals. For on-shell/physical processes, one can restrict the space-time dimension of the external particles to $D = 4$ and directly construct projectors for individual helicity amplitudes [562–564]. The integrals are related through integration-by-parts identities (IBPs) [565, 566] and Lorentz-invariance identities (LIs) [567]. Redundancies can be eliminated using the Laporta algorithm [568], leading to a set of *master integrals*, the evaluation of which is one of the biggest obstacles in obtaining multi-loop/multi-leg amplitudes. A useful technique for avoiding the intermediate expression swell in the reduction to master integrals is the use of *finite fields*, typically integers modulo some prime number [569–571]. A modern introduction to various techniques for

TABLE IV. Summary of the LesHouches precision wishlist for hadron colliders [558]. HTL stands for calculations in heavy top limit, VBF* stands for structure function approximation.

process	known	desired
$pp \to H$	N^3LO_{HTL}, $NNLO^{(t)}_{QCD}$, $N^{(1,1)}LO^{(HTL)}_{QCD\otimes EW}$	N^4LO_{HTL} (incl.), $NNLO^{(b,c)}_{QCD}$
$pp \to H + j$	$NNLO_{HTL}$, NLO_{QCD}, $N^{(1,1)}LO_{QCD\otimes EW}$	$NNLO_{HTL} \otimes NLO_{QCD} + NLO_{EW}$
$pp \to H + 2j$	$NLO_{HTL} \otimes LO_{QCD}$ $N^3LO^{(VBF^*)}_{QCD}$ (incl.), $NNLO^{(VBF^*)}_{QCD}$, $NLO^{(VBF)}_{EW}$	$NNLO_{HTL} \otimes NLO_{QCD} + NLO_{EW}$, $NNLO^{(VBF)}_{QCD}$
$pp \to H + 3j$	NLO_{HTL}, $NLO^{(VBF)}_{QCD}$	$NLO_{QCD} + NLO_{EW}$
$pp \to VH$	$NNLO_{QCD} + NLO_{EW}$, $NLO^{(t,b)}_{gg\to HZ}$	
$pp \to VH + j$	$NNLO_{QCD}$	$NNLO_{QCD} + NLO_{EW}$
$pp \to HH$	$N^3LO_{HTL} \otimes NLO_{QCD}$	NLO_{EW}
$pp \to HHH$	$NNLO_{HTL}$	
$pp \to H + t\bar{t}$	$NLO_{QCD} + NLO_{EW}$, $NNLO_{QCD}$ (off-diag.)	$NNLO_{QCD}$
$pp \to H + t/\bar{t}$	NLO_{QCD}	$NNLO_{QCD}$, $NLO_{QCD} + NLO_{EW}$
$pp \to V$	N^3LO_{QCD}, $N^{(1,1)}LO_{QCD\otimes EW}$, NLO_{EW}	$N^3LO_{QCD} + N^{(1,1)}LO_{QCD\otimes EW}$, N^2LO_{EW}
$pp \to VV'$	$NNLO_{QCD} + NLO_{EW}$, $+NLO_{QCD}$ (gg)	NLO_{QCD} $(gg$,massive loops)
$pp \to V + j$	$NNLO_{QCD} + NLO_{EW}$	hadronic decays
$pp \to V + 2j$	$NLO_{QCD} + NLO_{EW}$, NLO_{EW}	$NNLO_{QCD}$
$pp \to V + b\bar{b}$	NLO_{QCD}	$NNLO_{QCD} + NLO_{EW}$
$pp \to VV' + 1j$	$NLO_{QCD} + NLO_{EW}$	$NNLO_{QCD}$
$pp \to VV' + 2j$	NLO_{QCD} (QCD), $NLO_{QCD} + NLO_{EW}$ (EW)	Full $NLO_{QCD} + NLO_{EW}$
$pp \to W^+W^+ + 2j$	Full $NLO_{QCD} + NLO_{EW}$	
$pp \to W^+W^- + 2j$	$NLO_{QCD} + NLO_{EW}$ (EW component)	
$pp \to W^+Z + 2j$	$NLO_{QCD} + NLO_{EW}$ (EW component)	
$pp \to ZZ + 2j$	Full $NLO_{QCD} + NLO_{EW}$	
$pp \to VV'V''$	NLO_{QCD}, NLO_{EW} (w/o decays)	$NLO_{QCD} + NLO_{EW}$
$pp \to W^\pm W^+ W^-$	$NLO_{QCD} + NLO_{EW}$	
$pp \to \gamma\gamma$	$NNLO_{QCD} + NLO_{EW}$	N^3LO_{QCD}
$pp \to \gamma + j$	$NNLO_{QCD} + NLO_{EW}$	N^3LO_{QCD}
$pp \to \gamma\gamma + j$	$NNLO_{QCD} + NLO_{EW}$, $+NLO_{QCD}$ $(gg$ channel)	
$pp \to \gamma\gamma\gamma$	$NNLO_{QCD}$	$NNLO_{QCD} + NLO_{EW}$
$pp \to 2\,\text{jets}$	$NNLO_{QCD}$, $NLO_{QCD} + NLO_{EW}$	$N^3LO_{QCD} + NLO_{EW}$
$pp \to 3\,\text{jets}$	$NNLO_{QCD} + NLO_{EW}$	
$pp \to t\bar{t}$	$NNLO_{QCD}$ (w/ decays)+ NLO_{EW} (w/o decays) $NLO_{QCD} + NLO_{EW}$ (w/ decays, off-shell) $NNLO_{QCD}$	N^3LO_{QCD}
$pp \to t\bar{t} + j$	NLO_{QCD} (w/ decays, off-shell) NLO_{EW} (w/o decays)	$NNLO_{QCD} + NLO_{EW}$ (w/ decays)
$pp \to t\bar{t} + 2j$	NLO_{QCD} (w/o decays)	$NLO_{QCD} + NLO_{EW}$ (w/ decays)
$pp \to t\bar{t} + Z$	$NLO_{QCD} + NLO_{EW}$ (w/o decays) NLO_{QCD} (w/ decays, off-shell)	$NNLO_{QCD} + NLO_{EW}$ (w/ decays)
$pp \to t\bar{t} + W$	$NLO_{QCD} + NLO_{EW}$ (w/ decays, off-shell)	$NNLO_{QCD} + NLO_{EW}$ (w/ decays)
$pp \to t/\bar{t}$	$NNLO_{QCD}$*(w/ decays) NLO_{EW} (w/o decays)	$NNLO_{QCD} + NLO_{EW}$ (w/ decays)
$pp \to tZj$	$NLO_{QCD} + NLO_{EW}$ (w/ decays)	$NNLO_{QCD} + NLO_{EW}$ (w/o decays)

computing multi-loop Feynman integrals can be found in Ref. [572], and further details on recent developments can be found in [573, 574]. Another technique that has been recently developed to compute multi-scale two-loop scattering amplitudes is based on numerical unitarity [575–577], which effectively sidesteps tensor integral reduction and directly delivers helicity amplitudes.

The use of the differential equations technique [567, 578], and particularly Henn's canonical form [579] remains as one of the most important methods for computing Feynman Integrals. New developments concerning the use of differential equations and their application to cutting edge multi-loop integrals can be found in, e.g., Refs. [580–586]. In Ref. [587], a procedure for introducing an auxiliary dimensionless parameter into the kinematics of a process and deriving differential equations with respect to this parameter, known as the simplified differential equations approach, was described. It has recently been used to compute the 2-loop planar [588] and non-planar [584] 5-point functions with one massive leg. The method of differential equations is reviewed in [589, 590].

It is not only the amplitude community that has seen impressive development recently. There have been significant steps forward on the side of subtraction schemes. While a full automation of NLO subtractions has been achieved, this is not yet the case at NNLO. This puts the next frontier in NNLO calculations to $2 \rightarrow 3$ processes, as well as revisiting prior approximations that could potentially limit the interpretation of theory–data comparisons (*e.g.* combination of production and decay subprocesses, flavoured jet definition, photon-jet separation and hadron fragmentation, on-shell vs. off-shell, etc.). Antenna subtraction [591, 592] is applicable to processes with hadronic initial and final states with analytically integrated counterterms. It has been extended to cope with identified jet flavours [593, 594] and the photon fragmentation function [595, 596]. Sector-improved residue subtraction [597–599] is capable of treating hadronic initial and final states through a fully local subtraction that incorporates ideas of the FKS approach at NLO [600, 601] and a sector decomposition [602] approach for real radiation singularities [603–605]. It has been extended to deal with flavoured jets [606] and B-hadron production [607]. q_T-subtraction [608] is a slicing approach for processes with a colourless final state and/or a pair of massive coloured particles and is publicly available in the Matrix program [609] and the MCFM program [610]. It has been extended to cope with a pair of massive coloured particles [611, 612] and applied to top-pair production [613, 614] and $b\bar{b}$ production [615]. N-jettiness [616–618] is a slicing approach based on the resolution variable τ_N (N-jettiness) that is suited for processes beyond the scope of the q_T method, i.e. involving final-state jets and is available in the MCFM program [619, 620]. ColorFul subtraction [621] is a fully local subtraction extending the ideas of the Catani–Seymour dipole method at NLO [622]. Nested soft–collinear subtraction [623–625] is a fully local subtraction with analytic results for integrated subtraction counterterms. Analytic local sector subtraction [626, 627] is a local subtraction with analytic integration of the counterterms aiming to combine the respective advantages from two NLO approaches of FKS subtraction [600, 601] and dipole subtraction [622]. Finally, projection to Born [628] is a method based on knowledge of inclusive calculations that retain the full differential information with respect to Born kinematics. All these developments will lead to more NNLO precise results becoming available for use by experiments in the near future.

A separate challenge is to make the NNLO $2 \rightarrow 2$ predictions or complex NLO predictions publicly available to experimental analyses. Root nTuples have been a useful tool for complicated final states at NLO and allow for very flexible re-weighting and analysis. An extension of AP-PLgrid [629] and fastNLO [630] to NNLO offers a convenient method to distribute higher-order predictions. Despite progress in this direction [631], more of these grids should become publicly available.

IX.2.   Monte-Carlo simulations

Most QCD experimental programs rely on the modeling of hadronic final states provided by particle-level Monte-Carlo event generators. Uncertainties on the results of experimental analyses are often dominated by effects associated with these simulations. They arise from the underlying physics models and theory, the truncation of perturbative expansions, the PDFs and their implementation, the modeling of nonperturbative effects, the tuning of model parameters, and the fundamental parameters of the theory.

The types of experiments discussed in Sec. I span a wide range of energies, beam particles, targets (collider vs. fixed target), temperature and chemical potential. An event generator employed for a given experimental configuration may require some dedicated physics models, while other parts can be similar or even identical to those used for other configurations. A particular strength of event generators derives from the factorization or assumed factorization of physics at different energy scales. This principle allows some physics models to be universal and often enables the modular assembly of (parts of) a generator from existing tools when targeting a new experiment. In this manner, previously gained knowledge and experience can be transferred, and a more comprehensive understanding of the physics models is made possible by allowing them to be tested against a wealth of data gathered in past and current experiments. These cross-cutting topics in event generation have been identified as a particular opportunity for the theory community [11].

A shared feature of all experiments is the hard interaction, which probes the colliding beams or fixed targets at the shortest distance scales. This component of any reaction is often the most interesting, since it is most susceptible to new physics effects. It is described in simulations using full quantum mechanical calculations, including interference, and typically at the highest order in perturbation theory that is practicable. Since measurements happen at much larger distance scales, the particles produced in hard interactions can radiate a substantial number of additional quanta before being detected. This radiation is implemented in quasi-classical cascade models, which are matched to the quantum mechanical calculation of the hard process to increase precision. If the active degrees of freedom at the hard scale are the asymptotically free quarks and gluons of QCD, the transition to color-neutral hadrons must be accounted for, typically through the cluster or string model. Particles produced in this simulation chain may undergo transport through nuclear matter. They may also still be unstable and decay on timescales that can in some cases be resolved by detectors. Uncertainties on the results of experimental analyses are often dominated by effects associated with the simulation of the above effects in event generators. They arise from the underlying physics models and theory, the truncation of perturbative expansions, the PDFs and their implementation, the modeling of non-perturbative effects, the tuning of model parameters, and the extraction of fundamental parameters of the theory. The need to address these uncertainties for various facilities and experiments is the driving force behind the efforts of the community of Monte-Carlo event generator developers. Ref. [11] discusses these questions in the context of the larger facilities that continue to drive the development in the near term.

High Energy Colliders: In the coming decade experiments at the LHC will make precise measurements of Standard Model parameters, such as the W mass and the Higgs boson couplings. Both the extraction of these parameters and their interpretation will be limited primarily by the precision of perturbative QCD and EW calculations, both fixed order and resummed. The results of some analyses will however also be limited by the number of Monte Carlo events that can be generated, and computing efficiency will play a crucial role. Future highest-energy colliders, including a potential muon collider, may/will require electroweak effects to be treated on the same footing as QCD and QED effects.

Neutrino Experiments: The next generation neutrino experiments DUNE and HyperK will make precise measurements of the CP violating phase, mixing angles and the mass hierarchy.

The SBN program will focus on precise measurements of neutrino cross sections and searches for new physics. None of these experiments will be limited by statistical uncertainties. Since all running and planned experiments use nuclear targets, one of the leading systematic uncertainties to the measurements arises from the modeling of neutrino-nucleus interactions. This requires the use of state-of-the-art nuclear-structure and -reaction theory calculations. The implementation of physics models with complete error budgets will be required to reach the precision goals of these experiments.

Electron-Ion Collider: The EIC will investigate the structure of nucleons and nuclei at an unprecedented level. This will be accomplished by performing precise measurements of DIS and other processes over the complete relevant kinematic range including the transition region from perturbative to non-perturbative QCD. Highly polarized beams and high luminosity will allow probes of the spatial and spin structure of nucleons, which will need to be simulated at high precision. This currently not possible with standard event generators and requires the development of new tools at the interface between particle and nuclear physics. It is expected that measurements at the LHC will greatly benefit from these developments.

Forward Physics Facility: The Forward Physics Facility at the LHC will leverage the intense beam of neutrinos, and possibly undiscovered particles, in the far-forward direction to search for new physics and calibrate forward particle production. These measurements will require an improved description of forward heavy flavor – particularly charm – production, neutrino scattering in the TeV range, and hadronization inside nuclear matter, including uncertainty quantification.

Lepton Colliders: Future lepton colliders would provide per mill level measurements of Higgs boson couplings and W and top-quark masses. The unprecedented experimental precision will require event generators to cover a much wider range of processes than at previous facilities, both in the Standard Model and beyond. In addition, predictions for the signal processes must be made with extreme precision. Some of the methodology is available from the LEP era, while other components will need to be developed.

Event generation for the above facilities contains many common physics components, such as higher-order QCD and electroweak perturbative corrections, factorization theorems and parton evolution equations, resummation of QCD and QED effects, hadronization, and final-state modeling. Various experiments also require the understanding of heavy-ion collisions and nuclear dynamics at high energies as well as heavy-flavor effects. In addition to the physics components, there are similar computational ingredients, such as interfaces to external tools for analysis, handling of tuning and systematics, and the need for improved computing efficiency. Many of these aspects may profit from developments in artificial intelligence and machine learning. A detailed discussion of all these aspects can be found in [557].

X. ANALYSIS TECHNIQUES

X.1. Jet Substructure

Jets produced from high energy quarks and gluons through QCD have a complex composition. This jet substructure has emerged as a powerful framework for studying the SM at particle colliders, and provides a key set of tools for probing nature at the highest energy scales accessible by terrestrial experiments [34, 35, 632–637]. In general, jet substructure techniques are applied to explore the structure of the strong force in final state radiation on small angular scales, and to identify Lorentz-boosted massive particles ($H/W/Z$ bosons, top quarks, and BSM particles). For all of these signatures, there are a variety of physics backgrounds that obfuscate the target signatures. At hadron colliders, this is the result of multiple, nearly simultaneous collisions (pileup) as well as

underlying event, and multi-parton interactions. A variety of *jet grooming* techniques have been developed to mitigate these effects (see e.g., Refs. [632–635]). While similar backgrounds in e^+e^- are often much smaller, beam-induced backgrounds in muon colliders [50] could potentially benefit from similar techniques developed for hadron colliders.

There are several detector technologies that will improve jet substructure and related techniques. These include finer calorimeter granularity [638, 639], more hermetic coverage of tracking detectors, and precise measurements of timing information. The experience of the LHC has shown that such information can be used to more accurately reconstruct the interaction of hadrons with various detector elements, much of which is used in the 'particle flow' (PF) concept already deployed by the LHC experiments. At future muon colliders, 'beam background' detectors could also in principle be deployed to reduce the impact on jet substructure.

X.1.0.1. Light Quark and Gluon Jets High-energy quark and gluon jets are important probes of a variety of QCD phenomena. These jets can be used to study perturbative aspects of QCD as well as features of QCD that cannot currently be described with perturbation theory. For the latter case, there are cases where scaling relations can be predicated and tested across a wide range of energies. These final states can be used to measure the strong coupling constant, to extract various universal objects within factorized QCD, to tune parton-shower Monte Carlo generators, as well as other tasks. Quark and gluon jets were also studied at previous colliders, but higher energy machines allow for a suppression of nonperturbative effects as well as a larger lever arm for testing scaling behaviors.

Quark and gluon jets are statistically distinguishable due to their different fragmentation processes. Quark versus gluon jet tagging has been a standard benchmark for the development of new classical and machine learning-based jet taggers. Many SM and BSM final states of interest are dominated either by quark or gluon jets, in contrast to the dominant background processes. Quark versus gluon jet tagging can help enhance such signals, although these jets are not as separable as other objects. See also references [39, 191, 640] for further details.

Currently, quark vs. gluon tagging has not fulfilled its promise due to large uncertainties in the modelling of gluon jets. Having pure samples of gluon jets in QCD would significantly change this situation and have a major impact on the LHC physics program. This would be a particular advantage of future lepton colliders for the study of QCD, as they provide pure samples of gluon jets through the process $e^+e^- \to HZ$, with Z decay to leptons and Higgs boson decay to gg [38–40]. Although the understanding of gluon jets is quite poor, there in fact exist a wide range of precision perturbative calculations of event shapes on $H \to gg$, which have never been compared to data. Since the perturbative features of gluon jets are well understood, and already available to high accuracies, comparison with data would enable detailed studies of the nonperturbative structure of gluon jets.

X.1.0.2. Heavy Flavor Jets Bottom quark jets are highly separable from other jets due to the long lifetime of the bottom quark and the heavy mass of bottom-flavored hadrons. In addition to lifetime information, jet substructure can be used to further separate these jets from other jets [641, 642]. A similar conclusion holds to a lesser extent for charm quark jets [643, 644] and to an even lesser extent for strange quark jets [645–647].

X.1.0.3. Strahlung Jets Many future collider scenarios result in H, W, and Z bosons radiating off of very high energy jets ("Weak-strahlung"). In the $H \to b\bar{b}$ and $H \to c\bar{c}$ final states, flavor and lifetime information can be used in addition to the jet substructure to improve categorization. The identification of W and Z bosons is similar to the H boson, however the masses are slightly lower and they often do not decay to bottom or charm quarks, so there are fewer handles to use to identify them.

There may also be top quark production within a jet that originates from light quarks or gluons via gluon splitting to $t\bar{t}$, similar to the case at the Tevatron and LHC for bottom quarks. These

types of events will need to be handled separately from events without these gluon splittings. The jet substructure of top quarks is, in some sense, an ideal case, since there are two heavy SM particle masses to utilize (the top quark and W boson), as well as lifetime and flavor information in the final state particles. This provides a strong handle to identify top quarks. Especially at higher-energy future colliders, the analysis of collisions containing top quarks will be reliant on jet substructure and boosted topologies.

X.1.0.4. *Unconventional Jets*   Unconventional signatures include cases where jets are composed of leptons and hadrons, only leptons, only photons, hadrons and missing transverse energy etc. In addition to the jet kinematics and substructure, the jet timing [648] information and other information can be used for classification. Examples include jets containing one or more hard leptons [649–653], displaced vertices [651], hard photons [654, 655], or significant missing transverse momentum [656, 657]. Some of these anomalous signatures are already started being explored at the LHC [658–662].

X.2.   Event Shapes and Energy Correlations

Measurements of the flow of radiation provide one of the most interesting tests of our understanding of QCD. High energy collisions are particularly interesting, since they provide a probe of the dynamics of QCD from asymptotically free quarks and gluons, through the confining phase transition to free hadrons at asymptotic infinity. Energy flow can be studied either using event shapes or using correlation functions. Both approaches have seen significant progress driven by jet substructure at the LHC, giving rise to many interesting new observables that could be measured at future colliders, providing a significantly extended understanding of energy flow in quantum field theory.

Energy correlation functions [663–668] exhibit simple structures in QCD perturbation theory. A measurement of the two-point correlator using Open Data from the CMS experiment is shown in Fig. 25, illustrating beautiful scaling behavior of weakly coupled quarks and gluons, and a transition to the scaling of free hadrons [669]. Measurements of this quality at future lepton colliders would provide remarkable insights into the dynamics of QCD jets, and the hadronization transition [670].

An insight of the jet substructure program has been the introduction of grooming algorithms that systematically remove low-energy soft radiation [671, 672], thereby reducing traditional double logarithmic observables to single logarithmic observables, and reducing nonperturbative corrections [12]. Fig. 25 shows the groomed hemisphere mass as an example. Although the corresponding groomed observables are theoretically cumbersome, they are practically very useful. The most precise extractions of α_s from event shapes are currently based on thrust and the C-parameter [36, 37], which are closely related double logarithmic observables. Using the standard methodology, one of the complexities in the measurement is the determination of nonperturbative corrections. These corrections cannot be computed from first principles. Theoretical progress in understanding these power corrections has been made in [673–675]. Nevertheless, they must be simultaneously fit for along with the value of α_s. Due to the differing theoretical structure of groomed event shapes, an extraction of α_s from the groomed thrust would provide a relatively independent measurement of the value of the strong coupling. The groomed thrust can be computed to high perturbative accuracy, using a factorization formula, as shown in Fig. 25. Nonperturbative corrections to the groomed thrust distribution have been studied in [676].

While the groomed thrust provides many complementary features to the standard thrust based extraction of α_s, it is ultimately based on the same event shape paradigm, and therefore similar assumptions enter in the treatment of nonperturbative effects. Another interesting complementary measurement would be to perform a measurement of the two-point energy correlator (EEC) in
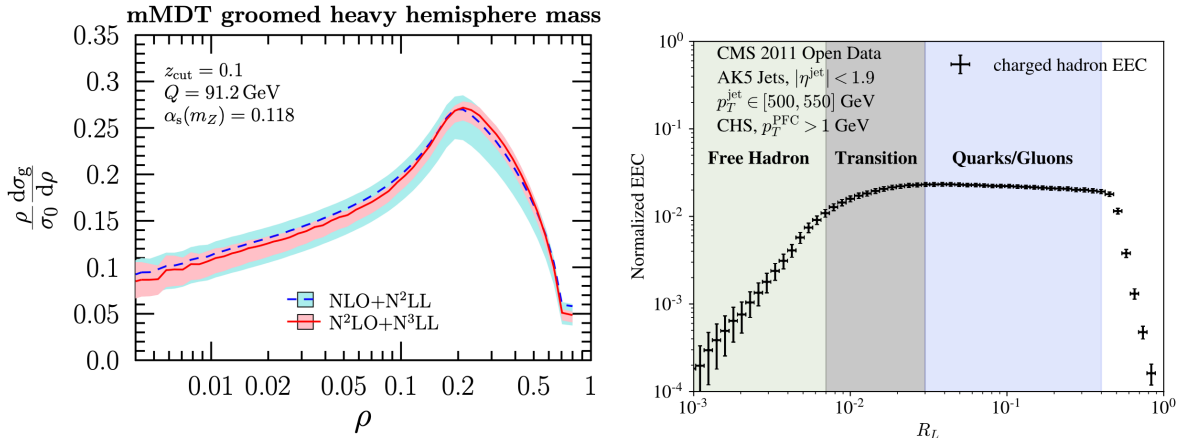
FIG. 25. (a) The groomed mass observable in e^+e^-. The hadronization region is to the left. Figure taken from [681]. (b) A precision measurement of the two-point correlator in the collinear limit at the LHC [669]. Both of these new observables provide interesting probes of α_s
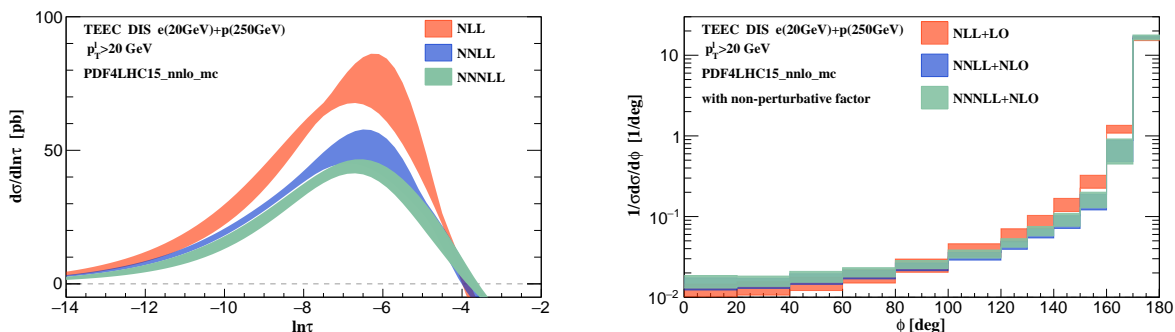

FIG. 26. Left: resummed distributions in the back-to-back limit up to N^3LL accuracy. Note that results are not normalized by σ in the τ interval shown. Right: TEEC ϕ distribution matched with a nonperturbative model. The orange, blue and green bands are the final predictions with scale uncertainties up to $N^3LL+NLO$.

the collinear limit [677]. Due to new analytic results at NLO [678, 679] and the resummation at N^3LL' in the back-to-back limit [680], the EEC has seen a resurgence of interest. Its collinear limit is described by completely different physics (fixed spin DGLAP) than the Sudakov region, and furthermore, since the energy correlators are not event shape observables, they have a different structure for their nonperturbative effects. Despite being an old observable that was measured at LEP, extractions of α_s from the collinear limit were never performed at LEP. Comparing the measurement of the two-point correlator at LEP vs. using the modern calorimetry of the LHC shows a completely different understanding of the collinear limit. Achieving a similarly precise measurement in the clean e^+e^- environment of the ILC or FCC-ee would be extremely valuable for precision measurements of α_s (once it reaches NNLO, or beyond, pQCD accuracy), and might resolve the longstanding tensions in the values extracted from event shapes.

Moreover, the EEC/TEEC event shape observables can be studied in e^+e^-, ep and pp collisions, which provides a way to test the universality of QCD factorization in different colliding systems. These observables can also be used to study TMD physics, which is one of the most important goals of the EIC. Hadron colliders present a more complex environment than e^+e^- or ep colliders, nevertheless, high accuracy can still be achieved. Once EEC/TEEC are computed at NNLO

pQCD accuracy, a new avenue will be opened for the rich HL-LHC data to be combined with precision resummed QCD predictions to obtain precision measurement of SM parameters, such as strong coupling constant and various TMD functions. The simplicity in the theoretical structure of EEC/TEEC makes higher-order calculation feasible and can shed light on the structure of perturbation theory. Both of these lead to valuable addition to our understanding of QCD. Finally, the EEC/TEEC observables can be generalized to eA, pA, and AA collisions. They can shed new light on the many-body QCD dynamics in reactions with nuclei, specifically multi-parton interactions and the formation of parton showers in matter. In these environments, precise extraction of transport properties of various forms of nuclear matter will greatly benefit from the high perturbative accuracy achieved in the baseline ep and pp reactions.

XI. CROSS-CUTTING QCD

QCD interactions play a ubiquitous and multifaceted role in collider phenomenology, and hence successes across many areas depend on future developments at the intersections of QCD and other domains. To take the full advantage of precise perturbative QCD calculations discussed in Sec. IX.1, commensurate advances must be achieved in determinations of long-distance QCD contributions including PDFs, computations of electroweak radiative contributions, event generation, machine learning, and last but not least, accurate and fast practical implementations. These tasks require collaboration between experimentalists and theorists, model-builders and QCD experts, and, more broadly, support of the *QCD infrastructure* that adapts theoretical tools for experimental analyses and provides protocols to validate these tools and assess uncertainties from experimental or theoretical sides. This subsection presents examples of such cross-cutting issues.

XI.1. Comprehensive uncertainty estimates

Achieving the targeted accuracy on the PDFs and key measurements such as W boson mass at the HL-LHC requires better control of systematic uncertainties at all stages [13], in experimental measurements as well as in numerical computations. This requires a close collaboration between experimentalists and theorists on the consistent usage of QCD predictions and the conversion from parton to particle level (see also Sec. IX.2). Making higher-order calculations for complex final states available in a form suitable for experimental analyses remains a significant part of this challenge [629, 630, 682]. In addition, more efforts are necessary to present models of systematic uncertainties in the complete form that can be interpreted by external users [683].
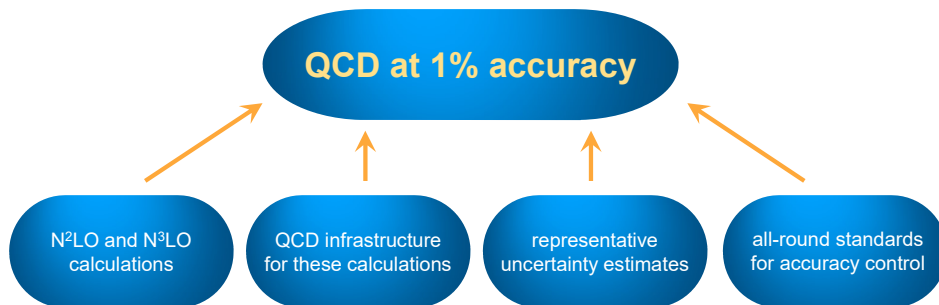

FIG. 27. Prerequisites for achieving percent-level accuracy in QCD calculations.

New types of complexity issues emerge in comparisons of models with many parameters to very large data samples expected at the LHC Run-3 and HL-LHC. Such comparisons may be subject to increased risks of undetected biases due to non-representative exploration of contributing systematic factors [684], as has been recently demonstrated on the example of a PDF global fit [186]. In short, elevating the accuracy of QCD calculations to one percent requires both individual precise theoretical calculations as well as accurate supporting theoretical infrastructure that would allow, in particular, to explore exhaustively the relevant systematic factors. Reaching this target also requires agreed-upon standards and practices for accuracy control at all stages of the analyses, as is illustrated in Fig. 27.

XI.2. AI/ML innovation for QCD

QCD applications are a fertile ground to explore innovative developments in machine learning (ML) and artificial intelligence (AI) [685]. ML methods have been proposed to solve a variety of tasks both in experiment (particle reconstruction, event unfolding, anomaly detection) and theory (phase space integration, calculations of scattering amplitudes, simulations of parton showers, and modeling of parton distribution and fragmentation functions) [686]. ML methods are explored at the same time in the context of lattice QCD calculations [687]. Conceptually, there are significant overlaps between ML and methods of large-scale and multivariate data analysis and fitting that traditionally have been used e.g. for collider particle detection and fitting of nonperturbative functions. ML provides technical tools that can facilitate many advances. Across-the-board outstanding questions also need to be resolved, notably interpretability and faithful estimation of uncertainties of ML/AI results, as detailed in the dedicated Snowmass whitepaper [688].

XI.3. QCD in new physics searches and SM EFT fits

The energy reach of many BSM searches depends on the interplay between precision calculations of matrix elements and global PDF analyses. Examples include searches for new vector bosons, referred to as Z's and W's. Current LHC bounds on mass disfavor extra vector bosons lighter than approximately 4-5 TeV. BSM searches of W'/Z's with even larger masses are progressively more sensitive to PDFs at large x where uncertainties are still large [174] and affected by nuclear corrections, higher-twist contributions, intrinsic heavy-quark components. Either forward particle production at the LHC or, often more cleanly, DIS at the EIC can constrain PDFs in the large-x region and increase sensitivity of BSM searches in the TeV mass range.

Search for deviations from SM examined in the language of Effective Field Theories (EFTs) [689] can set lower bounds on the scales in a number of new physics scenarios. Such analyses is an active research area covered in the other EF reports, for example, in a widely adopted EFT expansion of the Standard Model, or SMEFT [690]. SMEFT contributions extracted from collider data may significantly depend on including subleading (dimension-eight) SMEFT operators as well as SM radiative contributions, as examined, e.g., in Refs. [691–698]. This dependence must be kept in mind when interpreting the SMEFT fits to data from both lepton and hadron colliders.

As an example, Fig. 28(a) illustrates the change in confidence regions for SMEFT coefficients extracted from LEP data upon adding higher-order (dimension-8) operators into the analysis [694]. As illustrated in Fig. 28(b), when including high-mass LHC data in a fit of PDFs and in a fit of SMEFT coefficients, and neglecting the interplay between them, the uncertainties on the EFT parameters may be underestimated. Although the proton structure parametrized by PDFs is intrinsically a low-energy input and should in principle be separable from the imprints of SMEFT operators, the complexity of the LHC environment might well intertwine them [699–704]. The
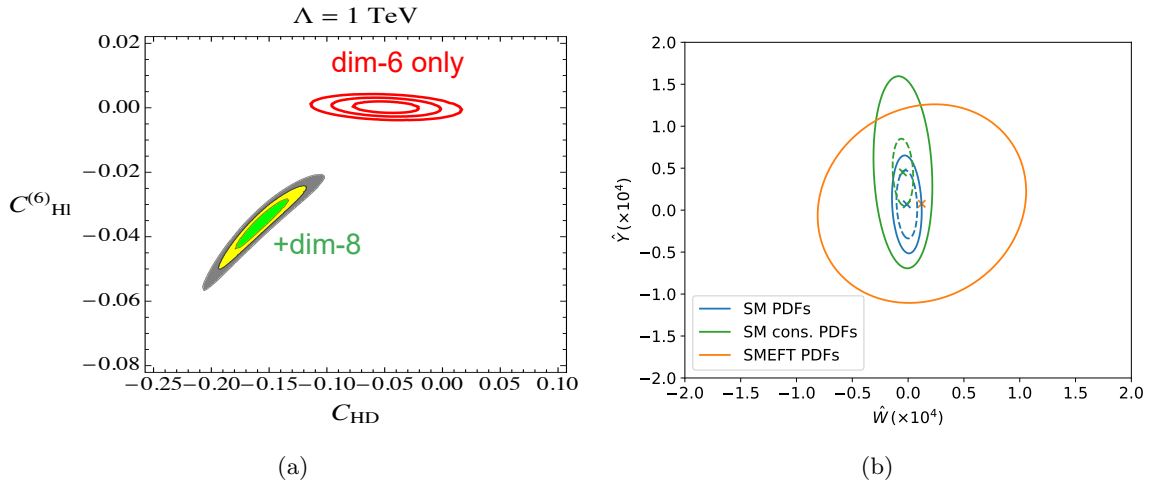
FIG. 28. (a) 68%/95%/99.9% exclusion limits on select SMEFT coefficients up to dim-6 and dim-8 in an analysis of LEP electroweak precision data [694]. (b) The 95% confidence level bounds on the plane of the Wilson coefficients considered in Ref. [699] obtained using either fixed SM PDFs (blue) or conservative SM PDFs that do not include high-energy data (green). PDF uncertainties are included in the solid lines and not included in the dashed lines. Results are compared to those obtained in a simultaneous fit of SMEFT and PDFs, when the PDFs are allowed to vary when varying the values of the Wilson coefficients (orange).

bounds on the respective Wilson coefficients are relaxed once the are fitted together with the PDFs. Constraints on either the PDFs or EFT operators in low-energy experiments, where at least some new physics contributions are absent, can be crucial for disentangling the SM/BSM degeneracies. In this light, the SM and SMEFT studies at the EIC and other low-energy facilities again are synergistic to those at the (HL-)LHC [705, 706], especially for spin-dependent EFT operators.

XI.4. QCD theory for FCC-hh

In 100 TeV pp collisions, in addition to the unprecedented experimental environment reviewed in Sec. I.8, synergistic developments across multiple areas of QCD theory will be necessary to meet objectives of the FCC-hh experimental program. Hadronic and electromagnetic shower components up to several TeV need to be simulated, where extrapolations to these high energies come with large uncertainties. Differences in the hadronic shower simulation models in Geant4 [707] have been reported for pions in the energy range 2–10 GeV [708], warranting future detailed studies of hadronic showers for the highest-energy regime. Multi-loop perturbative calculations combining both QCD and EW radiative contributions will be combined with PDFs of commensurate precision at multi-TeV energy scales. A BFKL-like QCD formalism will be necessary to predict parton scattering at momentum fractions as low as 10^{-7}. Electroweak gauge bosons W and Z, leptons, and top quarks will be copiously produced at the FCC-hh energy and will need to be included into the PDFs together with quarks and gluons [709].

XI.5. Legacy data preservation

Electron-positron and lepton-hadron colliders still provide the most precise data for a number of QCD studies and will likely not be superseded by the LHC dataset. Legacy data from LEP/SLC and HERA therefore continue to be important for QCD analysis (including event generator tuning

and other studies). In particular, there has been significant theory and experimental innovation (including with machine learning) since these data were collected. These new insights can be used to extract novel information from these pristine datasets. A funding model for supporting such analysis does not currently exist, but even a modest investment could produce significant physics results.

XII. SUMMARY

In this report, we reviewed the rich landscape, wide impact, and interconnectedness of QCD studies in 2020's. During the Snowmass 2021 process, QCD has drawn strong interest in numerous discussions as the only QFT that can be experimentally studied in perturbative and nonperturbative phases, and as the key theory in HEP phenomenology now and in the future. QCD is rich both in data and in ideas. While being the least accurately known fundamental force of the Standard Model, the strong force plays the central role in many measurements. In particular, success of many precision measurements in Higgs, top, electroweak boson production channels relies on both advancements in perturbative QCD calculations and detailed modeling of nonperturbative contributions. Various domains of QCD theory undergo rapid development. Completion of the HL-LHC and EIC programs, together with a Higgs factory, will provide unprecedented levels of precision in QCD, in turn impacting most areas in the Energy Frontier.

ACKNOWLEDGMENTS

[1] **ATLAS** Collaboration, "Snowmass White Paper Contribution: Physics with the Phase-2 ATLAS and CMS Detectors." ATL-PHYS-PUB-2022-018, 2022.

[2] L. A. Anchordoqui *et al.*, "The Forward Physics Facility: Sites, experiments, and physics potential," *Phys. Rept.* **968** (2022) 1–50, arXiv:2109.10905 [hep-ph].

[3] J. L. Feng *et al.*, "The Forward Physics Facility at the High-Luminosity LHC," arXiv:2203.05090 [hep-ex].

[4] R. Abdul Khalek *et al.*, "Snowmass 2021 White Paper: Electron Ion Collider for High Energy Physics," in *2022 Snowmass Summer Study*. 3, 2022. arXiv:2203.13199 [hep-ph].

[5] S. V. Chekanov and S. Magill, "Some aspects of impact of the Electron Ion Collider on particle physics at the Energy Frontier," in *2022 Snowmass Summer Study*. 2, 2022. arXiv:2202.11529 [hep-ph].

[6] ν-**Test** Collaboration, B. Batell, T. Ghosh, and K. Xie, "Heavy Neutral Lepton Searches at the Electron-Ion Collider: A Snowmass Whitepaper," in *2022 Snowmass Summer Study*. 3, 2022. arXiv:2203.06705 [hep-ph].

[7] A. Accardi *et al.*, "Opportunities for precision QCD physics in hadronization at Belle II – a snowmass whitepaper," in *2022 Snowmass Summer Study*. 4, 2022. arXiv:2204.02280 [hep-ex].

[8] G. Bernardi *et al.*, "The Future Circular Collider: a Summary for the US 2021 Snowmass Process," arXiv:2203.06520 [hep-ex].

[9] **ILC International Development Team** Collaboration, A. Aryshev *et al.*, "The International Linear Collider: Report to Snowmass 2021," arXiv:2203.07622 [physics.acc-ph].

[10] D. Acosta, E. Barberis, N. Hurley, W. Li, O. M. Colin, D. Wood, and X. Zuo, "The Potential of a TeV-Scale Muon-Ion Collider," in *2022 Snowmass Summer Study*. 3, 2022. arXiv:2203.06258 [hep-ex].

[11] J. M. Campbell *et al.*, "Event Generators for High-Energy Physics Experiments," arXiv:2203.11110 [hep-ph].

[12] D. d'Enterria *et al.*, "The strong coupling constant: State of the art and the decade ahead," arXiv:2203.08271 [hep-ph].

[13] S. Amoroso *et al.*, "Snowmass 2021 whitepaper: Proton structure at the precision frontier," arXiv:2203.13923 [hep-ph].

[14] M. Constantinou *et al.*, "Lattice QCD Calculations of Parton Physics," arXiv:2202.07193 [hep-lat].

[15] T.-J. Hou, H.-W. Lin, M. Yan, and C. P. Yuan, "Impact of lattice $s(x) - \bar{s}(x)$ data in the CTEQ-TEA global analysis," arXiv:2204.07944 [hep-ph].

[16] M. Hentschinski *et al.*, "White Paper on Forward Physics, BFKL, Saturation Physics and Diffraction," arXiv:2203.08129 [hep-ph].

[17] W. Bai, M. V. Diwan, M. V. Garzelli, Y. S. Jeong, K. Kumar, and M. H. Reno, "Prompt electron and tau neutrinos and antineutrinos in the forward region at the LHC," *JHEAp* **34** (2022) 212–216, arXiv:2203.07212 [hep-ph].

[18] B. Nachman *et al.*, "Jets and Jet Substructure at Future Colliders," arXiv:2203.07462 [hep-ph].

[19] The xFitter Collaboration, "xFitter: An Open Source QCD Analysis Framework,". Text available at https://tinyurl.com/xFitterSnowmass21WP; the collaboration website: https://www.xfitter.org/.

[20] D. d'Enterria *et al.*, "Opportunities for new physics searches with heavy ions at colliders," in *2022 Snowmass Summer Study*. 3, 2022. arXiv:2203.05939 [hep-ph].

[21] I. Anikin, A. Besse, D. Yu. Ivanov, B. Pire, L. Szymanowski, and S. Wallon, "A phenomenological study of helicity amplitudes of high energy exclusive leptoproduction of the rho meson," *Phys. Rev. D* **84** (2011) 054004, arXiv:1105.1761 [hep-ph].

[22] A. Besse, L. Szymanowski, and S. Wallon, "Saturation effects in exclusive rhoT, rhoL meson electroproduction," *JHEP* **11** (2013) 062, arXiv:1302.1766 [hep-ph].

[23] A. D. Bolognino, F. G. Celiberto, D. Yu. Ivanov, and A. Papa, "Unintegrated gluon distribution from forward polarized ρ-electroproduction," *Eur. Phys. J.* **C78** no. 12, (2018) 1023, arXiv:1808.02395 [hep-ph].

[24] F. G. Celiberto, "Unraveling the Unintegrated Gluon Distribution in the Proton via ρ-Meson

Leptoproduction," *Nuovo Cim.* **C42** (2019) 220, `arXiv:1912.11313 [hep-ph]`.

[25] A. D. Bolognino, A. Szczurek, and W. Schaefer, "Exclusive production of ϕ meson in the $\gamma^* p \to \phi p$ reaction at large photon virtualities within k_T-factorization approach," *Phys. Rev. D* **101** no. 5, (2020) 054041, `arXiv:1912.06507 [hep-ph]`.

[26] I. Bautista, A. Fernandez Tellez, and M. Hentschinski, "BFKL evolution and the growth with energy of exclusive J/ψ and Υ photoproduction cross sections," *Phys. Rev. D* **94** no. 5, (2016) 054002, `arXiv:1607.05203 [hep-ph]`.

[27] A. Arroyo García, M. Hentschinski, and K. Kutak, "QCD evolution based evidence for the onset of gluon saturation in exclusive photo-production of vector mesons," *Phys. Lett. B* **795** (2019) 569–575, `arXiv:1904.04394 [hep-ph]`.

[28] M. Hentschinski and E. Padrón Molina, "Exclusive J/Ψ and $\Psi(2s)$ photo-production as a probe of QCD low x evolution equations," *Phys. Rev. D* **103** no. 7, (2021) 074008, `arXiv:2011.02640 [hep-ph]`.

[29] National Academies of Sciences, Engineering, and Medicine, *An Assessment of U.S.-Based Electron-Ion Collider Science*. The National Academies Press, Washington, DC, 2018.

[30] R. Abdul Khalek *et al.*, "Science Requirements and Detector Concepts for the Electron-Ion Collider: EIC Yellow Report," `arXiv:2103.05419 [physics.ins-det]`.

[31] M. Thomson, "Model-independent measurement of the e$^+$ e$^-$ → HZ cross section at a future e$^+$ e$^-$ linear collider using hadronic Z decays," *Eur. Phys. J. C* **76** no. 2, (2016) 72, `arXiv:1509.02853 [hep-ex]`.

[32] P.-Z. Lai, M. Ruan, and C.-M. Kuo, "Jet performance at the circular electron-positron collider," *JINST* **16** no. 07, (2021) P07037, `arXiv:2104.05029 [hep-ex]`.

[33] M. Boronat, J. Fuster, I. Garcia, P. Roloff, R. Simoniello, and M. Vos, "Jet reconstruction at high-energy electron–positron colliders," *Eur. Phys. J. C* **78** no. 2, (2018) 144, `arXiv:1607.05039 [hep-ex]`.

[34] A. J. Larkoski, I. Moult, and B. Nachman, "Jet Substructure at the Large Hadron Collider: A Review of Recent Advances in Theory and Machine Learning," `arXiv:1709.04464 [hep-ph]`.

[35] S. Marzani, G. Soyez, and M. Spannowsky, *Looking inside jets: an introduction to jet substructure and boosted-object phenomenology*, vol. 958. Springer, 2019. `arXiv:1901.10342 [hep-ph]`.

[36] R. Abbate, M. Fickinger, A. H. Hoang, V. Mateu, and I. W. Stewart, "Thrust at N^3LL with Power Corrections and a Precision Global Fit for alphas(mZ)," *Phys.Rev.* **D83** (2011) 074021, `arXiv:1006.3080 [hep-ph]`.

[37] A. H. Hoang, D. W. Kolodrubetz, V. Mateu, and I. W. Stewart, "Precise determination of α_s from the C-parameter distribution," *Phys. Rev. D* **91** no. 9, (2015) 094018, `arXiv:1501.04111 [hep-ph]`.

[38] D. d'Enterria, K. Krajczár, and H. Paukkunen, "Top-quark production in proton–nucleus and nucleus–nucleus collisions at LHC energies and beyond," *Phys. Lett. B* **746** (2015) 64–72, `arXiv:1501.05879 [hep-ph]`.

[39] P. Gras, S. Höche, D. Kar, A. Larkoski, L. Lönnblad, S. Plätzer, A. Siódmok, P. Skands, G. Soyez, and J. Thaler, "Systematics of quark/gluon tagging," *JHEP* **07** (2017) 091, `arXiv:1704.03878 [hep-ph]`.

[40] J. Gao, Y. Gong, W.-L. Ju, and L. L. Yang, "Thrust distribution in Higgs decays at the next-to-leading order and beyond," *JHEP* **03** (2019) 030, `arXiv:1901.02253 [hep-ph]`.

[41] D. d'Enterria and C. Yan, "Revised QCD effects on the Z → $b\bar{b}$ forward-backward asymmetry," `arXiv:2011.00530 [hep-ph]`.

[42] **ILD** Collaboration, H. Abramowicz *et al.*, "The ILD detector at the ILC," `arXiv:1912.04601 [physics.ins-det]`.

[43] M. Breidenbach, J. E. Brau, P. Burrows, T. Markiewicz, M. Stanitzki, J. Strube, and A. P. White, "Updating the SiD Detector concept," `arXiv:2110.09965 [physics.ins-det]`.

[44] **CLICdp** Collaboration, D. Arominski *et al.*, "A detector for CLIC: main parameters and performance," `arXiv:1812.07337 [physics.ins-det]`.

[45] N. Bacchetta *et al.*, "CLD – A Detector Concept for the FCC-ee," `arXiv:1911.12230 [physics.ins-det]`.

[46] **CALICE** Collaboration, C. Adloff *et al.*, "Hadronic energy resolution of a highly granular scintillator-steel hadron calorimeter using software compensation techniques," *JINST* **7** (2012) P09017, `arXiv:1207.4210 [physics.ins-det]`.

[47] R. Ström and P. Roloff, "Physics potential for boosted topologies in top-quark pair production at a multi-TeV Compact Linear Collider," `arXiv:2008.05526 [hep-ex]`.

[48] M. Boronat, J. Fuster, I. Garcia, E. Ros, and M. Vos, "A robust jet reconstruction algorithm for high-energy lepton colliders," *Phys. Lett. B* **750** (2015) 95–99, `arXiv:1404.4294 [hep-ex]`.

[49] I. W. Stewart, F. J. Tackmann, J. Thaler, C. K. Vermilion, and T. F. Wilkason, "XCone: N-jettiness as an Exclusive Cone Jet Algorithm," *JHEP* **11** (2015) 072, `arXiv:1508.01516 [hep-ph]`.

[50] F. Collamati, C. Curatolo, D. Lucchesi, A. Mereghetti, N. Mokhov, M. Palmer, and P. Sala, "Advanced assessment of beam-induced background at a muon collider," *JINST* **16** no. 11, (2021) P11009, `arXiv:2105.09116 [physics.acc-ph]`.

[51] D. Ally, L. Carpenter, T. Holmes, L. Lee, and P. Wagenknecht, "Strategies for Beam-Induced Background Reduction at Muon Colliders," `arXiv:2203.06773 [physics.ins-det]`.

[52] **Muon Collider** Collaboration, N. Bartosik *et al.*, "Simulated Detector Performance at the Muon Collider," in *2022 Snowmass Summer Study*. 3, 2022. `arXiv:2203.07964 [hep-ex]`.

[53] J. Thaler and K. Van Tilburg, "Identifying Boosted Objects with N-subjettiness," *JHEP* **03** (2011) 015, `arXiv:1011.2268 [hep-ph]`.

[54] J. Thaler and K. Van Tilburg, "Maximizing Boosted Top Identification by Minimizing N-subjettiness," *JHEP* **02** (2012) 093, `arXiv:1108.2701 [hep-ph]`.

[55] A. J. Larkoski, I. Moult, and D. Neill, "Power Counting to Better Jet Observables," `arXiv:1409.6298 [hep-ph]`.

[56] D. P. Anderle *et al.*, "Electron-ion collider in China," *Front. Phys. (Beijing)* **16** no. 6, (2021) 64701, `arXiv:2102.09222 [nucl-ex]`.

[57] "Proceedings, ECFA-CERN Workshop on large hadron collider in the LEP tunnel: Lausanne and Geneva, Switzerland, March 21-27 March, 1984." CERN-84-10-V-2, CERN-84-10-V-1, ECFA-84-85, CERN-YELLOW-84-10-V-1, 1984.

[58] **LHeC Study Group** Collaboration, J. L. Abelleira Fernandez *et al.*, "A Large Hadron Electron Collider at CERN: Report on the Physics and Design Concepts for Machine and Detector," *J. Phys. G* **39** (2012) 075001, `arXiv:1206.2913 [physics.acc-ph]`.

[59] **LHeC, FCC-he Study Group** Collaboration, P. Agostini *et al.*, "The Large Hadron-Electron Collider at the HL-LHC," *J. Phys. G* **48** no. 11, (2021) 110501, `arXiv:2007.14491 [hep-ex]`.

[60] K. D. J. André *et al.*, "An experiment for electron-hadron scattering at the LHC," *Eur. Phys. J. C* **82** no. 1, (2022) 40, `arXiv:2201.02436 [hep-ex]`.

[61] E. Coleman, M. Freytsis, A. Hinzmann, M. Narain, J. Thaler, N. Tran, and C. Vernieri, "The importance of calorimetry for highly-boosted jet substructure," *Journal of Instrumentation* **13** no. 01, (Jan, 2018) T01003–T01003. `http://dx.doi.org/10.1088/1748-0221/13/01/T01003`.

[62] A. J. Larkoski, F. Maltoni, and M. Selvaggi, "Tracking down hyper-boosted top quarks," `arXiv:1503.03347 [hep-ph]`.

[63] H.-M. Chang, M. Procura, J. Thaler, and W. J. Waalewijn, "Calculating Track-Based Observables for the LHC," *Phys. Rev. Lett.* **111** (2013) 102002, `arXiv:1303.6637 [hep-ph]`.

[64] B. T. Elder and J. Thaler, "Aspects of Track-Assisted Mass," *JHEP* **03** (2019) 104, `arXiv:1805.11109 [hep-ph]`.

[65] M. Spannowsky and M. Stoll, "Tracking New Physics at the LHC and beyond," *Phys. Rev. D* **92** no. 5, (2015) 054033, `arXiv:1505.01921 [hep-ph]`.

[66] **ATLAS** Collaboration, "Jet mass reconstruction with the ATLAS Detector in early Run 2 data." ATLAS-CONF-2016-035, Jul, 2016. `http://cds.cern.ch/record/2200211`.

[67] L. Gouskos, A. Sung, and J. Incandela, "Search for stop scalar quarks at FCC-hh," tech. rep., CERN, Geneva, Oct, 2018. `https://cds.cern.ch/record/2642475`.

[68] M. Aleksa *et al.*, "Calorimeters for the FCC-hh," `arXiv:1912.09962 [physics.ins-det]`.

[69] **Particle Data Group** Collaboration, R. L. Workman, "Review of Particle Physics," *PTEP* **2022** (2022) 083C01.

[70] D. d'Enterria and V. Jacobsen, "Improved strong coupling determinations from hadronic decays of electroweak bosons at N³LO accuracy," `arXiv:2005.04545 [hep-ph]`.

[71] **Particle Data Group** Collaboration, P. A. Zyla *et al.*, "Review of Particle Physics," *PTEP* **2020** no. 8, (2020) 083C01.

[72] Y. Aoki *et al.*, "FLAG Review 2021," `arXiv:2111.09849 [hep-lat]`.

[73] A. Blondel and E. Gianfelice, "The challenges of beam polarization and keV-scale centre-of-mass

energy calibration at the FCC-ee," *Eur. Phys. J. Plus* **136** no. 11, (2021) 1103.

[74] **FCC** Collaboration, A. Abada *et al.*, "FCC-ee: The Lepton Collider: Future Circular Collider Conceptual Design Report Volume 2," *Eur. Phys. J. ST* **228** no. 2, (2019) 261–623.

[75] P. Janot, "Direct measurement of $\alpha_{QED}(m_Z^2)$ at the FCC-ee," *JHEP* **02** (2016) 053, `arXiv:1512.05544 [hep-ph]`. [Erratum: JHEP 11, 164 (2017)].

[76] A. Blondel, J. Gluza, S. Jadach, P. Janot, and T. Riemann, eds., *Theory for the FCC-ee: Report on the 11th FCC-ee Workshop Theory and Experiments*, vol. 3/2020 of *CERN Yellow Reports: Monographs*. CERN, Geneva, May, 2019. `arXiv:1905.05078 [hep-ph]`.

[77] A. Accardi *et al.*, "Electron Ion Collider: The Next QCD Frontier: Understanding the glue that binds us all," *Eur. Phys. J. A* **52** no. 9, (2016) 268, `arXiv:1212.1701 [nucl-ex]`.

[78] T.-J. Hou *et al.*, "New CTEQ global analysis of quantum chromodynamics with high-precision data from the LHC," *Phys. Rev. D* **103** no. 1, (2021) 014013, `arXiv:1912.10053 [hep-ph]`.

[79] A. Deur, Y. Prok, V. Burkert, D. Crabb, F. X. Girod, K. A. Griffioen, N. Guler, S. E. Kuhn, and N. Kvaltine, "High precision determination of the Q^2 evolution of the Bjorken Sum," *Phys. Rev. D* **90** no. 1, (2014) 012009, `arXiv:1405.7854 [nucl-ex]`.

[80] K. Kovařík, P. M. Nadolsky, and D. E. Soper, "Hadronic structure in high-energy collisions," *Rev. Mod. Phys.* **92** no. 4, (2020) 045003, `arXiv:1905.06957 [hep-ph]`.

[81] M. Luscher, P. Weisz, and U. Wolff, "A Numerical method to compute the running coupling in asymptotically free theories," *Nucl. Phys. B* **359** (1991) 221–243.

[82] M. Luscher, R. Sommer, P. Weisz, and U. Wolff, "A Precise determination of the running coupling in the SU(3) Yang-Mills theory," *Nucl. Phys. B* **413** (1994) 481–502, `arXiv:hep-lat/9309005`.

[83] **Alpha** Collaboration, G. de Divitiis, R. Frezzotti, M. Guagnelli, M. Luscher, R. Petronzio, R. Sommer, P. Weisz, and U. Wolff, "Universality and the approach to the continuum limit in lattice gauge theory," *Nucl. Phys. B* **437** (1995) 447–470, `arXiv:hep-lat/9411017`.

[84] K. Jansen, C. Liu, M. Luscher, H. Simma, S. Sint, R. Sommer, P. Weisz, and U. Wolff, "Nonperturbative renormalization of lattice QCD at all scales," *Phys. Lett. B* **372** (1996) 275–282, `arXiv:hep-lat/9512009`.

[85] K. Symanzik, "Schrodinger Representation and Casimir Effect in Renormalizable Quantum Field Theory," *Nucl. Phys. B* **190** (1981) 1–44.

[86] M. Luscher, "SCHRODINGER REPRESENTATION IN QUANTUM FIELD THEORY," *Nucl. Phys. B* **254** (1985) 52–57.

[87] M. Luscher, R. Narayanan, P. Weisz, and U. Wolff, "The Schrödinger functional: A Renormalizable probe for nonAbelian gauge theories," *Nucl. Phys. B* **384** (1992) 168–228, `arXiv:hep-lat/9207009`.

[88] S. Sint, "On the Schrodinger functional in QCD," *Nucl. Phys. B* **421** (1994) 135–158, `arXiv:hep-lat/9312079`.

[89] **ALPHA** Collaboration, A. Bode, P. Weisz, and U. Wolff, "Two loop computation of the Schrodinger functional in lattice QCD," *Nucl. Phys. B* **576** (2000) 517–539, `arXiv:hep-lat/9911018`. [Erratum: Nucl.Phys.B 608, 481–481 (2001), Erratum: Nucl.Phys.B 600, 453–453 (2001)].

[90] **ALPHA** Collaboration, M. Bruno, M. Dalla Brida, P. Fritzsch, T. Korzec, A. Ramos, S. Schaefer, H. Simma, S. Sint, and R. Sommer, "QCD Coupling from a Nonperturbative Determination of the Three-Flavor Λ Parameter," *Phys. Rev. Lett.* **119** no. 10, (2017) 102001, `arXiv:1706.03821 [hep-lat]`.

[91] **HPQCD, UKQCD** Collaboration, Q. Mason, H. D. Trottier, C. T. H. Davies, K. Foley, A. Gray, G. P. Lepage, M. Nobes, and J. Shigemitsu, "Accurate determinations of alpha(s) from realistic lattice QCD," *Phys. Rev. Lett.* **95** (2005) 052002, `arXiv:hep-lat/0503005`.

[92] **HPQCD** Collaboration, C. T. H. Davies, K. Hornbostel, I. D. Kendall, G. P. Lepage, C. McNeile, J. Shigemitsu, and H. Trottier, "Update: Accurate Determinations of alpha(s) from Realistic Lattice QCD," *Phys. Rev. D* **78** (2008) 114507, `arXiv:0807.1687 [hep-lat]`.

[93] K. Maltman, D. Leinweber, P. Moran, and A. Sternbeck, "The Realistic Lattice Determination of alpha(s)(M(Z)) Revisited," *Phys. Rev. D* **78** (2008) 114504, `arXiv:0807.2020 [hep-lat]`.

[94] C. McNeile, C. T. H. Davies, E. Follana, K. Hornbostel, and G. P. Lepage, "High-Precision c and b Masses, and QCD Coupling from Current-Current Correlators in Lattice and Continuum QCD," *Phys. Rev. D* **82** (2010) 034512, `arXiv:1004.4285 [hep-lat]`.

[95] A. Pineda and J. Soto, "The Renormalization group improvement of the QCD static potentials," *Phys. Lett. B* **495** (2000) 323–328, `arXiv:hep-ph/0007197`.

[96] N. Brambilla, A. Pineda, J. Soto, and A. Vairo, "Effective Field Theories for Heavy Quarkonium," *Rev. Mod. Phys.* **77** (2005) 1423, `arXiv:hep-ph/0410047`.

[97] N. Brambilla, A. Vairo, X. Garcia i Tormo, and J. Soto, "The QCD static energy at NNNLL," *Phys. Rev. D* **80** (2009) 034016, `arXiv:0906.1390 [hep-ph]`.

[98] A. Bazavov, N. Brambilla, X. G. Tormo, I, P. Petreczky, J. Soto, and A. Vairo, "Determination of α_s from the QCD static energy: An update," *Phys. Rev. D* **90** no. 7, (2014) 074038, `arXiv:1407.8437 [hep-ph]`. [Erratum: Phys.Rev.D 101, 119902 (2020)].

[99] H. Takaura, T. Kaneko, Y. Kiyo, and Y. Sumino, "Determination of α_s from static QCD potential with renormalon subtraction," *Phys. Lett. B* **789** (2019) 598–602, `arXiv:1808.01632 [hep-ph]`.

[100] H. Takaura, T. Kaneko, Y. Kiyo, and Y. Sumino, "Determination of α_s from static QCD potential: OPE with renormalon subtraction and lattice QCD," *JHEP* **04** (2019) 155, `arXiv:1808.01643 [hep-ph]`.

[101] **TUMQCD** Collaboration, A. Bazavov, N. Brambilla, P. Petreczky, A. Vairo, and J. H. Weber, "Color screening in (2+1)-flavor QCD," *Phys. Rev. D* **98** no. 5, (2018) 054511, `arXiv:1804.10600 [hep-lat]`.

[102] **TUMQCD** Collaboration, A. Bazavov, N. Brambilla, X. Garcia i Tormo, P. Petreczky, J. Soto, A. Vairo, and J. H. Weber, "Determination of the QCD coupling from the static energy and the free energy," *Phys. Rev. D* **100** no. 11, (2019) 114511, `arXiv:1907.11747 [hep-lat]`.

[103] C. Ayala, X. Lobregat, and A. Pineda, "Determination of $\alpha(M_z)$ from an hyperasymptotic approximation to the energy of a static quark-antiquark pair," *JHEP* **09** (2020) 016, `arXiv:2005.12301 [hep-ph]`.

[104] J. Komijani, P. Petreczky, and J. H. Weber, "Strong coupling constant and quark masses from lattice QCD," *Prog. Part. Nucl. Phys.* **113** (2020) 103788, `arXiv:2003.11703 [hep-lat]`.

[105] C. Sturm, "Moments of Heavy Quark Current Correlators at Four-Loop Order in Perturbative QCD," *JHEP* **09** (2008) 075, `arXiv:0805.3358 [hep-ph]`.

[106] Y. Kiyo, A. Maier, P. Maierhofer, and P. Marquard, "Reconstruction of heavy quark current correlators at O(alpha(s)**3)," *Nucl. Phys. B* **823** (2009) 269–287, `arXiv:0907.2120 [hep-ph]`.

[107] A. Maier, P. Maierhofer, P. Marquard, and A. V. Smirnov, "Low energy moments of heavy quark current correlators at four loops," *Nucl. Phys. B* **824** (2010) 1–18, `arXiv:0907.2117 [hep-ph]`.

[108] **HPQCD** Collaboration, I. Allison *et al.*, "High-Precision Charm-Quark Mass from Current-Current Correlators in Lattice and Continuum QCD," *Phys. Rev. D* **78** (2008) 054513, `arXiv:0805.2999 [hep-lat]`.

[109] B. Chakraborty, C. T. H. Davies, B. Galloway, P. Knecht, J. Koponen, G. C. Donald, R. J. Dowdall, G. P. Lepage, and C. McNeile, "High-precision quark masses and QCD coupling from $n_f = 4$ lattice QCD," *Phys. Rev. D* **91** no. 5, (2015) 054508, `arXiv:1408.4169 [hep-lat]`.

[110] Y. Maezawa and P. Petreczky, "Quark masses and strong coupling constant in 2+1 flavor QCD," *Phys. Rev. D* **94** no. 3, (2016) 034507, `arXiv:1606.08798 [hep-lat]`.

[111] P. Petreczky and J. H. Weber, "Strong coupling constant and heavy quark masses in (2+1)-flavor QCD," *Phys. Rev. D* **100** no. 3, (2019) 034519, `arXiv:1901.06424 [hep-lat]`.

[112] P. Petreczky and J. H. Weber, "Strong coupling constant from moments of quarkonium correlators revisited," *Eur. Phys. J. C* **82** no. 1, (2022) 64, `arXiv:2012.06193 [hep-lat]`.

[113] P. A. Baikov, K. G. Chetyrkin, and J. H. Kuhn, "Order alpha**4(s) QCD Corrections to Z and tau Decays," *Phys. Rev. Lett.* **101** (2008) 012002, `arXiv:0801.1821 [hep-ph]`.

[114] **JLQCD, TWQCD** Collaboration, E. Shintani, S. Aoki, T. W. Chiu, S. Hashimoto, T. H. Hsieh, T. Kaneko, H. Matsufuru, J. Noaki, T. Onogi, and N. Yamada, "Lattice study of the vacuum polarization function and determination of the strong coupling constant," *Phys. Rev. D* **79** (2009) 074510, `arXiv:0807.0556 [hep-lat]`.

[115] E. Shintani, S. Aoki, H. Fukaya, S. Hashimoto, T. Kaneko, T. Onogi, and N. Yamada, "Strong coupling constant from vacuum polarization functions in three-flavor lattice QCD with dynamical overlap fermions," *Phys. Rev. D* **82** no. 7, (2010) 074505, `arXiv:1002.0371 [hep-lat]`. [Erratum: Phys.Rev.D 89, 099903 (2014)].

[116] R. J. Hudspith, R. Lewis, K. Maltman, and E. Shintani, "α_s from the Lattice Hadronic Vacuum Polarisation," `arXiv:1804.10286 [hep-lat]`.

[117] S. Cali, K. Cichy, P. Korcyl, and J. Simeth, "Running coupling constant from position-space current-current correlation functions in three-flavor lattice QCD," *Phys. Rev. Lett.* **125** (2020)

242002, `arXiv:2003.05781 [hep-lat]`.

[118] B. Alles, D. Henty, H. Panagopoulos, C. Parrinello, C. Pittori, and D. G. Richards, "α_s from the nonperturbatively renormalised lattice three gluon vertex," *Nucl. Phys. B* **502** (1997) 325–342, `arXiv:hep-lat/9605033`.

[119] P. Boucaud, J. P. Leroy, H. Moutarde, J. Micheli, O. Pene, J. Rodriguez-Quintero, and C. Roiesnel, "Preliminary calculation of alpha(s) from Green functions with dynamical quarks," *JHEP* **01** (2002) 046, `arXiv:hep-ph/0107278`.

[120] **ETM** Collaboration, B. Blossier, P. Boucaud, F. De soto, V. Morenas, M. Gravina, O. Pene, and J. Rodriguez-Quintero, "Ghost-gluon coupling, power corrections and $\Lambda_{\overline{MS}}$ from twisted-mass lattice QCD at Nf=2," *Phys. Rev. D* **82** (2010) 034510, `arXiv:1005.5290 [hep-lat]`.

[121] B. Blossier, P. Boucaud, M. Brinet, F. De Soto, X. Du, M. Gravina, V. Morenas, O. Pene, K. Petrov, and J. Rodriguez-Quintero, "Ghost-gluon coupling, power corrections and $\Lambda_{\overline{MS}}$ from lattice QCD with a dynamical charm," *Phys. Rev. D* **85** (2012) 034503, `arXiv:1110.5829 [hep-lat]`.

[122] B. Blossier, P. Boucaud, M. Brinet, F. De Soto, X. Du, V. Morenas, O. Pene, K. Petrov, and J. Rodriguez-Quintero, "The Strong running coupling at τ and Z_0 mass scales from lattice QCD," *Phys. Rev. Lett.* **108** (2012) 262002, `arXiv:1201.5770 [hep-ph]`.

[123] **ETM** Collaboration, B. Blossier, P. Boucaud, M. Brinet, F. De Soto, V. Morenas, O. Pene, K. Petrov, and J. Rodriguez-Quintero, "High statistics determination of the strong coupling constant in Taylor scheme and its OPE Wilson coefficient from lattice QCD with a dynamical charm," *Phys. Rev. D* **89** no. 1, (2014) 014507, `arXiv:1310.3763 [hep-ph]`.

[124] S. Zafeiropoulos, P. Boucaud, F. De Soto, J. Rodríguez-Quintero, and J. Segovia, "Strong Running Coupling from the Gauge Sector of Domain Wall Lattice QCD with Physical Quark Masses," *Phys. Rev. Lett.* **122** no. 16, (2019) 162002, `arXiv:1902.08148 [hep-ph]`.

[125] **ALPHA** Collaboration, M. Dalla Brida, R. Höllwieser, F. Knechtli, T. Korzec, A. Ramos, and R. Sommer, "Non-perturbative renormalization by decoupling," *Phys. Lett. B* **807** (2020) 135571, `arXiv:1912.06001 [hep-lat]`.

[126] K. G. Chetyrkin and J. H. Kuhn, "Quartic mass corrections to R(had)," *Nucl. Phys. B* **432** (1994) 337–350, `arXiv:hep-ph/9406299`.

[127] J.-L. Kneur and A. Neveu, "Chiral condensate from renormalization group optimized perturbation," *Phys. Rev. D* **92** no. 7, (2015) 074027, `arXiv:1506.07506 [hep-ph]`.

[128] M. Dalla Brida, "Past, present, and future of precision determinations of the QCD parameters from lattice QCD," *Eur. Phys. J. A* **57** no. 2, (2021) 66, `arXiv:2012.01232 [hep-lat]`.

[129] L. Del Debbio and A. Ramos, "Lattice determinations of the strong coupling," `arXiv:2101.04762 [hep-lat]`.

[130] S. Aoki *et al.*, "Review of Lattice Results Concerning Low-Energy Particle Physics," *Eur. Phys. J. C* **74** (2014) 2890, `arXiv:1310.8555 [hep-lat]`.

[131] S. Aoki *et al.*, "Review of lattice results concerning low-energy particle physics," *Eur. Phys. J. C* **77** no. 2, (2017) 112, `arXiv:1607.00299 [hep-lat]`.

[132] **Flavour Lattice Averaging Group** Collaboration, S. Aoki *et al.*, "FLAG Review 2019: Flavour Lattice Averaging Group (FLAG)," *Eur. Phys. J. C* **80** no. 2, (2020) 113, `arXiv:1902.08191 [hep-lat]`.

[133] J. Vermaseren, S. Larin, and T. van Ritbergen, "The four loop quark mass anomalous dimension and the invariant quark mass," *Phys.Lett.* **B405** (1997) 327–333, `arXiv:hep-ph/9703284 [hep-ph]`.

[134] K. G. Chetyrkin, "Quark mass anomalous dimension to O (alpha-s**4)," *Phys. Lett. B* **404** (1997) 161–165, `arXiv:hep-ph/9703278`.

[135] P. A. Baikov, K. G. Chetyrkin, and J. H. Kühn, "Quark Mass and Field Anomalous Dimensions to $\mathcal{O}(\alpha_s^5)$," *JHEP* **10** (2014) 076, `arXiv:1402.6611 [hep-ph]`.

[136] F. Herren and M. Steinhauser, "Version 3 of RunDec and CRunDec," *Comput. Phys. Commun.* **224** (2018) 333–345, `arXiv:1703.03751 [hep-ph]`.

[137] A. H. Hoang, C. Lepenik, and V. Mateu, "REvolver: Automated running and matching of couplings and masses in QCD," `arXiv:2102.01085 [hep-ph]`.

[138] S. Narison, "$\overline{m}_c$ and $\overline{m}_b$ from M_{Bc} and improved estimates of f_{Bc} and $f_{Bc(2S)}$," *Phys. Lett. B* **802** (2020) 135221, `arXiv:1906.03614 [hep-ph]`.

[139] C. Peset, A. Pineda, and J. Segovia, "The charm/bottom quark mass from heavy quarkonium at N3LO," *JHEP* **09** (2018) 167, `arXiv:1806.05197 [hep-ph]`.

[140] Y. Kiyo, G. Mishima, and Y. Sumino, "Determination of m_c and m_b from quarkonium 1S energy levels in perturbative QCD," *Phys. Lett.* **B752** (2016) 122–127, arXiv:1510.07072 [hep-ph]. [Erratum: Phys. Lett.B772,878(2017)].

[141] A. A. Penin and N. Zerf, "Bottom Quark Mass from Υ Sum Rules to $\mathcal{O}(\alpha_s^3)$," *JHEP* **04** (2014) 120, arXiv:1401.7035 [hep-ph].

[142] A. Alberti, P. Gambino, K. J. Healey, and S. Nandi, "Precision Determination of the Cabibbo-Kobayashi-Maskawa Element V_{cb}," *Phys. Rev. Lett.* **114** no. 6, (2015) 061802, arXiv:1411.6560 [hep-ph].

[143] M. Beneke, A. Maier, J. Piclum, and T. Rauh, "The bottom-quark mass from non-relativistic sum rules at NNNLO," *Nucl. Phys. B* **891** (2015) 42–72, arXiv:1411.3132 [hep-ph].

[144] B. Dehnadi, A. H. Hoang, and V. Mateu, "Bottom and Charm Mass Determinations with a Convergence Test," *JHEP* **08** (2015) 155, arXiv:1504.07638 [hep-ph].

[145] W. Lucha, D. Melikhov, and S. Simula, "Accurate bottom-quark mass from Borel QCD sum rules for f_B and f_{B_s}," *Phys. Rev. D* **88** (2013) 056011, arXiv:1305.7099 [hep-ph].

[146] S. Bodenstein, J. Bordes, C. Dominguez, J. Penarrocha, and K. Schilcher, "Bottom-quark mass from finite energy QCD sum rules," *Phys. Rev. D* **85** (2012) 034003, arXiv:1111.5742 [hep-ph].

[147] A. Laschka, N. Kaiser, and W. Weise, "Quark-antiquark potential to order 1/m and heavy quark masses," *Phys. Rev. D* **83** (2011) 094002, arXiv:1102.0945 [hep-ph].

[148] K. Chetyrkin, J. Kuhn, A. Maier, P. Maierhofer, P. Marquard, M. Steinhauser, and C. Sturm, "Charm and Bottom Quark Masses: An Update," *Phys. Rev. D* **80** (2009) 074010, arXiv:0907.2110 [hep-ph].

[149] **Fermilab Lattice, MILC, TUMQCD** Collaboration, A. Bazavov *et al.*, "Up-, down-, strange-, charm-, and bottom-quark masses from four-flavor lattice QCD," *Phys. Rev. D* **98** no. 5, (2018) 054517, arXiv:1802.04248 [hep-lat].

[150] B. Colquhoun, R. Dowdall, C. Davies, K. Hornbostel, and G. Lepage, "Υ and Υ' Leptonic Widths, a_μ^b and m_b from full lattice QCD," *Phys. Rev. D* **91** no. 7, (2015) 074514, arXiv:1408.5768 [hep-lat].

[151] F. Bernardoni *et al.*, "The b-quark mass from non-perturbative $N_f = 2$ Heavy Quark Effective Theory at $O(1/m_h)$," *Phys. Lett. B* **730** (2014) 171–177, arXiv:1311.5498 [hep-lat].

[152] **HPQCD** Collaboration, A. Lee, C. Monahan, R. Horgan, C. Davies, R. Dowdall, and J. Koponen, "Mass of the b quark from lattice NRQCD and lattice perturbation theory," *Phys. Rev. D* **87** no. 7, (2013) 074018, arXiv:1302.3739 [hep-lat].

[153] **ETM** Collaboration, P. Dimopoulos *et al.*, "Lattice QCD determination of m_b, f_B and f_{Bs} with twisted mass Wilson fermions," *JHEP* **01** (2012) 046, arXiv:1107.1441 [hep-lat].

[154] **Flavour Lattice Averaging Group** Collaboration, S. Aoki *et al.*, "FLAG Review 2019: Flavour Lattice Averaging Group (FLAG)," *Eur. Phys. J. C* **80** no. 2, (2020) 113, arXiv:1902.08191 [hep-lat].

[155] **H1, ZEUS** Collaboration, H. Abramowicz *et al.*, "Combination and QCD analysis of charm and beauty production cross-section measurements in deep inelastic ep scattering at HERA," *Eur. Phys. J. C* **78** no. 6, (2018) 473, arXiv:1804.01019 [hep-ex].

[156] **Belle** Collaboration, C. Schwanda *et al.*, "Measurement of the Moments of the Photon Energy Spectrum in B —> X(s) gamma Decays and Determination of —V(cb)— and m(b) at Belle," *Phys. Rev. D* **78** (2008) 032016, arXiv:0803.2158 [hep-ex].

[157] **BaBar** Collaboration, B. Aubert *et al.*, "Measurement and interpretation of moments in inclusive semileptonic decays anti-B —> X(c) l- anti-nu," *Phys. Rev. D* **81** (2010) 032003, arXiv:0908.0415 [hep-ex].

[158] **DELPHI** Collaboration, P. Abreu *et al.*, "m_b at M_Z," *Phys. Lett.* **B418** (1998) 430–442.

[159] **ALEPH** Collaboration, R. Barate *et al.*, "A Measurement of the b quark mass from hadronic Z decays," *Eur. Phys. J.* **C18** (2000) 1–13, arXiv:hep-ex/0008013 [hep-ex].

[160] **OPAL** Collaboration, G. Abbiendi *et al.*, "Determination of the b quark mass at the Z mass scale," *Eur. Phys. J.* **C21** (2001) 411–422, arXiv:hep-ex/0105046 [hep-ex].

[161] **DELPHI** Collaboration, J. Abdallah *et al.*, "Determination of the b quark mass at the M(Z) scale with the DELPHI detector at LEP," *Eur. Phys. J.* **C46** (2006) 569–583, arXiv:hep-ex/0603046 [hep-ex].

[162] **DELPHI** Collaboration, J. Abdallah *et al.*, "Study of b-quark mass effects in multijet topologies

with the DELPHI detector at LEP," *Eur. Phys. J.* **C55** (2008) 525–538, `arXiv:0804.3883 [hep-ex]`.

[163] A. Brandenburg, P. N. Burrows, D. Muller, N. Oishi, and P. Uwer, "Measurement of the running b quark mass using $e^+e^- \to b\bar{b}g$ events," *Phys. Lett.* **B468** (1999) 168–177, `arXiv:hep-ph/9905495 [hep-ph]`.

[164] **SLD** Collaboration, K. Abe *et al.*, "An Improved test of the flavor independence of strong interactions," *Phys. Rev.* **D59** (1999) 012002, `arXiv:hep-ex/9805023 [hep-ex]`.

[165] J. Aparisi *et al.*, "mb at mH: The Running Bottom Quark Mass and the Higgs Boson," *Phys. Rev. Lett.* **128** no. 12, (2022) 122001, `arXiv:2110.10202 [hep-ph]`.

[166] ATLAS Collaboration, "A combination of measurements of Higgs boson production and decay using up to 139 fb^{-1} of proton–proton collision data at $\sqrt{s} = 13$ TeV collected with the ATLAS experiment." ATLAS-CONF-2020-027, 2020. `https://cds.cern.ch/record/2725733`.

[167] CMS collaboration, "Combined measurements of Higgs boson couplings in proton–proton collisions at $\sqrt{s} = 13$ TeV," *Eur. Phys. J.* **C79** no. 5, (2019) 421, `arXiv:1809.10733 [hep-ex]`.

[168] J. Aparisi *et al.*, "Snowmass White Paper: prospects for measurements of the bottom quark mass," `arXiv:2203.16994 [hep-ex]`.

[169] A. Gizhko *et al.*, "Running of the Charm-Quark Mass from HERA Deep-Inelastic Scattering Data," *Phys. Lett. B* **775** (2017) 233–238, `arXiv:1705.08863 [hep-ph]`.

[170] J. Fuster, A. Irles, G. Rodrigo, S. Tairafune, M. Vos, H. Yamamoto, and R. Yonamine, "Prospects for the measurement of the b-quark mass at the ILC," in *International Workshop on Future Linear Colliders*. 4, 2021. `arXiv:2104.09924 [hep-ex]`.

[171] J. de Blas *et al.*, "Higgs Boson Studies at Future Particle Colliders," *JHEP* **01** (2020) 139, `arXiv:1905.03764 [hep-ph]`.

[172] M. Cepeda *et al.*, "Report from Working Group 2: Higgs Physics at the HL-LHC and HE-LHC," *CERN Yellow Rep. Monogr.* **7** (2019) 221–584, `arXiv:1902.00134 [hep-ph]`.

[173] J. Yan, S. Watanuki, K. Fujii, A. Ishikawa, D. Jeans, J. Strube, J. Tian, and H. Yamamoto, "Measurement of the Higgs boson mass and $e^+e^- \to ZH$ cross section using $Z \to \mu^+\mu^-$ and $Z \to e^+e^-$ at the ILC," *Phys. Rev. D* **94** no. 11, (2016) 113002, `arXiv:1604.07524 [hep-ex]`. [Erratum: Phys.Rev.D 103, 099903 (2021)].

[174] L. T. Brady, A. Accardi, W. Melnitchouk, and J. F. Owens, "Impact of PDF uncertainties at large x on heavy boson production," *JHEP* **06** (2012) 019, `arXiv:1110.5398 [hep-ph]`.

[175] R. D. Ball, V. Bertone, M. Bonvini, S. Marzani, J. Rojo, and L. Rottoli, "Parton distributions with small-x resummation: evidence for BFKL dynamics in HERA data," *Eur. Phys. J. C* **78** no. 4, (2018) 321, `arXiv:1710.05935 [hep-ph]`.

[176] J. Campbell *et al.*, "Working Group Report: Quantum Chromodynamics," in *Community Summer Study 2013: Snowmass on the Mississippi*. 10, 2013. `arXiv:1310.5189 [hep-ph]`.

[177] L. A. Harland-Lang, A. D. Martin, P. Motylinski, and R. S. Thorne, "Parton distributions in the LHC era: MMHT 2014 PDFs," *Eur. Phys. J. C* **75** no. 5, (2015) 204, `arXiv:1412.3989 [hep-ph]`.

[178] S. Dulat, T.-J. Hou, J. Gao, M. Guzzi, J. Huston, P. Nadolsky, J. Pumplin, C. Schmidt, D. Stump, and C. P. Yuan, "New parton distribution functions from a global analysis of quantum chromodynamics," *Phys. Rev.* **D93** no. 3, (2016) 033006, `arXiv:1506.07443 [hep-ph]`.

[179] **H1, ZEUS** Collaboration, H. Abramowicz *et al.*, "Combination of measurements of inclusive deep inelastic $e^\pm p$ scattering cross sections and QCD analysis of HERA data," *Eur. Phys. J. C* **75** no. 12, (2015) 580, `arXiv:1506.06042 [hep-ex]`.

[180] A. Accardi, L. T. Brady, W. Melnitchouk, J. F. Owens, and N. Sato, "Constraints on large-x parton distributions from new weak boson production and deep-inelastic scattering data," *Phys. Rev. D* **93** no. 11, (2016) 114017, `arXiv:1602.03154 [hep-ph]`.

[181] S. Alekhin, J. Blümlein, S. Moch, and R. Placakyte, "Parton distribution functions, α_s, and heavy-quark masses for LHC Run II," *Phys. Rev. D* **96** no. 1, (2017) 014011, `arXiv:1701.05838 [hep-ph]`.

[182] **NNPDF** Collaboration, R. D. Ball *et al.*, "Parton distributions from high-precision collider data," *Eur. Phys. J. C* **77** no. 10, (2017) 663, `arXiv:1706.00428 [hep-ph]`.

[183] S. Bailey, T. Cridge, L. A. Harland-Lang, A. D. Martin, and R. S. Thorne, "Parton distributions from LHC, HERA, Tevatron and fixed target data: MSHT20 PDFs," *Eur. Phys. J. C* **81** no. 4, (2021) 341, `arXiv:2012.04684 [hep-ph]`.

[184] **NNPDF** Collaboration, R. D. Ball *et al.*, "The path to proton structure at 1% accuracy," *Eur. Phys. J. C* **82** no. 5, (2022) 428, arXiv:2109.02653 [hep-ph].

[185] **ATLAS** Collaboration, G. Aad *et al.*, "Determination of the parton distribution functions of the proton using diverse ATLAS data from pp collisions at $\sqrt{s} = 7$, 8 and 13 TeV," *Eur. Phys. J. C* **82** no. 5, (2022) 438, arXiv:2112.11266 [hep-ex].

[186] A. Courtoy, J. Huston, P. Nadolsky, K. Xie, M. Yan, and C. P. Yuan, "Parton distributions need representative sampling," arXiv:2205.10444 [hep-ph].

[187] The PDF4LHC working group. https://www.hep.ucl.ac.uk/pdf4lhc/.

[188] R. D. Ball *et al.*, "The PDF4LHC21 combination of global PDF fits for the LHC Run III," arXiv:2203.05506 [hep-ph].

[189] J. Butterworth *et al.*, "PDF4LHC recommendations for LHC Run II," *J. Phys. G* **43** (2016) 023001, arXiv:1510.03865 [hep-ph].

[190] R. Abdul Khalek, S. Bailey, J. Gao, L. Harland-Lang, and J. Rojo, "Towards Ultimate Parton Distributions at the High-Luminosity LHC," *Eur. Phys. J. C* **78** no. 11, (2018) 962, arXiv:1810.03639 [hep-ph].

[191] S. Amoroso *et al.*, "Les Houches 2019: Physics at TeV Colliders: Standard Model Working Group Report," in *11th Les Houches Workshop on Physics at TeV Colliders: PhysTeV Les Houches*. 3, 2020. arXiv:2003.01700 [hep-ph].

[192] ATLAS Collaboration, "Prospects for jet and photon physics at the HL-LHC and HE-LHC." ATL-PHYS-PUB-2018-051, 2018. https://cds.cern.ch/record/2652285.

[193] CMS Collaboration, "Projection of measurements of differential ttbar production cross sections in the e/u+jets channels in pp collisions at the HL-LHC," CMS Physics Analysis Summary CMS-PAS-FTR-18-015, CERN, 2018. http://cds.cern.ch/record/2651195.

[194] J. Gao, L. Harland-Lang, and J. Rojo, "The Structure of the Proton in the LHC Precision Era," *Phys. Rept.* **742** (2018) 1–121, arXiv:1709.04922 [hep-ph].

[195] J. Campbell, J. Huston, and F. Krauss, *The Black Book of Quantum Chromodynamics: A Primer for the LHC Era*. Oxford University Press, 2018.

[196] T. J. Hobbs, B.-T. Wang, P. M. Nadolsky, and F. I. Olness, "Charting the coming synergy between lattice QCD and high-energy phenomenology," *Phys. Rev. D* **100** no. 9, (2019) 094040, arXiv:1904.00022 [hep-ph].

[197] A. Accardi, T. J. Hobbs, X. Jing, and P. M. Nadolsky, "Deuterium scattering experiments in CTEQ global QCD analyses: a comparative investigation," *Eur. Phys. J. C* **81** no. 7, (2021) 603, arXiv:2102.01107 [hep-ph].

[198] **Jefferson Lab Angular Momentum** Collaboration, J. Cammarota, L. Gamberg, Z.-B. Kang, J. A. Miller, D. Pitonyak, A. Prokudin, T. C. Rogers, and N. Sato, "Origin of single transverse-spin asymmetries in high-energy collisions," *Phys. Rev. D* **102** no. 5, (2020) 054002, arXiv:2002.08384 [hep-ph].

[199] R. Gupta, Y.-C. Jang, B. Yoon, H.-W. Lin, V. Cirigliano, and T. Bhattacharya, "Isovector Charges of the Nucleon from 2+1+1-flavor Lattice QCD," *Phys. Rev.* **D98** (2018) 034503, arXiv:1806.09006 [hep-lat].

[200] C. Alexandrou, S. Bacchio, M. Constantinou, J. Finkenrath, K. Hadjiyiannakou, K. Jansen, G. Koutsou, and A. Vaquero Aviles-Casco, "Nucleon axial, tensor, and scalar charges and σ-terms in lattice QCD," *Phys. Rev. D* **102** no. 5, (2020) 054517, arXiv:1909.00485 [hep-lat].

[201] M. Arratia, Y. Furletova, T. J. Hobbs, F. Olness, and S. J. Sekula, "Charm jets as a probe for strangeness at the future Electron-Ion Collider," *Phys. Rev. D* **103** no. 7, (2021) 074023, arXiv:2006.12520 [hep-ph].

[202] F. Gelis, E. Iancu, J. Jalilian-Marian, and R. Venugopalan, "The Color Glass Condensate," *Ann. Rev. Nucl. Part. Sci.* **60** (2010) 463–489, arXiv:1002.0333 [hep-ph].

[203] CMS Collaboration, "Constraining nuclear parton distributions with heavy ion collisions at the HL-LHC with the CMS experiment," CMS Physics Analysis Summary CMS-PAS-FTR-18-027, CERN, 2018. http://cds.cern.ch/record/2652030.

[204] ATLAS Collaboration, "Expected ATLAS Measurement Capabilities of Observables Sensitive to Nuclear Parton Distributions." ATL-PHYS-PUB-2018-039, 2018. https://cds.cern.ch/record/2649445.

[205] K. J. Eskola, P. Paakkinen, H. Paukkunen, and C. A. Salgado, "EPPS16: Nuclear parton

distributions with LHC data," *Eur. Phys. J. C* **77** no. 3, (2017) 163, `arXiv:1612.05741 [hep-ph]`.

[206] **NNPDF** Collaboration, R. Abdul Khalek, J. J. Ethier, and J. Rojo, "Nuclear parton distributions from lepton-nucleus scattering and the impact of an electron-ion collider," *Eur. Phys. J. C* **79** no. 6, (2019) 471, `arXiv:1904.00018 [hep-ph]`.

[207] R. Abdul Khalek, J. J. Ethier, J. Rojo, and G. van Weelden, "nNNPDF2.0: quark flavor separation in nuclei from LHC data," *JHEP* **09** (2020) 183, `arXiv:2006.14629 [hep-ph]`.

[208] **ALICE** Collaboration, S. Acharya *et al.*, "Coherent J/ψ and ψ' photoproduction at midrapidity in ultra-peripheral Pb-Pb collisions at $\sqrt{s_{\mathrm{NN}}}$ = 5.02 TeV" *Eur. Phys. J. C* **81** no. 8, (2021) 712, `arXiv:2101.04577 [nucl-ex]`.

[209] **LHCb** Collaboration, W. Duan, "Charmonia photo-production in ultra-peripheral and peripheral PbPb collisions with LHCb," in *Low-x Workshop 2021*. 12, 2021. `arXiv:2112.10300 [nucl-ex]`.

[210] **CMS** Collaboration, V. Khachatryan *et al.*, "Coherent J/ψ photoproduction in ultra-peripheral PbPb collisions at $\sqrt{s_{NN}} = 2.76$ TeV with the CMS experiment," *Phys. Lett. B* **772** (2017) 489–511, `arXiv:1605.06966 [nucl-ex]`.

[211] V. Guzey, E. Kryshen, M. Strikman, and M. Zhalov, "Nuclear suppression from coherent J/ψ photoproduction at the Large Hadron Collider," *Phys. Lett. B* **816** (2021) 136202, `arXiv:2008.10891 [hep-ph]`.

[212] K. J. Eskola, C. A. Flett, V. Guzey, T. Löytäinen, and H. Paukkunen, "Exclusive J/ψ photoproduction in ultraperipheral Pb+Pb collisions at the LHC to next-to-leading order perturbative QCD," `arXiv:2203.11613 [hep-ph]`.

[213] **ATLAS** Collaboration, "Photo-nuclear dijet production in ultra-peripheral Pb+Pb collisions." ATLAS-CONF-2017-011, 2017.

[214] V. Emel'yanov, A. Khodinov, S. R. Klein, and R. Vogt, "The Effect of shadowing on initial conditions, transverse energy and hard probes in ultrarelativistic heavy ion collisions," *Phys. Rev. C* **61** (2000) 044904, `arXiv:hep-ph/9909427`.

[215] L. Frankfurt, V. Guzey, and M. Strikman, "Leading Twist Nuclear Shadowing Phenomena in Hard Processes with Nuclei," *Phys. Rept.* **512** (2012) 255–393, `arXiv:1106.2091 [hep-ph]`.

[216] A. C. Aguilar *et al.*, "Pion and Kaon Structure at the Electron-Ion Collider," *Eur. Phys. J. A* **55** no. 10, (2019) 190, `arXiv:1907.08218 [nucl-ex]`.

[217] C. D. Roberts, D. G. Richards, T. Horn, and L. Chang, "Insights into the emergence of mass from studies of pion and kaon structure," *Prog. Part. Nucl. Phys.* **120** (2021) 103883, `arXiv:2102.01765 [hep-ph]`.

[218] P. C. Barry *et al.*, "Complementarity of experimental and lattice QCD data on pion parton distributions," `arXiv:2204.00543 [hep-ph]`.

[219] A. Metz and A. Vossen, "Parton Fragmentation Functions," *Prog. Part. Nucl. Phys.* **91** (2016) 136–202, `arXiv:1607.02521 [hep-ex]`.

[220] M. Anselmino, A. Mukherjee, and A. Vossen, "Transverse spin effects in hard semi-inclusive collisions," *Prog. Part. Nucl. Phys.* **114** (2020) 103806, `arXiv:2001.05415 [hep-ph]`.

[221] M. Burkardt, "Transverse force on quarks in deep-inelastic scattering," *Phys. Rev. D* **88** (2013) 114502, `arXiv:0810.3589 [hep-ph]`.

[222] **CLAS** Collaboration, M. Mirazita *et al.*, "Beam Spin Asymmetry in Semi-Inclusive Electroproduction of Hadron Pairs," *Phys. Rev. Lett.* **126** no. 6, (2021) 062002, `arXiv:2010.09544 [hep-ex]`.

[223] T. B. Hayward *et al.*, "Observation of Beam Spin Asymmetries in the Process $ep \to e'\pi^+\pi^- X$ with CLAS12," *Phys. Rev. Lett.* **126** (2021) 152501, `arXiv:2101.04842 [hep-ex]`.

[224] A. Courtoy, A. S. Miramontes, H. Avakian, M. Mirazita, and S. Pisano, "Extraction of the higher-twist parton distribution e(x) from CLAS data," *Phys. Rev. D* **106** no. 1, (2022) 014027, `arXiv:2203.14975 [hep-ph]`.

[225] T. Sjöstrand, S. Ask, J. R. Christiansen, R. Corke, N. Desai, P. Ilten, S. Mrenna, S. Prestel, C. O. Rasmussen, and P. Z. Skands, "An Introduction to PYTHIA 8.2" *Comput. Phys. Commun.* **191** (2015) 159–177, `arXiv:1410.3012 [hep-ph]`.

[226] J. Bellm *et al.*, "Herwig 7.2 release note," *Eur. Phys. J. C* **80** no. 5, (2020) 452, `arXiv:1912.06509 [hep-ph]`.

[227] **Sherpa** Collaboration, E. Bothmann *et al.*, "Event Generation with Sherpa 2.2" *SciPost Phys.* **7** no. 3, (2019) 034, `arXiv:1905.09127 [hep-ph]`.

[228] J. Brehmer, F. Kling, I. Espejo, and K. Cranmer, "MadMiner: Machine learning-based inference for particle physics," *Comput. Softw. Big Sci.* **4** no. 1, (2020) 3, `arXiv:1907.10621 [hep-ph]`.

[229] **ATLAS** Collaboration, G. Aad *et al.*, "Measurement of the Lund Jet Plane Using Charged Particles in 13 TeV Proton-Proton Collisions with the ATLAS Detector," *Phys. Rev. Lett.* **124** no. 22, (2020) 222002, `arXiv:2004.03540 [hep-ex]`.

[230] D. d'Enterria, K. J. Eskola, I. Helenius, and H. Paukkunen, "Confronting current NLO parton fragmentation functions with inclusive charged-particle spectra at hadron colliders," *Nucl. Phys. B* **883** (2014) 615–628, `arXiv:1311.1415 [hep-ph]`.

[231] S. Albino *et al.*, "Parton fragmentation in the vacuum and in the medium," `arXiv:0804.2021 [hep-ph]`.

[232] A. Accardi, F. Arleo, W. K. Brooks, D. D'Enterria, and V. Muccifora, "Parton Propagation and Fragmentation in QCD Matter," *Riv. Nuovo Cim.* **32** no. 9-10, (2009) 439–554, `arXiv:0907.3534 [nucl-th]`.

[233] M. Boglione and A. Simonelli, "Kinematic regions in the $e^+e^- \to h\,X$ factorized cross section in a 2-jet topology with thrust," *JHEP* **02** (2022) 013, `arXiv:2109.11497 [hep-ph]`.

[234] M. Boglione and A. Simonelli, "Factorization of $e^+e^- \to H\,X$ cross section, differential in z_h, P_T and thrust, in the 2-jet limit," *JHEP* **02** (2021) 076, `arXiv:2011.07366 [hep-ph]`.

[235] M. Boglione and A. Simonelli, "Universality-breaking effects in e^+e^- hadronic production processes," *Eur. Phys. J. C* **81** no. 1, (2021) 96, `arXiv:2007.13674 [hep-ph]`.

[236] H.-M. Chang, M. Procura, J. Thaler, and W. J. Waalewijn, "Calculating Track Thrust with Track Functions," *Phys. Rev. D* **88** (2013) 034030, `arXiv:1306.6630 [hep-ph]`.

[237] M. Jaarsma, Y. Li, I. Moult, W. Waalewijn, and H. X. Zhu, "Renormalization Group Flows for Track Function Moments," `arXiv:2201.05166 [hep-ph]`.

[238] Y. Li, I. Moult, S. S. van Velzen, W. J. Waalewijn, and H. X. Zhu, "Extending Precision Perturbative QCD with Track Functions," *Phys. Rev. Lett.* **128** no. 18, (2022) 182001, `arXiv:2108.01674 [hep-ph]`.

[239] V. A. Khoze and T. Sjostrand, "Color correlations and multiplicities in top events," *Phys. Lett. B* **328** (1994) 466, `arXiv:hep-ph/9403394`.

[240] S. Argyropoulos and T. Sjöstrand, "Effects of color reconnection on $t\bar{t}$ final states at the LHC," *JHEP* **11** (2014) 043, `arXiv:1407.6653 [hep-ph]`.

[241] D. d'Enterria, P. Z. Skands, *et al.*, "Parton radiation and fragmentation from LHC to FCC-ee," `arXiv:1702.01329 [hep-ph]`.

[242] J. R. Christiansen and T. Sjöstrand, "Color reconnection at future e$^+$ e$^-$ colliders," *Eur. Phys. J. C* **75** no. 9, (2015) 441, `arXiv:1506.09085 [hep-ph]`.

[243] T. Sjostrand and V. A. Khoze, "On Color rearrangement in hadronic W+ W- events," *Z. Phys. C* **62** (1994) 281–310, `hep-ph/9310242`.

[244] **ALEPH, DELPHI, L3, OPAL, LEP Electroweak** Collaboration, S. Schael *et al.*, "Electroweak Measurements in Electron-Positron Collisions at W-Boson-Pair Energies at LEP," *Phys. Rept.* **532** (2013) 119–244, `arXiv:1302.3415 [hep-ex]`.

[245] **FCC** Collaboration, A. Abada *et al.*, "FCC Physics Opportunities," *Eur. Phys. J.* **C79** no. 6, (2019) 474.

[246] CMS Collaboration, "High-p_T jet measurements at the HL-LHC," CMS Physics Analysis Summary CMS-PAS-FTR-18-032, CERN, 2018. `http://cds.cern.ch/record/2651219`.

[247] ATLAS Collaboration, "Measurement of the inclusive and dijet cross-sections of b-jets in pp collisions at $\sqrt{s} = 7\,\text{TeV}$ with the ATLAS detector," *Eur. Phys. J. C* **71** (2011) 1846, `arXiv:1109.6833 [hep-ex]`.

[248] ATLAS Collaboration, "Measurement of the $b\bar{b}$ dijet cross section in pp collisions at $\sqrt{s} = 7\,\text{TeV}$ with the ATLAS detector," *Eur. Phys. J. C* **76** (2016) 670, `arXiv:1607.08430 [hep-ex]`.

[249] CMS Collaboration, "Studies of inclusive four-jet production with two b-tagged jets in proton–proton collisions at 7 TeV," *Phys. Rev. D* **94** (2016) 112005, `arXiv:1609.03489 [hep-ex]`.

[250] CMS Collaboration, "Inclusive b-jet production in pp collisions at $\sqrt{s} = 7\,\text{TeV}$," *JHEP* **04** (2012) 084, `arXiv:1202.4617 [hep-ex]`.

[251] GEANT4 Collaboration, S. Agostinelli, *et al.*, "GEANT4 – a simulation toolkit," *Nucl. Instrum. Meth. A* **506** (2003) 250.

[252] F. Dreyer, G. Soyez, and A. Takacs, "Quarks and gluons in the Lund plane," `arXiv:2112.09140`

[253] H.-W. Lin *et al.*, "Parton distributions and lattice QCD calculations: a community white paper," *Prog. Part. Nucl. Phys.* **100** (2018) 107–160, `arXiv:1711.07916 [hep-ph]`.

[254] M. Constantinou *et al.*, "Parton distributions and lattice-QCD calculations: Toward 3D structure," *Prog. Part. Nucl. Phys.* **121** (2021) 103908, `arXiv:2006.08636 [hep-ph]`.

[255] X. Ji, Y.-S. Liu, Y. Liu, J.-H. Zhang, and Y. Zhao, "Large-momentum effective theory," *Rev. Mod. Phys.* **93** no. 3, (2021) 035005, `arXiv:2004.03543 [hep-ph]`.

[256] X. Ji, "Why is LaMET an effective field theory for partonic structure?," `arXiv:2007.06613 [hep-ph]`.

[257] H.-W. Lin, W. Melnitchouk, A. Prokudin, N. Sato, and H. Shows, "First Monte Carlo Global Analysis of Nucleon Transversity with Lattice QCD Constraints," *Phys. Rev. Lett.* **120** no. 15, (2018) 152502, `arXiv:1710.09858 [hep-ph]`.

[258] K. Cichy, L. Del Debbio, and T. Giani, "Parton distributions from lattice data: the nonsinglet case," *JHEP* **10** (2019) 137, `arXiv:1907.06037 [hep-ph]`.

[259] J. Bringewatt, N. Sato, W. Melnitchouk, J.-W. Qiu, F. Steffens, and M. Constantinou, "Confronting lattice parton distributions with global QCD analysis," *Phys. Rev. D* **103** no. 1, (2021) 016003, `arXiv:2010.00548 [hep-ph]`.

[260] L. Del Debbio, T. Giani, J. Karpie, K. Orginos, A. Radyushkin, and S. Zafeiropoulos, "Neural-network analysis of Parton Distribution Functions from Ioffe-time pseudodistributions," *JHEP* **02** (2021) 138, `arXiv:2010.03996 [hep-ph]`.

[261] K.-F. Liu and S.-J. Dong, "Origin of difference between anti-d and anti-u partons in the nucleon," *Phys. Rev. Lett.* **72** (1994) 1790–1793, `arXiv:hep-ph/9306299`.

[262] K.-F. Liu, "Parton degrees of freedom from the path integral formalism," *Phys. Rev. D* **62** (2000) 074501, `arXiv:hep-ph/9910306`.

[263] **XQCD** Collaboration, J. Liang, T. Draper, K.-F. Liu, A. Rothkopf, and Y.-B. Yang, "Towards the nucleon hadronic tensor from lattice QCD," *Phys. Rev. D* **101** no. 11, (2020) 114503, `arXiv:1906.05312 [hep-ph]`.

[264] χ**QCD** Collaboration, J. Liang and K.-F. Liu, "PDFs and Neutrino-Nucleon Scattering from Hadronic Tensor," *PoS* **LATTICE2019** (2020) 046, `arXiv:2008.12389 [hep-lat]`.

[265] U. Aglietti, M. Ciuchini, G. Corbo, E. Franco, G. Martinelli, and L. Silvestrini, "Model independent determination of the light cone wave functions for exclusive processes," *Phys. Lett. B* **441** (1998) 371–375, `arXiv:hep-ph/9806277`.

[266] X.-d. Ji and C.-w. Jung, "Studying hadronic structure of the photon in lattice QCD," *Phys. Rev. Lett.* **86** (2001) 208, `arXiv:hep-lat/0101014`.

[267] W. Detmold and C. J. D. Lin, "Deep-inelastic scattering and the operator product expansion in lattice QCD," *Phys. Rev. D* **73** (2006) 014501, `arXiv:hep-lat/0507007`.

[268] A. J. Chambers, R. Horsley, Y. Nakamura, H. Perlt, P. E. L. Rakow, G. Schierholz, A. Schiller, K. Somfleth, R. D. Young, and J. M. Zanotti, "Nucleon Structure Functions from Operator Product Expansion on the Lattice," *Phys. Rev. Lett.* **118** no. 24, (2017) 242001, `arXiv:1703.01153 [hep-lat]`.

[269] **HOPE** Collaboration, W. Detmold, A. V. Grebe, I. Kanamori, C. J. D. Lin, R. J. Perry, and Y. Zhao, "Parton physics from a heavy-quark operator product expansion: Formalism and Wilson coefficients," *Phys. Rev. D* **104** no. 7, (2021) 074511, `arXiv:2103.09529 [hep-lat]`.

[270] V. Braun and D. Müller, "Exclusive processes in position space and the pion distribution amplitude," *Eur. Phys. J. C* **55** (2008) 349–361, `arXiv:0709.1348 [hep-ph]`.

[271] Y.-Q. Ma and J.-W. Qiu, "Extracting Parton Distribution Functions from Lattice QCD Calculations," *Phys. Rev. D* **98** no. 7, (2018) 074021, `arXiv:1404.6860 [hep-ph]`.

[272] Y.-Q. Ma and J.-W. Qiu, "Exploring Partonic Structure of Hadrons Using ab initio Lattice QCD Calculations," *Phys. Rev. Lett.* **120** no. 2, (2018) 022003, `arXiv:1709.03018 [hep-ph]`.

[273] G. S. Bali, V. M. Braun, B. Gläßle, M. Göckeler, M. Gruber, F. Hutzler, P. Korcyl, A. Schäfer, P. Wein, and J.-H. Zhang, "Pion distribution amplitude from Euclidean correlation functions: Exploring universality and higher-twist effects," *Phys. Rev. D* **98** no. 9, (2018) 094507, `arXiv:1807.06671 [hep-lat]`.

[274] B. Joó, J. Karpie, K. Orginos, A. V. Radyushkin, D. G. Richards, and S. Zafeiropoulos, "Parton Distribution Functions from Ioffe Time Pseudodistributions from Lattice Calculations: Approaching

the Physical Point," *Phys. Rev. Lett.* **125** no. 23, (2020) 232003, `arXiv:2004.01687 [hep-lat]`.

[275] X. Gao, L. Jin, C. Kallidonis, N. Karthik, S. Mukherjee, P. Petreczky, C. Shugert, S. Syritsyn, and Y. Zhao, "Valence parton distribution of the pion from lattice QCD: Approaching the continuum limit," *Phys. Rev. D* **102** no. 9, (2020) 094513, `arXiv:2007.06590 [hep-lat]`.

[276] R. S. Sufian, C. Egerer, J. Karpie, R. G. Edwards, B. Joó, Y.-Q. Ma, K. Orginos, J.-W. Qiu, and D. G. Richards, "Pion Valence Quark Distribution from Current-Current Correlation in Lattice QCD," *Phys. Rev. D* **102** no. 5, (2020) 054508, `arXiv:2001.04960 [hep-lat]`.

[277] A. V. Radyushkin, "Quasi-parton distribution functions, momentum distributions, and pseudo-parton distribution functions," *Phys. Rev. D* **96** no. 3, (2017) 034025, `arXiv:1705.01488 [hep-ph]`.

[278] J. D. Bjorken and E. A. Paschos, "Inelastic Electron Proton and gamma Proton Scattering, and the Structure of the Nucleon," *Phys. Rev.* **185** (1969) 1975–1982.

[279] T. Izubuchi, X. Ji, L. Jin, I. W. Stewart, and Y. Zhao, "Factorization Theorem Relating Euclidean and Light-Cone Parton Distributions," *Phys. Rev. D* **98** no. 5, (2018) 056004, `arXiv:1801.03917 [hep-ph]`.

[280] X. Ji, "Parton Physics from Large-Momentum Effective Field Theory," *Sci. China Phys. Mech. Astron.* **57** (2014) 1407–1412, `arXiv:1404.6680 [hep-ph]`.

[281] H.-W. Lin, J.-W. Chen, and R. Zhang, "Lattice Nucleon Isovector Unpolarized Parton Distribution in the Physical-Continuum Limit," `arXiv:2011.14971 [hep-lat]`.

[282] J.-W. Chen, L. Jin, H.-W. Lin, Y.-S. Liu, Y.-B. Yang, J.-H. Zhang, and Y. Zhao, "Lattice Calculation of Parton Distribution Function from LaMET at Physical Pion Mass with Large Nucleon Momentum," `arXiv:1803.04393 [hep-lat]`.

[283] C. Alexandrou, K. Cichy, M. Constantinou, K. Jansen, A. Scapellato, and F. Steffens, "Light-Cone Parton Distribution Functions from Lattice QCD," *Phys. Rev. Lett.* **121** no. 11, (2018) 112001, `arXiv:1803.02685 [hep-lat]`.

[284] M. Bhat, K. Cichy, M. Constantinou, and A. Scapellato, "Flavor nonsinglet parton distribution functions from lattice QCD at physical quark masses via the pseudodistribution approach," *Phys. Rev. D* **103** no. 3, (2021) 034510, `arXiv:2005.02102 [hep-lat]`.

[285] H.-W. Lin, J.-W. Chen, X. Ji, L. Jin, R. Li, Y.-S. Liu, Y.-B. Yang, J.-H. Zhang, and Y. Zhao, "Proton Isovector Helicity Distribution on the Lattice at Physical Pion Mass," *Phys. Rev. Lett.* **121** no. 24, (2018) 242003, `arXiv:1807.07431 [hep-lat]`.

[286] Y.-S. Liu, J.-W. Chen, L. Jin, R. Li, H.-W. Lin, Y.-B. Yang, J.-H. Zhang, and Y. Zhao, "Nucleon Transversity Distribution at the Physical Pion Mass from Lattice QCD," `arXiv:1810.05043 [hep-lat]`.

[287] C. Alexandrou, K. Cichy, M. Constantinou, K. Jansen, A. Scapellato, and F. Steffens, "Transversity parton distribution functions from lattice QCD," *Phys. Rev. D* **98** no. 9, (2018) 091503, `arXiv:1807.00232 [hep-lat]`.

[288] C. Alexandrou, K. Cichy, M. Constantinou, K. Hadjiyiannakou, K. Jansen, A. Scapellato, and F. Steffens, "Systematic uncertainties in parton distribution functions from lattice QCD simulations at the physical point," *Phys. Rev. D* **99** no. 11, (2019) 114504, `arXiv:1902.00587 [hep-lat]`.

[289] **NNPDF** Collaboration, E. R. Nocera, R. D. Ball, S. Forte, G. Ridolfi, and J. Rojo, "A first unbiased global determination of polarized PDFs and their uncertainties," *Nucl. Phys.* **B887** (2014) 276–308, `arXiv:1406.5539 [hep-ph]`.

[290] J. J. Ethier, N. Sato, and W. Melnitchouk, "First simultaneous extraction of spin-dependent parton distributions and fragmentation functions from a global QCD analysis," *Phys. Rev. Lett.* **119** no. 13, (2017) 132001, `arXiv:1705.05889 [hep-ph]`.

[291] D. de Florian, R. Sassot, M. Stratmann, and W. Vogelsang, "Extraction of Spin-Dependent Parton Densities and Their Uncertainties," *Phys. Rev. D* **80** (2009) 034030, `arXiv:0904.3821 [hep-ph]`.

[292] J. Benel, A. Courtoy, and R. Ferro-Hernandez, "A constrained fit of the valence transversity distributions from dihadron production," *Eur. Phys. J. C* **80** no. 5, (2020) 465, `arXiv:1912.03289 [hep-ph]`.

[293] M. Radici and A. Bacchetta, "First Extraction of Transversity from a Global Analysis of Electron-Proton and Proton-Proton Data," *Phys. Rev. Lett.* **120** no. 19, (2018) 192001, `arXiv:1802.05212 [hep-ph]`.

[294] **LP3** Collaboration, H.-W. Lin, J.-W. Chen, T. Ishikawa, and J.-H. Zhang, "Improved parton

distribution functions at the physical pion mass," *Phys. Rev. D* **98** no. 5, (2018) 054504, `arXiv:1708.05301 [hep-lat]`.

[295] Z. Fan, R. Zhang, and H.-W. Lin, "Nucleon gluon distribution function from $2 + 1 + 1$-flavor lattice QCD," *Int. J. Mod. Phys. A* **36** no. 13, (2021) 2150080, `arXiv:2007.16113 [hep-lat]`.

[296] **HadStruc** Collaboration, T. Khan *et al.*, "Unpolarized gluon distribution in the nucleon from lattice quantum chromodynamics," *Phys. Rev. D* **104** no. 9, (2021) 094516, `arXiv:2107.08960 [hep-lat]`.

[297] X. Gao, A. D. Hanlon, S. Mukherjee, P. Petreczky, P. Scior, S. Syritsyn, and Y. Zhao, "Lattice QCD Determination of the Bjorken-x Dependence of Parton Distribution Functions at Next-to-Next-to-Leading Order," *Phys. Rev. Lett.* **128** no. 14, (2022) 142003, `arXiv:2112.02208 [hep-lat]`.

[298] H.-W. Lin, J.-W. Chen, Z. Fan, J.-H. Zhang, and R. Zhang, "Valence-Quark Distribution of the Kaon and Pion from Lattice QCD," *Phys. Rev. D* **103** no. 1, (2021) 014516, `arXiv:2003.14128 [hep-lat]`.

[299] **CMS** Collaboration, S. Chatrchyan *et al.*, "Measurement of the Muon Charge Asymmetry in Inclusive $pp \to W + X$ Production at $\sqrt{s} = 7$ TeV and an Improved Determination of Light Parton Distribution Functions," *Phys. Rev. D* **90** no. 3, (2014) 032004, `arXiv:1312.6283 [hep-ex]`.

[300] **ATLAS** Collaboration, G. Aad *et al.*, "Measurement of the production of a W boson in association with a charm quark in pp collisions at $\sqrt{s} = 7$ TeV with the ATLAS detector," *JHEP* **05** (2014) 068, `arXiv:1402.6263 [hep-ex]`.

[301] S. Alekhin, J. Blümlein, and S. Moch, "Strange sea determination from collider data," *Phys. Lett. B* **777** (2018) 134–140, `arXiv:1708.01067 [hep-ph]`.

[302] F. Faura, S. Iranipour, E. R. Nocera, J. Rojo, and M. Ubiali, "The Strangest Proton?," *Eur. Phys. J. C* **80** no. 12, (2020) 1168, `arXiv:2009.00014 [hep-ph]`.

[303] P. M. Nadolsky *et al.*, "Implications of CTEQ global analysis for collider observables," *Phys. Rev. D78* (2008) 013004, `arXiv:0802.0007 [hep-ph]`.

[304] Z.-Y. Fan, Y.-B. Yang, A. Anthony, H.-W. Lin, and K.-F. Liu, "Gluon Quasi-Parton-Distribution Functions from Lattice QCD," *Phys. Rev. Lett.* **121** no. 24, (2018) 242001, `arXiv:1808.02077 [hep-lat]`.

[305] I. Balitsky, W. Morris, and A. Radyushkin, "Gluon Pseudo-Distributions at Short Distances: Forward Case," *Phys. Lett. B* **808** (2020) 135621, `arXiv:1910.13963 [hep-ph]`.

[306] W. Wang, J.-H. Zhang, S. Zhao, and R. Zhu, "Complete matching for quasidistribution functions in large momentum effective theory," *Phys. Rev. D* **100** no. 7, (2019) 074509, `arXiv:1904.00978 [hep-ph]`.

[307] J.-H. Zhang, X. Ji, A. Schäfer, W. Wang, and S. Zhao, "Accessing Gluon Parton Distributions in Large Momentum Effective Theory," *Phys. Rev. Lett.* **122** no. 14, (2019) 142001, `arXiv:1808.10824 [hep-ph]`.

[308] J.-H. Zhang, J.-W. Chen, L. Jin, H.-W. Lin, A. Schäfer, and Y. Zhao, "First direct lattice-QCD calculation of the x-dependence of the pion parton distribution function," *Phys. Rev. D* **100** no. 3, (2019) 034505, `arXiv:1804.01483 [hep-lat]`.

[309] R. S. Sufian, J. Karpie, C. Egerer, K. Orginos, J.-W. Qiu, and D. G. Richards, "Pion Valence Quark Distribution from Matrix Element Calculated in Lattice QCD," *Phys. Rev. D* **99** no. 7, (2019) 074507, `arXiv:1901.03921 [hep-lat]`.

[310] T. Izubuchi, L. Jin, C. Kallidonis, N. Karthik, S. Mukherjee, P. Petreczky, C. Shugert, and S. Syritsyn, "Valence parton distribution function of pion from fine lattice," *Phys. Rev. D* **100** no. 3, (2019) 034516, `arXiv:1905.06349 [hep-lat]`.

[311] B. Joó, J. Karpie, K. Orginos, A. V. Radyushkin, D. G. Richards, R. S. Sufian, and S. Zafeiropoulos, "Pion valence structure from Ioffe-time parton pseudodistribution functions," *Phys. Rev. D* **100** no. 11, (2019) 114512, `arXiv:1909.08517 [hep-lat]`.

[312] C. Shugert, X. Gao, T. Izubichi, L. Jin, C. Kallidonis, N. Karthik, S. Mukherjee, P. Petreczky, S. Syritsyn, and Y. Zhao, "Pion valence quark PDF from lattice QCD," in *37th International Symposium on Lattice Field Theory*. 1, 2020. `arXiv:2001.11650 [hep-lat]`.

[313] L.-B. Chen, W. Wang, and R. Zhu, "Next-to-Next-to-Leading Order Calculation of Quasiparton Distribution Functions," *Phys. Rev. Lett.* **126** no. 7, (2021) 072002, `arXiv:2006.14825 [hep-ph]`.

[314] Z.-Y. Li, Y.-Q. Ma, and J.-W. Qiu, "Extraction of Next-to-Next-to-Leading-Order Parton Distribution Functions from Lattice QCD Calculations," *Phys. Rev. Lett.* **126** no. 7, (2021) 072001,

arXiv:2006.12370 [hep-ph].

[315] G. R. Farrar and D. R. Jackson, "Pion and Nucleon Structure Functions Near x=1," *Phys. Rev. Lett.* **35** (1975) 1416.

[316] D. E. Soper, "The Parton Model and the Bethe-Salpeter Wave Function," *Phys. Rev. D* **15** (1977) 1141.

[317] K. D. Bednar, I. C. Cloët, and P. C. Tandy, "Distinguishing Quarks and Gluons in Pion and Kaon Parton Distribution Functions," *Phys. Rev. Lett.* **124** no. 4, (2020) 042002, arXiv:1811.12310 [nucl-th].

[318] M. Ding, K. Raya, D. Binosi, L. Chang, C. D. Roberts, and S. M. Schmidt, "Symmetry, symmetry breaking, and pion parton distributions," *Phys. Rev. D* **101** no. 5, (2020) 054014, arXiv:1905.05208 [nucl-th].

[319] I. Novikov *et al.*, "Parton Distribution Functions of the Charged Pion Within The xFitter Framework," *Phys. Rev. D* **102** no. 1, (2020) 014040, arXiv:2002.02902 [hep-ph].

[320] A. Courtoy and P. M. Nadolsky, "Testing momentum dependence of the nonperturbative hadron structure in a global QCD analysis," *Phys. Rev. D* **103** no. 5, (2021) 054029, arXiv:2011.10078 [hep-ph].

[321] **ETM** Collaboration, C. Alexandrou, S. Bacchio, I. Cloët, M. Constantinou, K. Hadjiyiannakou, G. Koutsou, and C. Lauer, "Pion and kaon $\langle x3 \rangle$ from lattice QCD and PDF reconstruction from Mellin moments," *Phys. Rev. D* **104** no. 5, (2021) 054504, arXiv:2104.02247 [hep-lat].

[322] A. Salas-Chavira, Z. Fan, and H.-W. Lin, "First Glimpse into the Kaon Gluon Parton Distribution Using Lattice QCD," arXiv:2112.03124 [hep-lat].

[323] J.-H. Zhang, J.-W. Chen, X. Ji, L. Jin, and H.-W. Lin, "Pion Distribution Amplitude from Lattice QCD," *Phys. Rev. D* **95** no. 9, (2017) 094514, arXiv:1702.00008 [hep-lat].

[324] **LP3** Collaboration, J.-H. Zhang, L. Jin, H.-W. Lin, A. Schäfer, P. Sun, Y.-B. Yang, R. Zhang, Y. Zhao, and J.-W. Chen, "Kaon Distribution Amplitude from Lattice QCD and the Flavor SU(3) Symmetry," *Nucl. Phys. B* **939** (2019) 429–446, arXiv:1712.10025 [hep-ph].

[325] G. S. Bali *et al.*, "Pion distribution amplitude from Euclidean correlation functions," *Eur. Phys. J. C* **78** no. 3, (2018) 217, arXiv:1709.04325 [hep-lat].

[326] **RQCD** Collaboration, G. S. Bali, V. M. Braun, S. Bürger, M. Göckeler, M. Gruber, F. Hutzler, P. Korcyl, A. Schäfer, A. Sternbeck, and P. Wein, "Light-cone distribution amplitudes of pseudoscalar mesons from lattice QCD," *JHEP* **08** (2019) 065, arXiv:1903.08038 [hep-lat]. [Addendum: JHEP 11, 037 (2020)].

[327] **Lattice Parton** Collaboration, J. Hua, M.-H. Chu, P. Sun, W. Wang, J. Xu, Y.-B. Yang, J.-H. Zhang, and Q.-A. Zhang, "Distribution Amplitudes of K* and ϕ at the Physical Pion Mass from Lattice QCD," *Phys. Rev. Lett.* **127** no. 6, (2021) 062002, arXiv:2011.09788 [hep-lat].

[328] R. Zhang, C. Honkala, H.-W. Lin, and J.-W. Chen, "Pion and kaon distribution amplitudes in the continuum limit," *Phys. Rev. D* **102** no. 9, (2020) 094519, arXiv:2005.13955 [hep-lat].

[329] **HOPE** Collaboration, W. Detmold, A. V. Grebe, I. Kanamori, C. J. D. Lin, S. Mondal, R. J. Perry, and Y. Zhao, "Parton physics from a heavy-quark operator product expansion: Lattice QCD calculation of the second moment of the pion distribution amplitude," *Phys. Rev. D* **105** no. 3, (2022) 034506, arXiv:2109.15241 [hep-lat].

[330] N. Juliano, R. Zhang, C. Honkala, and H.-W. Lin, "Pion Distribution Amplitudes in the Continuum Limit," *PoS* **LATTICE2021** (2022) 436, arXiv:2108.04326 [hep-lat].

[331] J. Hua *et al.*, "Pion and Kaon Distribution Amplitudes from Lattice QCD," arXiv:2201.09173 [hep-lat].

[332] X. Gao, A. D. Hanlon, N. Karthik, S. Mukherjee, P. Petreczky, P. Scior, S. Syritsyn, and Y. Zhao, "Pion distribution amplitude at the physical point using the leading-twist expansion of the quasi-DA matrix element," arXiv:2206.04084 [hep-lat].

[333] I. W. Stewart, "Theoretical introduction to B decays and the soft collinear effective theory," in *38th Rencontres de Moriond on QCD and High-Energy Hadronic Interactions*. 8, 2003. arXiv:hep-ph/0308185.

[334] J.-W. Chen, H.-W. Lin, and J.-H. Zhang, "Pion generalized parton distribution from lattice QCD," *Nucl. Phys. B* **952** (2020) 114940, arXiv:1904.12376 [hep-lat].

[335] C. Alexandrou, K. Cichy, M. Constantinou, K. Hadjiyiannakou, K. Jansen, A. Scapellato, and F. Steffens, "Unpolarized and helicity generalized parton distributions of the proton within lattice

QCD," *Phys. Rev. Lett.* **125** no. 26, (2020) 262001, `arXiv:2008.10573 [hep-lat]`.

[336] H.-W. Lin, "Nucleon Tomography and Generalized Parton Distribution at Physical Pion Mass from Lattice QCD," *Phys. Rev. Lett.* **127** no. 18, (2021) 182001, `arXiv:2008.12474 [hep-ph]`.

[337] H.-W. Lin, "Nucleon helicity generalized parton distribution at physical pion mass from lattice QCD," *Phys. Lett. B* **824** (2022) 136821, `arXiv:2112.07519 [hep-lat]`.

[338] B. U. Musch, P. Hagler, J. W. Negele, and A. Schafer, "Exploring quark transverse momentum distributions with lattice QCD," *Phys. Rev. D* **83** (2011) 094507, `arXiv:1011.1213 [hep-lat]`.

[339] B. U. Musch, P. Hagler, M. Engelhardt, J. W. Negele, and A. Schafer, "Sivers and Boer-Mulders observables from lattice QCD," *Phys. Rev. D* **85** (2012) 094510, `arXiv:1111.4249 [hep-lat]`.

[340] M. Engelhardt, P. Hägler, B. Musch, J. Negele, and A. Schäfer, "Lattice QCD study of the Boer-Mulders effect in a pion," *Phys. Rev. D* **93** no. 5, (2016) 054501, `arXiv:1506.07826 [hep-lat]`.

[341] B. Yoon, T. Bhattacharya, M. Engelhardt, J. Green, R. Gupta, P. Hägler, B. Musch, J. Negele, A. Pochinsky, and S. Syritsyn, "Lattice QCD calculations of nucleon transverse momentum-dependent parton distributions using clover and domain wall fermions," in *33rd International Symposium on Lattice Field Theory.* SISSA, 11, 2015. `arXiv:1601.05717 [hep-lat]`.

[342] B. Yoon, M. Engelhardt, R. Gupta, T. Bhattacharya, J. R. Green, B. U. Musch, J. W. Negele, A. V. Pochinsky, A. Schäfer, and S. N. Syritsyn, "Nucleon Transverse Momentum-dependent Parton Distributions in Lattice QCD: Renormalization Patterns and Discretization Effects," *Phys. Rev. D* **96** no. 9, (2017) 094508, `arXiv:1706.03406 [hep-lat]`.

[343] P. Shanahan, M. Wagman, and Y. Zhao, "Collins-Soper kernel for TMD evolution from lattice QCD," *Phys. Rev. D* **102** no. 1, (2020) 014511, `arXiv:2003.06063 [hep-lat]`.

[344] **Lattice Parton** Collaboration, Q.-A. Zhang *et al.*, "Lattice-QCD Calculations of TMD Soft Function Through Large-Momentum Effective Theory," *Phys. Rev. Lett.* **125** no. 19, (2020) 192001, `arXiv:2005.14572 [hep-lat]`.

[345] M. Schlemmer, A. Vladimirov, C. Zimmermann, M. Engelhardt, and A. Schäfer, "Determination of the Collins-Soper Kernel from Lattice QCD," *JHEP* **08** (2021) 004, `arXiv:2103.16991 [hep-lat]`.

[346] Y. Li *et al.*, "Lattice QCD Study of Transverse-Momentum Dependent Soft Function," *Phys. Rev. Lett.* **128** no. 6, (2022) 062002, `arXiv:2106.13027 [hep-lat]`.

[347] **Lattice Parton** Collaboration, Q.-A. Zhang *et al.*, "Lattice-QCD Calculations of TMD Soft Function Through Large-Momentum Effective Theory," *Phys. Rev. Lett.* **125** no. 19, (2020) 192001, `arXiv:2005.14572 [hep-lat]`.

[348] P. Shanahan, M. Wagman, and Y. Zhao, "Lattice QCD calculation of the Collins-Soper kernel from quasi-TMDPDFs," *Phys. Rev. D* **104** no. 11, (2021) 114502, `arXiv:2107.11930 [hep-lat]`.

[349] B. Yoon, T. Bhattacharya, M. Engelhardt, J. Green, R. Gupta, P. Hägler, B. Musch, J. Negele, A. Pochinsky, and S. Syritsyn, "Lattice QCD calculations of nucleon transverse momentum-dependent parton distributions using clover and domain wall fermions," in *33rd International Symposium on Lattice Field Theory.* SISSA, 11, 2015. `arXiv:1601.05717 [hep-lat]`.

[350] V. S. Fadin, E. A. Kuraev, and L. N. Lipatov, "On the Pomeranchuk Singularity in Asymptotically Free Theories," *Phys. Lett. B* **60** (1975) 50–52.

[351] E. A. Kuraev, L. N. Lipatov, and V. S. Fadin, "Multi - Reggeon Processes in the Yang-Mills Theory," *Sov. Phys. JETP* **44** (1976) 443–450.

[352] E. A. Kuraev, L. N. Lipatov, and V. S. Fadin, "The Pomeranchuk Singularity in Nonabelian Gauge Theories," *Sov. Phys. JETP* **45** (1977) 199–204.

[353] I. I. Balitsky and L. N. Lipatov, "The Pomeranchuk Singularity in Quantum Chromodynamics," *Sov. J. Nucl. Phys.* **28** (1978) 822–829.

[354] M. Boonekamp, A. Dechambre, V. Juranek, O. Kepka, M. Rangel, C. Royon, and R. Staszewski, "FPMC: A Generator for forward physics," `arXiv:1102.2531 [hep-ph]`.

[355] H. Jung and A. de Roeck, eds., *Proceedings, HERA and the LHC Workshop Series on the implications of HERA for LHC physics: 2006-2008.* DESY, Hamburg, Germany, 3, 2009. `arXiv:0903.3861 [hep-ph]`.

[356] C. Marquet, C. Royon, M. Saimpert, and D. Werder, "Probing the Pomeron structure using dijets and γ+jet events at the LHC," *Phys. Rev. D* **88** no. 7, (2013) 074029, `arXiv:1306.4901 [hep-ph]`.

[357] O. Kepka and C. Royon, "Search for exclusive events using the dijet mass fraction at the Tevatron," *Phys. Rev. D* **76** (2007) 034012, `arXiv:0704.1956 [hep-ph]`.

[358] C. Marquet, D. E. Martins, A. V. Pereira, M. Rangel, and C. Royon, "Diffractive di-jet production at the LHC with a Reggeon contribution," *Phys. Lett. B* **766** (2017) 23–28, `arXiv:1608.05674 [hep-ph]`.

[359] A. Chuinard, C. Royon, and R. Staszewski, "Testing Pomeron flavour symmetry with diffractive W charge asymmetry," *JHEP* **04** (2016) 092, `arXiv:1510.04218 [hep-ph]`.

[360] L. Lukaszuk and B. Nicolescu, "A Possible interpretation of p p rising total cross-sections," *Lett. Nuovo Cim.* **8** (1973) 405–413.

[361] E. Martynov and B. Nicolescu, "Odderon effects in the differential cross-sections at Tevatron and LHC energies," *Eur. Phys. J. C* **79** no. 6, (2019) 461, `arXiv:1808.08580 [hep-ph]`.

[362] A. Breakstone *et al.*, "A Measurement of $\bar{p}p$ and pp Elastic Scattering in the Dip Region at $\sqrt{s}$ = 53-GeV," *Phys. Rev. Lett.* **54** (1985) 2180.

[363] S. Erhan *et al.*, "Comparison of $\bar{p}p$ and pp Elastic Scattering With $0.6 - \text{GeV}^< t < 2.1 - \text{GeV}^2$ at the CERN ISR," *Phys. Lett. B* **152** (1985) 131–134.

[364] **UA4** Collaboration, D. Bernard *et al.*, "Large T Elastic Scattering at the CERN SPS Collider at $\sqrt{s}$ = 630-GeV," *Phys. Lett. B* **171** (1986) 142–144.

[365] **UA4** Collaboration, M. Bozzo *et al.*, "Elastic Scattering at the CERN SPS Collider Up to a Four Momentum Transfer of 1.55-GeV**2," *Phys. Lett. B* **155** (1985) 197–202.

[366] E. Nagy *et al.*, "Measurements of Elastic Proton Proton Scattering at Large Momentum Transfer at the CERN Intersecting Storage Rings," *Nucl. Phys. B* **150** (1979) 221–267.

[367] **D0** Collaboration, V. M. Abazov *et al.*, "Measurement of the differential cross section $d\sigma/dt$ in elastic $p\bar{p}$ scattering at $\sqrt{s}$ = 1.96 TeV," *Phys. Rev. D* **86** (2012) 012009, `arXiv:1206.0687 [hep-ex]`.

[368] **TOTEM** Collaboration, G. Antchev *et al.*, "Elastic differential cross-section $d\sigma/dt$ at $\sqrt{s}$ = 2.76 TeV and implications on the existence of a colourless C-odd three-gluon compound state," *Eur. Phys. J. C* **80** no. 2, (2020) 91, `arXiv:1812.08610 [hep-ex]`.

[369] **TOTEM** Collaboration, G. Antchev *et al.*, "Proton-proton elastic scattering at the LHC energy of s** (1/2) = 7-TeV," *EPL* **95** no. 4, (2011) 41001, `arXiv:1110.1385 [hep-ex]`.

[370] **TOTEM** Collaboration, G. Antchev *et al.*, "Evidence for non-exponential elastic proton–proton differential cross-section at low —t— and $\sqrt{s}$=8 TeV by TOTEM," *Nucl. Phys. B* **899** (2015) 527–546, `arXiv:1503.08111 [hep-ex]`.

[371] **TOTEM** Collaboration, G. Antchev *et al.*, "Elastic differential cross-section measurement at $\sqrt{s}$ = 13 TeV by TOTEM," *Eur. Phys. J. C* **79** no. 10, (2019) 861, `arXiv:1812.08283 [hep-ex]`.

[372] **TOTEM, D0** Collaboration, V. M. Abazov *et al.*, "Odderon Exchange from Elastic Scattering Differences between pp and $p\bar{p}$ Data at 1.96 TeV and from pp Forward Scattering Measurements," *Phys. Rev. Lett.* **127** no. 6, (2021) 062003, `arXiv:2012.03981 [hep-ex]`.

[373] **ALICE** Collaboration, C. Loizides, W. Riegler, *et al.*, "Letter of Intent: A Forward Calorimeter (FoCal) in the ALICE experiment,". `https://cds.cern.ch/record/2719928`.

[374] P. Azzi *et al.*, "Report from Working Group 1: Standard Model Physics at the HL-LHC and HE-LHC," *CERN Yellow Rep. Monogr.* **7** (2019) 1–220, `arXiv:1902.04070 [hep-ph]`.

[375] **FCC** Collaboration, A. Abada *et al.*, "FCC-hh: The Hadron Collider: Future Circular Collider Conceptual Design Report Volume 3," *Eur. Phys. J. ST* **228** no. 4, (2019) 755–1107.

[376] **FCC** Collaboration, A. Abada *et al.*, "FCC Physics Opportunities: Future Circular Collider Conceptual Design Report Volume 1," *Eur. Phys. J. C* **79** no. 6, (2019) 474.

[377] M. L. Mangano *et al.*, "Physics at a 100 TeV pp Collider: Standard Model Processes," `arXiv:1607.01831 [hep-ph]`.

[378] J. Rojo, "Parton Distributions at a 100 TeV Hadron Collider," *PoS* **DIS2016** (2016) 275, `arXiv:1605.08302 [hep-ph]`.

[379] **PROSA** Collaboration, O. Zenaiev *et al.*, "Impact of heavy-flavour production cross sections measured by the LHCb experiment on parton distribution functions at low x," *Eur. Phys. J. C* **75** no. 8, (2015) 396, `arXiv:1503.04581 [hep-ph]`.

[380] R. Gauld and J. Rojo, "Precision determination of the small-x gluon from charm production at LHCb," *Phys. Rev. Lett.* **118** no. 7, (2017) 072001, `arXiv:1610.09373 [hep-ph]`.

[381] **PROSA** Collaboration, O. Zenaiev, M. V. Garzelli, K. Lipka, S. O. Moch, A. Cooper-Sarkar, F. Olness, A. Geiser, and G. Sigl, "Improved constraints on parton distributions using LHCb, ALICE and HERA heavy-flavour measurements and implications for the predictions for prompt

atmospheric-neutrino fluxes," *JHEP* **04** (2020) 118, `arXiv:1911.13164 [hep-ph]`.

[382] M. V. Garzelli, L. Kemmler, S. Moch, and O. Zenaiev, "Heavy-flavor hadro-production with heavy-quark masses renormalized in the $\overline{\text{MS}}$, MSR and on-shell schemes," *JHEP* **04** (2021) 043, `arXiv:2009.07763 [hep-ph]`.

[383] S. J. Brodsky, A. Kusina, F. Lyonnet, I. Schienbein, H. Spiesberger, and R. Vogt, "A review of the intrinsic heavy quark content of the nucleon," *Adv. High Energy Phys.* **2015** (2015) 231547, `arXiv:1504.06287 [hep-ph]`.

[384] **LHCb** Collaboration, R. Aaij *et al.*, "Prompt charm production in pp collisions at sqrt(s)=7 TeV," *Nucl. Phys. B* **871** (2013) 1–20, `arXiv:1302.2864 [hep-ex]`.

[385] **LHCb** Collaboration, R. Aaij *et al.*, "Measurements of prompt charm production cross-sections in pp collisions at $\sqrt{s} = 13$ TeV," *JHEP* **03** (2016) 159, `arXiv:1510.01707 [hep-ex]`. [Erratum: JHEP 09, 013 (2016), Erratum: JHEP 05, 074 (2017)].

[386] **LHCb** Collaboration, R. Aaij *et al.*, "Measurements of prompt charm production cross-sections in pp collisions at $\sqrt{s} = 5$ TeV," *JHEP* **06** (2017) 147, `arXiv:1610.02230 [hep-ex]`.

[387] **LHCb** Collaboration, R. Aaij *et al.*, "Study of Z bosons produced in association with charm in the forward region," `arXiv:2109.08084 [hep-ex]`.

[388] V. Bertone, R. Gauld, and J. Rojo, "Neutrino Telescopes as QCD Microscopes," *JHEP* **01** (2019) 217, `arXiv:1808.02034 [hep-ph]`.

[389] A. Garcia, R. Gauld, A. Heijboer, and J. Rojo, "Complete predictions for high-energy neutrino propagation in matter," *JCAP* **09** (2020) 025, `arXiv:2004.04756 [hep-ph]`.

[390] R. Gauld, J. Rojo, L. Rottoli, S. Sarkar, and J. Talbert, "The prompt atmospheric neutrino flux in the light of LHCb," *JHEP* **02** (2016) 130, `arXiv:1511.06346 [hep-ph]`.

[391] **PROSA** Collaboration, M. V. Garzelli, S. Moch, O. Zenaiev, A. Cooper-Sarkar, A. Geiser, K. Lipka, R. Placakyte, and G. Sigl, "Prompt neutrino fluxes in the atmosphere with PROSA parton distribution functions," *JHEP* **05** (2017) 004, `arXiv:1611.03815 [hep-ph]`.

[392] **IceCube** Collaboration, R. Abbasi *et al.*, "The IceCube high-energy starting event sample: Description and flux characterization with 7.5 years of data," *Phys. Rev. D* **104** (2020) 022002, `arXiv:2011.03545 [astro-ph.HE]`.

[393] **KM3Net** Collaboration, S. Adrian-Martinez *et al.*, "Letter of intent for KM3NeT 2.0" *J. Phys. G* **43** no. 8, (2016) 084001, `arXiv:1601.07459 [astro-ph.IM]`.

[394] M. Ackermann *et al.*, "High-energy and ultra-high-energy neutrinos: A Snowmass white paper," *JHEAp* **36** (2022) 55–110, `arXiv:2203.08096 [hep-ph]`.

[395] R. A. Khalek, J. J. Ethier, E. R. Nocera, and J. Rojo, "Self-consistent determination of proton and nuclear PDFs at the Electron Ion Collider," *Phys. Rev. D* **103** no. 9, (2021) 096005, `arXiv:2102.00018 [hep-ph]`.

[396] **NuTeV** Collaboration, M. Tzanov *et al.*, "Precise measurement of neutrino and anti-neutrino differential cross sections," *Phys. Rev. D* **74** (2006) 012008, `arXiv:hep-ex/0509010`.

[397] **NOMAD** Collaboration, O. Samoylov *et al.*, "A Precision Measurement of Charm Dimuon Production in Neutrino Interactions from the NOMAD Experiment," *Nucl. Phys. B* **876** (2013) 339–375, `arXiv:1308.4750 [hep-ex]`.

[398] **NuTeV** Collaboration, M. Goncharov *et al.*, "Precise Measurement of Dimuon Production Cross-Sections in ν_μ Fe and $\bar{\nu}_\mu$ Fe Deep Inelastic Scattering at the Tevatron.," *Phys. Rev. D* **64** (2001) 112006, `arXiv:hep-ex/0102049`.

[399] **CHORUS** Collaboration, E. Eskut *et al.*, "The CHORUS experiment to search for muon-neutrino –> tau-neutrino oscillation," *Nucl. Instrum. Meth. A* **401** (1997) 7–44.

[400] W.-C. Chang and J.-C. Peng, "Flavor Structure of the Nucleon Sea," *Prog. Part. Nucl. Phys.* **79** (2014) 95–135, `arXiv:1406.1260 [hep-ph]`.

[401] S. Alekhin, J. Blumlein, L. Caminadac, K. Lipka, K. Lohwasser, S. Moch, R. Petti, and R. Placakyte, "Determination of Strange Sea Quark Distributions from Fixed-target and Collider Data," *Phys. Rev. D* **91** no. 9, (2015) 094002, `arXiv:1404.6469 [hep-ph]`.

[402] G. Bevilacqua, M. V. Garzelli, A. Kardos, and L. Toth, "W+charm production with massive c quarks in PowHel," `arXiv:2106.11261 [hep-ph]`.

[403] J. Collins, *Foundations of perturbative QCD*, vol. 32. Cambridge University Press, 11, 2013.

[404] M. Nefedov, "Sudakov resummation from the BFKL evolution," *Phys. Rev. D* **104** no. 5, (2021) 054039, `arXiv:2105.13915 [hep-ph]`.

[405] M. Hentschinski, "Transverse momentum dependent gluon distribution within high energy factorization at next-to-leading order," *Phys. Rev. D* **104** no. 5, (2021) 054014, `arXiv:2107.06203 [hep-ph]`.

[406] A. Bacchetta, F. Delcarro, C. Pisano, M. Radici, and A. Signori, "Extraction of partonic transverse momentum distributions from semi-inclusive deep-inelastic scattering, Drell-Yan and Z-boson production," *JHEP* **06** (2017) 081, `arXiv:1703.10157 [hep-ph]`. [Erratum: JHEP 06, 051 (2019)].

[407] I. Scimemi and A. Vladimirov, "Analysis of vector boson production within TMD factorization," *Eur. Phys. J. C* **78** no. 2, (2018) 89, `arXiv:1706.01473 [hep-ph]`.

[408] I. Scimemi and A. Vladimirov, "Non-perturbative structure of semi-inclusive deep-inelastic and Drell-Yan scattering at small transverse momentum," *JHEP* **06** (2020) 137, `arXiv:1912.06532 [hep-ph]`.

[409] A. Bacchetta, V. Bertone, C. Bissolotti, G. Bozzi, F. Delcarro, F. Piacenza, and M. Radici, "Transverse-momentum-dependent parton distributions up to N³LL from Drell-Yan data," *JHEP* **07** (2020) 117, `arXiv:1912.07550 [hep-ph]`.

[410] P. J. Mulders and J. Rodrigues, "Transverse momentum dependence in gluon distribution and fragmentation functions," *Phys. Rev. D* **63** (2001) 094021, `arXiv:hep-ph/0009343`.

[411] P. M. Nadolsky, C. Balazs, E. L. Berger, and C. P. Yuan, "Gluon-gluon contributions to the production of continuum diphoton pairs at hadron colliders," *Phys. Rev. D* **76** (2007) 013008, `arXiv:hep-ph/0702003`.

[412] S. Catani and M. Grazzini, "QCD transverse-momentum resummation in gluon fusion processes," *Nucl. Phys. B* **845** (2011) 297–323, `arXiv:1011.3918 [hep-ph]`.

[413] D. Boer, S. J. Brodsky, P. J. Mulders, and C. Pisano, "Direct Probes of Linearly Polarized Gluons inside Unpolarized Hadrons," *Phys. Rev. Lett.* **106** (2011) 132001, `arXiv:1011.4225 [hep-ph]`.

[414] P. Sun, B.-W. Xiao, and F. Yuan, "Gluon Distribution Functions and Higgs Boson Production at Moderate Transverse Momentum," *Phys. Rev.* **D84** (2011) 094005, `arXiv:1109.1354 [hep-ph]`.

[415] D. Boer, W. J. den Dunnen, C. Pisano, M. Schlegel, and W. Vogelsang, "Linearly Polarized Gluons and the Higgs Transverse Momentum Distribution," *Phys. Rev. Lett.* **108** (2012) 032002, `arXiv:1109.1444 [hep-ph]`.

[416] C. Pisano, D. Boer, S. J. Brodsky, M. G. Buffing, and P. J. Mulders, "Linear polarization of gluons and photons in unpolarized collider experiments," *JHEP* **10** (2013) 024, `arXiv:1307.3417 [hep-ph]`.

[417] W. J. den Dunnen, J. P. Lansberg, C. Pisano, and M. Schlegel, "Accessing the Transverse Dynamics and Polarization of Gluons inside the Proton at the LHC," *Phys. Rev. Lett.* **112** (2014) 212001, `arXiv:1401.7611 [hep-ph]`.

[418] J.-P. Lansberg, C. Pisano, and M. Schlegel, "Associated production of a dilepton and a $\Upsilon(J/\psi)$ at the LHC as a probe of gluon transverse momentum dependent distributions," *Nucl. Phys.* **B920** (2017) 192–210, `arXiv:1702.00305 [hep-ph]`.

[419] E. Chapon *et al.*, "Prospects for quarkonium studies at the high-luminosity LHC," *Prog. Part. Nucl. Phys.* **122** (2022) 103906, `arXiv:2012.14161 [hep-ph]`.

[420] F. G. Celiberto, D. Y. Ivanov, and A. Papa, "Diffractive production of Λ hyperons in the high-energy limit of strong interactions," *Phys. Rev. D* **102** no. 9, (2020) 094019, `arXiv:2008.10513 [hep-ph]`.

[421] F. G. Celiberto, M. Fucilla, D. Y. Ivanov, and A. Papa, "High-energy resummation in Λ_c baryon production," *Eur. Phys. J. C* **81** no. 8, (2021) 780, `arXiv:2105.06432 [hep-ph]`.

[422] A. Bacchetta, F. G. Celiberto, M. Radici, and P. Taels, "Transverse-momentum-dependent gluon distribution functions in a spectator model," *Eur. Phys. J. C* **80** no. 8, (2020) 733, `arXiv:2005.02288 [hep-ph]`.

[423] T. C. Rogers and P. J. Mulders, "No Generalized TMD-Factorization in Hadro-Production of High Transverse Momentum Hadrons," *Phys. Rev. D* **81** (2010) 094006, `arXiv:1001.2977 [hep-ph]`.

[424] L. Frankfurt, V. Guzey, A. Stasto, and M. Strikman, "Selected topics in diffraction with protons and nuclei: past, present, and future," `arXiv:2203.12289 [hep-ph]`.

[425] C. A. Flett, S. P. Jones, A. D. Martin, M. G. Ryskin, and T. Teubner, "How to include exclusive J/ψ production data in global PDF analyses," *Phys. Rev. D* **101** no. 9, (2020) 094011, `arXiv:1908.08398 [hep-ph]`.

[426] C. A. Flett, A. D. Martin, M. G. Ryskin, and T. Teubner, "Very low x gluon density determined by LHCb exclusive J/ψ data," *Phys. Rev. D* **102** (2020) 114021, `arXiv:2006.13857 [hep-ph]`.

[427] S. R. Klein and H. Mäntysaari, "Imaging the nucleus with high-energy photons," *Nature Rev. Phys.* **1** no. 11, (2019) 662–674, `arXiv:1910.10858 [hep-ex]`.

[428] **STAR** Collaboration, L. Adamczyk *et al.*, "Coherent diffractive photoproduction of $\rho 0$ mesons on gold nuclei at 200 GeV/nucleon-pair at the Relativistic Heavy Ion Collider," *Phys. Rev. C* **96** no. 5, (2017) 054904, `arXiv:1702.07705 [nucl-ex]`.

[429] X.-d. Ji, "Viewing the proton through 'color' filters," *Phys. Rev. Lett.* **91** (2003) 062001, `arXiv:hep-ph/0304037`.

[430] A. V. Belitsky, X.-d. Ji, and F. Yuan, "Quark imaging in the proton via quantum phase space distributions," *Phys. Rev. D* **69** (2004) 074014, `arXiv:hep-ph/0307383`.

[431] S. Meissner, A. Metz, and M. Schlegel, "Generalized parton correlation functions for a spin-1/2 hadron," *JHEP* **08** (2009) 056, `arXiv:0906.5323 [hep-ph]`.

[432] S. Bhattacharya, A. Metz, and J. Zhou, "Generalized TMDs and the exclusive double Drell–Yan process," *Phys. Lett. B* **771** (2017) 396–400, `arXiv:1702.04387 [hep-ph]`. [Erratum: Phys.Lett.B 810, 135866 (2020)].

[433] Y. Hagiwara, Y. Hatta, R. Pasechnik, M. Tasevsky, and O. Teryaev, "Accessing the gluon Wigner distribution in ultraperipheral pA collisions," *Phys. Rev. D* **96** no. 3, (2017) 034009, `arXiv:1706.01765 [hep-ph]`.

[434] R. Boussarie, Y. Hatta, B.-W. Xiao, and F. Yuan, "Probing the Weizsäcker-Williams gluon Wigner distribution in pp collisions," *Phys. Rev. D* **98** no. 7, (2018) 074015, `arXiv:1807.08697 [hep-ph]`.

[435] **CMS** Collaboration, V. Khachatryan *et al.*, "Observation of Long-Range Near-Side Angular Correlations in Proton-Proton Collisions at the LHC," *JHEP* **09** (2010) 091, `arXiv:1009.4122 [hep-ex]`.

[436] **CMS** Collaboration, V. Khachatryan *et al.*, "Observation of Long-Range Near-Side Angular Correlations in Proton-Lead Collisions at the LHC," *Phys. Lett. B* **718** (2013) 795–814, `arXiv:1210.5482 [nucl-ex]`.

[437] **ATLAS** Collaboration, G. Aad *et al.*, "Observation of Associated Near-Side and Away-Side Long-Range Correlations in $\sqrt{s_{NN}}$=5.02 TeV Proton-Lead Collisions with the ATLAS Detector," *Phys. Rev. Lett.* **110** no. 18, (2013) 182302, `arXiv:1212.5198 [hep-ex]`.

[438] **ALICE** Collaboration, B. Abelev *et al.*, "Long-range angular correlations on the near and away side in p-Pb collisions at $\sqrt{s_{NN}} = 5.02$ TeV," *Phys. Lett. B* **719** (2013) 29–41, `arXiv:1212.2001 [nucl-ex]`.

[439] **LHCb** Collaboration, R. Aaij *et al.*, "Measurements of long-range near-side angular correlations in $\sqrt{s_{\text{NN}}} = 5$TeV proton-lead collisions in the forward region," *Phys. Lett. B* **762** (2016) 473–483, `arXiv:1512.00439 [nucl-ex]`.

[440] **ATLAS** Collaboration, G. Aad *et al.*, "Evidence for light-by-light scattering in heavy-ion collisions with the ATLAS detector at the LHC," *Nature Phys.* **13** no. 9, (2017) 852–858, `arXiv:1702.01625 [hep-ex]`.

[441] **CMS** Collaboration, A. M. Sirunyan *et al.*, "Evidence for light-by-light scattering and searches for axion-like particles in ultraperipheral PbPb collisions at $\sqrt{s_{\text{NN}}} = 5.02$ TeV," *Phys. Lett. B* **797** (2019) 134826, `arXiv:1810.04602 [hep-ex]`.

[442] A. Dainese, M. Mangano, A. B. Meyer, A. Nisati, G. Salam, and M. A. Vesterinen, "Report on the Physics at the HL-LHC, and Perspectives for the HE-LHC," CERN Yellow Report CERN-2019-007, CERN, 2019. `https://cds.cern.ch/record/2703572`.

[443] ATLAS Collaboration, "A Radiation-Hard Zero Degree Calorimeter for ATLAS in the HL-LHC era," 2021. `https://cds.cern.ch/record/2781150`.

[444] Y. Bashan, Z. Citron, B. Cole, M. Grosse Perdekamp, A. Hase, T. Koeth, C. Lantz, S. Lascio, R. Longo, D. MacLean, A. Mignerey, Y. Moyal, M. Murray, M. Nickel, M. Phipps, S. Popescu, N. Santiago, A. Sickles, S. Shenkar, P. Steinberg, L. Sudit, A. Tate, Q. Wang, and S. Yang, "A Run 4 Zero Degree Calorimeter for CMS," tech. rep., CERN, Geneva, Nov, 2021. `https://cds.cern.ch/record/2791533`. This is a joint project with the ATLAS heavy ion group.

[445] CMS Collaboration, "A MIP Timing Detector for the CMS Phase-2 Upgrade," tech. rep., CERN, Geneva, Mar, 2019. `https://cds.cern.ch/record/2667167`.

[446] C. ALICE, "Letter of intent for ALICE 3: A next generation heavy-ion experiment at the LHC," tech. rep., CERN, Geneva, Mar, 2022. `https://cds.cern.ch/record/2803563`.

[447] **PHENIX** Collaboration, A. Adare *et al.*, "An Upgrade Proposal from the PHENIX Collaboration,"

arXiv:1501.06197 [nucl-ex].

[448] **ATLAS** Collaboration, G. Aad *et al.*, "Observation of a Centrality-Dependent Dijet Asymmetry in Lead-Lead Collisions at $\sqrt{s_{NN}}$ = 2.77 TeV with the ATLAS Detector at the LHC," *Phys. Rev. Lett.* **105** (2010) 252303, arXiv:1011.6182 [hep-ex].

[449] **CMS** Collaboration, S. Chatrchyan *et al.*, "Observation and studies of jet quenching in PbPb collisions at nucleon-nucleon center-of-mass energy = 2.76 TeV," *Phys. Rev. C* **84** (2011) 024906, arXiv:1102.1957 [nucl-ex].

[450] **CMS** Collaboration, S. Chatrchyan *et al.*, "Jet momentum dependence of jet quenching in PbPb collisions at $\sqrt{s_{NN}}$ = 2.76 TeV," *Phys. Lett. B* **712** (2012) 176–197, arXiv:1202.5022 [nucl-ex].

[451] **CMS** Collaboration, S. Chatrchyan *et al.*, "Studies of jet quenching using isolated-photon+jet correlations in PbPb and *pp* collisions at $\sqrt{s_{NN}}$ = 2.76 TeV," *Phys. Lett. B* **718** (2013) 773–794, arXiv:1205.0206 [nucl-ex].

[452] **CMS** Collaboration, A. M. Sirunyan *et al.*, "Study of jet quenching with isolated-photon+jet correlations in PbPb and pp collisions at $\sqrt{s_{\mathrm{NN}}}$ = 5.02 TeV," *Phys. Lett. B* **785** (2018) 14–39, arXiv:1711.09738 [nucl-ex].

[453] **ATLAS** Collaboration, M. Aaboud *et al.*, "Measurement of photon–jet transverse momentum correlations in 5.02 TeV Pb + Pb and *pp* collisions with ATLAS," *Phys. Lett. B* **789** (2019) 167–190, arXiv:1809.07280 [nucl-ex].

[454] **CMS** Collaboration, A. M. Sirunyan *et al.*, "Study of Jet Quenching with Z + jet Correlations in Pb-Pb and *pp* Collisions at $\sqrt{s}_{NN}$ = 5.02 TeV," *Phys. Rev. Lett.* **119** no. 8, (2017) 082301, arXiv:1702.01060 [nucl-ex].

[455] **ATLAS** Collaboration, G. Aad *et al.*, "Measurement of the jet radius and transverse momentum dependence of inclusive jet suppression in lead-lead collisions at $\sqrt{s_{NN}}$= 2.76 TeV with the ATLAS detector," *Phys. Lett. B* **719** (2013) 220–241, arXiv:1208.1967 [hep-ex].

[456] **ATLAS** Collaboration, G. Aad *et al.*, "Measurements of the Nuclear Modification Factor for Jets in Pb+Pb Collisions at $\sqrt{s_{\mathrm{NN}}}$ = 2.76 TeV with the ATLAS Detector," *Phys. Rev. Lett.* **114** no. 7, (2015) 072302, arXiv:1411.2357 [hep-ex].

[457] **CMS** Collaboration, V. Khachatryan *et al.*, "Measurement of inclusive jet cross sections in *pp* and PbPb collisions at $\sqrt{s_{NN}}$ = 2.76 TeV," *Phys. Rev. C* **96** no. 1, (2017) 015202, arXiv:1609.05383 [nucl-ex].

[458] **ATLAS** Collaboration, M. Aaboud *et al.*, "Measurement of the nuclear modification factor for inclusive jets in Pb+Pb collisions at $\sqrt{s_{\mathrm{NN}}}$ = 5.02 TeV with the ATLAS detector," *Phys. Lett. B* **790** (2019) 108–128, arXiv:1805.05635 [nucl-ex].

[459] **CMS** Collaboration, A. M. Sirunyan *et al.*, "First measurement of large area jet transverse momentum spectra in heavy-ion collisions," *JHEP* **05** (2021) 284, arXiv:2102.13080 [hep-ex].

[460] **ALICE** Collaboration, J. Adam *et al.*, "Measurement of jet suppression in central Pb-Pb collisions at $\sqrt{s_{\mathrm{NN}}}$ = 2.76 TeV," *Phys. Lett. B* **746** (2015) 1–14, arXiv:1502.01689 [nucl-ex].

[461] **CMS** Collaboration, V. Khachatryan *et al.*, "Measurement of transverse momentum relative to dijet systems in PbPb and pp collisions at $\sqrt{s_{NN}}$ = 2.76 TeV," *JHEP* **01** (2016) 006, arXiv:1509.09029 [nucl-ex].

[462] **CMS** Collaboration, S. Chatrchyan *et al.*, "Modification of Jet Shapes in PbPb Collisions at $\sqrt{s_{NN}}$ = 2.76 TeV," *Phys. Lett. B* **730** (2014) 243–263, arXiv:1310.0878 [nucl-ex].

[463] **CMS** Collaboration, S. Chatrchyan *et al.*, "Measurement of Jet Fragmentation in PbPb and pp Collisions at $\sqrt{s_{NN}}$ = 2.76 TeV," *Phys. Rev. C* **90** no. 2, (2014) 024908, arXiv:1406.0932 [nucl-ex].

[464] **ATLAS** Collaboration, G. Aad *et al.*, "Measurement of inclusive jet charged-particle fragmentation functions in Pb+Pb collisions at $\sqrt{s_{NN}}$ = 2.76 TeV with the ATLAS detector," *Phys. Lett. B* **739** (2014) 320–342, arXiv:1406.2979 [hep-ex].

[465] **CMS** Collaboration, A. M. Sirunyan *et al.*, "Measurement of the Splitting Function in *pp* and Pb-Pb Collisions at $\sqrt{s_{\mathrm{NN}}}$ = 5.02 TeV," *Phys. Rev. Lett.* **120** no. 14, (2018) 142302, arXiv:1708.09429 [nucl-ex].

[466] **CMS** Collaboration, A. M. Sirunyan *et al.*, "Jet Shapes of Isolated Photon-Tagged Jets in Pb-Pb and pp Collisions at $\sqrt{s_{\mathrm{NN}}}$ = 5.02 TeV," *Phys. Rev. Lett.* **122** no. 15, (2019) 152001, arXiv:1809.08602 [hep-ex].

[467] **ATLAS** Collaboration, G. Aad *et al.*, "Medium-Induced Modification of Z-Tagged Charged Particle

Yields in $Pb + Pb$ Collisions at 5.02 TeV with the ATLAS Detector," *Phys. Rev. Lett.* **126** no. 7, (2021) 072301, `arXiv:2008.09811 [nucl-ex]`.

[468] **ATLAS** Collaboration, M. Aaboud *et al.*, "Measurement of jet fragmentation in Pb+Pb and *pp* collisions at $\sqrt{s_{NN}} = 5.02$ TeV with the ATLAS detector," *Phys. Rev. C* **98** no. 2, (2018) 024908, `arXiv:1805.05424 [nucl-ex]`.

[469] **CMS** Collaboration, A. M. Sirunyan *et al.*, "Observation of Medium-Induced Modifications of Jet Fragmentation in Pb-Pb Collisions at $\sqrt{s_{NN}} = 5.02$ TeV Using Isolated Photon-Tagged Jets," *Phys. Rev. Lett.* **121** no. 24, (2018) 242301, `arXiv:1801.04895 [hep-ex]`.

[470] **CMS** Collaboration, A. M. Sirunyan *et al.*, "Measurement of the groomed jet mass in PbPb and pp collisions at $\sqrt{s_{NN}} = 5.02$ TeV," *JHEP* **10** (2018) 161, `arXiv:1805.05145 [hep-ex]`.

[471] **ALICE** Collaboration, S. Acharya *et al.*, "Exploration of jet substructure using iterative declustering in pp and Pb–Pb collisions at LHC energies," *Phys. Lett. B* **802** (2020) 135227, `arXiv:1905.02512 [nucl-ex]`.

[472] **ALICE** Collaboration, S. Acharya *et al.*, "Medium modification of the shape of small-radius jets in central Pb-Pb collisions at $\sqrt{s_{NN}} = 2.76$ TeV," *JHEP* **10** (2018) 139, `arXiv:1807.06854 [nucl-ex]`.

[473] **CMS** Collaboration, A. M. Sirunyan *et al.*, "Measurement of quark- and gluon-like jet fractions using jet charge in PbPb and pp collisions at 5.02 TeV," *JHEP* **07** (2020) 115, `arXiv:2004.00602 [hep-ex]`.

[474] **CMS** Collaboration, A. M. Sirunyan *et al.*, "Using Z Boson Events to Study Parton-Medium Interactions in Pb-Pb Collisions," *Phys. Rev. Lett.* **128** no. 12, (2022) 122301, `arXiv:2103.04377 [hep-ex]`.

[475] CMS Collaboration, "Performance of jet quenching measurements in pp and PbPb collisions with CMS at the HL-LHC," CMS Physics Analysis Summary CMS-PAS-FTR-18-025, CERN, 2018. `http://cds.cern.ch/record/2651892`.

[476] ATLAS Collaboration, "Projections for ATLAS Measurements of Jet Modifications in Pb+Pb Collisions in LHC Runs 3 and 4." ATL-PHYS-PUB-2018-019, 2018. `https://cds.cern.ch/record/2644406`.

[477] **sPHENIX** Collaboration, C. A. Aidala *et al.*, "Design and Beam Test Results for the sPHENIX Electromagnetic and Hadronic Calorimeter Prototypes," *IEEE Trans. Nucl. Sci.* **65** no. 12, (2018) 2901–2919, `arXiv:1704.01461 [physics.ins-det]`.

[478] B. Z. Kopeliovich, I. K. Potashnikova, I. Schmidt, and M. Siddikov, "Survival of charmonia in a hot environment," *Phys. Rev. C* **91** no. 2, (2015) 024911, `arXiv:1409.5147 [hep-ph]`.

[479] S. Aronson, E. Borras, B. Odegard, R. Sharma, and I. Vitev, "Collisional and thermal dissociation of J/ψ and Υ states at the LHC," *Phys. Lett. B* **778** (2018) 384–391, `arXiv:1709.02372 [hep-ph]`.

[480] X. Du, R. Rapp, and M. He, "Color Screening and Regeneration of Bottomonia in High-Energy Heavy-Ion Collisions," *Phys. Rev. C* **96** no. 5, (2017) 054901, `arXiv:1706.08670 [hep-ph]`.

[481] **CMS** Collaboration, A. M. Sirunyan *et al.*, "Measurement of the $B^{\pm}$ Meson Nuclear Modification Factor in Pb-Pb Collisions at $\sqrt{s_{NN}} = 5.02$ TeV," *Phys. Rev. Lett.* **119** no. 15, (2017) 152301, `arXiv:1705.04727 [hep-ex]`.

[482] **CMS** Collaboration, A. M. Sirunyan *et al.*, "Measurement of B_s^0 meson production in pp and PbPb collisions at $\sqrt{s_{NN}} = 5.02$ TeV," *Phys. Lett. B* **796** (2019) 168–190, `arXiv:1810.03022 [hep-ex]`.

[483] **ALICE** Collaboration, S. Acharya *et al.*, "Measurement of D^0, D^+, D^{*+} and D_s^+ production in Pb-Pb collisions at $\sqrt{s_{NN}} = 5.02$ TeV," *JHEP* **10** (2018) 174, `arXiv:1804.09083 [nucl-ex]`.

[484] **CMS** Collaboration, A. M. Sirunyan *et al.*, "Nuclear modification factor of D^0 mesons in PbPb collisions at $\sqrt{s_{NN}} = 5.02$ TeV," *Phys. Lett. B* **782** (2018) 474–496, `arXiv:1708.04962 [nucl-ex]`.

[485] **ALICE** Collaboration, J. Adam *et al.*, "Transverse momentum dependence of D-meson production in Pb-Pb collisions at $\sqrt{s_{NN}} = 2.76$ TeV," *JHEP* **03** (2016) 081, `arXiv:1509.06888 [nucl-ex]`.

[486] **ALICE** Collaboration, S. Acharya *et al.*, "Measurement of beauty and charm production in pp collisions at $\sqrt{s} = 5.02$ TeV via non-prompt and prompt D mesons," *JHEP* **05** (2021) 220, `arXiv:2102.13601 [nucl-ex]`.

[487] **CMS** Collaboration, A. M. Sirunyan *et al.*, "Studies of Beauty Suppression via Nonprompt D^0 Mesons in Pb-Pb Collisions at $Q^2 = 4$ GeV^2," *Phys. Rev. Lett.* **123** no. 2, (2019) 022001, `arXiv:1810.11102 [hep-ex]`.

[488] **CMS** Collaboration, A. M. Sirunyan *et al.*, "Measurement of prompt and nonprompt J/ψ production in pp and pPb collisions at $\sqrt{s_{NN}} = 5.02$ TeV," *Eur. Phys. J. C* **77** no. 4, (2017) 269,

arXiv:1702.01462 [nucl-ex].

[489] **ATLAS** Collaboration, M. Aaboud *et al.*, "Prompt and non-prompt J/ψ and $\psi(2S)$ suppression at high transverse momentum in 5.02 TeV Pb+Pb collisions with the ATLAS experiment," *Eur. Phys. J. C* **78** no. 9, (2018) 762, arXiv:1805.04077 [nucl-ex].

[490] **CMS** Collaboration, S. Chatrchyan *et al.*, "Indications of suppression of excited Υ states in PbPb collisions at $\sqrt{S_{NN}} = 2.76$ TeV," *Phys. Rev. Lett.* **107** (2011) 052302, arXiv:1105.4894 [nucl-ex].

[491] **CMS** Collaboration, S. Chatrchyan *et al.*, "Suppression of non-prompt J/ψ, prompt J/ψ, and Y(1S) in PbPb collisions at $\sqrt{s_{NN}} = 2.76$ TeV," *JHEP* **05** (2012) 063, arXiv:1201.5069 [nucl-ex].

[492] **CMS** Collaboration, S. Chatrchyan *et al.*, "Observation of Sequential Upsilon Suppression in PbPb Collisions," *Phys. Rev. Lett.* **109** (2012) 222301, arXiv:1208.2826 [nucl-ex]. [Erratum: Phys.Rev.Lett. 120, 199903 (2018)].

[493] **CMS** Collaboration, V. Khachatryan *et al.*, "Suppression of $\Upsilon(1S), \Upsilon(2S)$ and $\Upsilon(3S)$ production in PbPb collisions at $\sqrt{s_{\mathrm{NN}}} = 2.76$ TeV," *Phys. Lett. B* **770** (2017) 357–379, arXiv:1611.01510 [nucl-ex].

[494] **ATLAS** Collaboration, G. Aad *et al.*, "Measurement of the centrality dependence of J/ψ yields and observation of Z production in lead–lead collisions with the ATLAS detector at the LHC," *Phys. Lett. B* **697** (2011) 294–312, arXiv:1012.5419 [hep-ex].

[495] **ALICE** Collaboration, B. Abelev *et al.*, "J/ψ suppression at forward rapidity in Pb-Pb collisions at $\sqrt{s_{NN}} = 2.76$ TeV," *Phys. Rev. Lett.* **109** (2012) 072301, arXiv:1202.1383 [hep-ex].

[496] **CMS** Collaboration, V. Khachatryan *et al.*, "Measurement of Prompt $\psi(2S) \to J/\psi$ Yield Ratios in Pb-Pb and $p - p$ Collisions at $\sqrt{s_{NN}} = 2.76$ TeV," *Phys. Rev. Lett.* **113** no. 26, (2014) 262301, arXiv:1410.1804 [nucl-ex].

[497] **ALICE** Collaboration, J. Adam *et al.*, "Differential studies of inclusive J/ψ and $\psi(2S)$ production at forward rapidity in Pb-Pb collisions at $\sqrt{s_{\mathrm{NN}}} = 2.76$ TeV," *JHEP* **05** (2016) 179, arXiv:1506.08804 [nucl-ex].

[498] **ALICE** Collaboration, F. Reidt, "Upgrade of the ALICE ITS detector," *Nucl. Instrum. Meth. A* **1032** (2022) 166632, arXiv:2111.08301 [physics.ins-det].

[499] **ALICE** Collaboration, D. Colella, "ALICE ITS 3: the first truly cylindrical inner tracker," in *12th International Conference on Position Sensitive Detectors.* 11, 2021. arXiv:2111.09689 [physics.ins-det].

[500] CMS Collaboration, "Open heavy flavor and quarkonia in heavy ion collisions at HL-LHC," CMS Physics Analysis Summary CMS-PAS-FTR-18-024, CERN, 2018. http://cds.cern.ch/record/2650897.

[501] CMS Collaboration, "Predictions on the precision achievable for small system flow observables in the context of HL-LHC," CMS Physics Analysis Summary CMS-PAS-FTR-18-026, CERN, 2018. http://cds.cern.ch/record/2650773.

[502] **ATLAS** Collaboration, ATLAS collaboration, "Projections for ATLAS Measurements of Bulk Properties of Pb+Pb, p+Pb, and pp Collisions in LHC Runs 3 and 4," tech. rep., CERN, Geneva, Oct, 2018. http://cds.cern.ch/record/2644407.

[503] **LHCb** Collaboration, R. Aaij *et al.*, "Observation of Multiplicity Dependent Prompt $\chi_{c1}(3872)$ and $\psi(2S)$ Production in pp Collisions," *Phys. Rev. Lett.* **126** no. 9, (2021) 092001, arXiv:2009.06619 [hep-ex].

[504] **CMS** Collaboration, A. M. Sirunyan *et al.*, "Evidence for X(3872) in Pb-Pb Collisions and Studies of its Prompt Production at $\sqrt{s_{NN}}$=5.02 TeV," *Phys. Rev. Lett.* **128** no. 3, (2022) 032001, arXiv:2102.13048 [hep-ex].

[505] **ALICE** Collaboration, ALICE Collaboration, "Correlated event-by-event fluctuations of flow harmonics in Pb-Pb collisions at $\sqrt{s_{\mathrm{NN}}} = 2.76$ TeV," *Phys. Rev. Lett.* **117** (2016) 182301, arXiv:1604.07663 [nucl-ex].

[506] CMS Collaboration, "Observation of long-range, near-side angular correlations in proton–proton collisions at the LHC," *JHEP* **09** (2010) 091, arXiv:1009.4122 [hep-ex].

[507] CMS Collaboration, "Observation of long-range, near-side angular correlations in pPb collisions at the LHC," *Phys. Lett. B* **718** (2013) 795, arXiv:1210.5482 [hep-ex].

[508] ATLAS Collaboration, "Observation of Associated Near-Side and Away-Side Long-Range Correlations in $\sqrt{s_{\mathrm{NN}}} = 5.02$ TeV Proton–Lead Collisions with the ATLAS Detector," *Phys. Rev. Lett.* **110** (2013) 182302, arXiv:1212.5198 [hep-ex].

[509] F. G. Gardim, F. Grassi, M. Luzum, and J.-Y. Ollitrault, "Breaking of factorization of two-particle correlations in hydrodynamics," *Phys. Rev. C* **87** no. 3, (2013) 031901, `arXiv:1211.0989 [nucl-th]`.

[510] C. A. Bertulani, S. R. Klein, and J. Nystrand, "Physics of ultra-peripheral nuclear collisions," *Ann. Rev. Nucl. Part. Sci.* **55** (2005) 271–310, `arXiv:nucl-ex/0502005`.

[511] J. G. Contreras and J. D. Tapia Takaki, "Ultra-peripheral heavy-ion collisions at the LHC," *Int. J. Mod. Phys. A* **30** (2015) 1542012.

[512] S. Klein and P. Steinberg, "Photonuclear and Two-photon Interactions at High-Energy Nuclear Colliders," *Ann. Rev. Nucl. Part. Sci.* **70** (2020) 323–354, `arXiv:2005.01872 [nucl-ex]`.

[513] A. J. Baltz, "The Physics of Ultraperipheral Collisions at the LHC," *Phys. Rept.* **458** (2008) 1–171, `arXiv:0706.3356 [nucl-ex]`.

[514] Z. Citron *et al.*, "Report from Working Group 5: Future physics opportunities for high-density QCD at the LHC with heavy-ion and proton beams," *CERN Yellow Rep. Monogr.* **7** (2019) 1159–1410, `arXiv:1812.06772 [hep-ph]`.

[515] N. Burmasov, "Central Diffraction and Ultra-Peripheral Collisions in ALICE in Run 3 and 4," *Phys. Part. Nucl.* **53** no. 2, (2022) 297–302, `arXiv:2010.09752 [hep-ex]`.

[516] S. R. Klein, "Ultra-peripheral collisions and hadronic structure," *Nucl. Phys. A* **967** (2017) 249–256, `arXiv:1704.04715 [nucl-ex]`.

[517] S. R. Klein, J. Nystrand, and R. Vogt, "Photoproduction of top in peripheral heavy ion collisions," *Eur. Phys. J. C* **21** (2001) 563–566, `arXiv:hep-ph/0005157`.

[518] S. R. Klein, J. Nystrand, and R. Vogt, "Heavy quark photoproduction in ultraperipheral heavy ion collisions," *Phys. Rev. C* **66** (2002) 044906, `arXiv:hep-ph/0206220`.

[519] V. P. Goncalves and M. V. T. Machado, "Diffractive photoproduction of heavy quarks in hadronic collisions," *Phys. Rev. D* **75** (2007) 031502, `arXiv:hep-ph/0612265`.

[520] A. Adeluyi and T. Nguyen, "Photoproduction of heavy quarks in ultraperipheral pp, pA, and AA collisions at the CERN Large Hadron Collider," `arXiv:1210.3327 [nucl-th]`.

[521] V. P. Gonçalves, G. Sampaio dos Santos, and C. R. Sena, "Inclusive heavy quark photoproduction in *pp*, *pPb* and *PbPb* collisions at Run 2 LHC energies," *Nucl. Phys. A* **976** (2018) 33–45, `arXiv:1711.04497 [hep-ph]`.

[522] L. Frankfurt, M. Strikman, D. Treleani, and C. Weiss, "Evidence for color fluctuations in the nucleon in high-energy scattering," *Phys. Rev. Lett.* **101** (2008) 202003, `arXiv:0808.0182 [hep-ph]`.

[523] S. Fichet, G. von Gersdorff, B. Lenzi, C. Royon, and M. Saimpert, "Light-by-light scattering with intact protons at the LHC: from Standard Model to New Physics," *JHEP* **02** (2015) 165, `arXiv:1411.6629 [hep-ph]`.

[524] S. Fichet, G. von Gersdorff, O. Kepka, B. Lenzi, C. Royon, and M. Saimpert, "Probing new physics in diphoton production with proton tagging at the Large Hadron Collider," *Phys. Rev. D* **89** (2014) 114004, `arXiv:1312.5153 [hep-ph]`.

[525] ATLAS Collaboration, "Prospects for Measurements of Photon-Induced Processes in Ultra-Peripheral Collisions of Heavy Ions with the ATLAS Detector in the LHC Runs 3 and 4." ATL-PHYS-PUB-2018-018, 2018. `https://cds.cern.ch/record/2641655`.

[526] D. d'Enterria and G. G. da Silveira, "Observing light-by-light scattering at the Large Hadron Collider," *Phys. Rev. Lett.* **111** (2013) 080405, `arXiv:1305.7142 [hep-ph]`. [Erratum: Phys.Rev.Lett. 116, 129901 (2016)].

[527] S. Knapen, T. Lin, H. K. Lou, and T. Melia, "Searching for Axionlike Particles with Ultraperipheral Heavy-Ion Collisions," *Phys. Rev. Lett.* **118** no. 17, (2017) 171801, `arXiv:1607.06083 [hep-ph]`.

[528] ATLAS Collaboration, "ATLAS Forward Proton Phase-I Upgrade: Technical Design Report," 2015. `https://cds.cern.ch/record/2017378`.

[529] CMS-TOTEM Collaboration, "CMS-TOTEM Precision Proton Spectrometer," tech. rep., CERN, Sep, 2014. `https://cds.cern.ch/record/1753795`.

[530] M. Bauer, M. Neubert, and A. Thamm, "Collider Probes of Axion-Like Particles," *JHEP* **12** (2017) 044, `arXiv:1708.00443 [hep-ph]`.

[531] CMS Collaboration, "Evidence for light-by-light scattering and searches for axion-like particles in ultraperipheral PbPb collisions at $\sqrt{s_{\mathrm{NN}}} = 5.02\,\mathrm{TeV}$," *Phys. Lett. B* **797** (2019) 134826, `arXiv:1810.04602 [hep-ex]`.

[532] D. Adamová *et al.*, "A next-generation LHC heavy-ion experiment," `arXiv:1902.01211`

[physics.ins-det].

[533] C. Baldenegro, S. Fichet, G. von Gersdorff, and C. Royon, "Searching for axion-like particles with proton tagging at the LHC," *JHEP* **06** (2018) 131, arXiv:1803.10835 [hep-ph].

[534] C. Baldenegro, S. Hassani, C. Royon, and L. Schoeffel, "Extending the constraint for axion-like particles as resonances at the LHC and laser beam experiments," *Phys. Lett. B* **795** (2019) 339–345, arXiv:1903.04151 [hep-ph].

[535] J. de Favereau de Jeneret, V. Lemaitre, Y. Liu, S. Ovyn, T. Pierzchala, K. Piotrzkowski, X. Rouby, N. Schul, and M. Vander Donckt, "High energy photon interactions at the LHC," arXiv:0908.2020 [hep-ph].

[536] T. Pierzchala and K. Piotrzkowski, "Sensitivity to anomalous quartic gauge couplings in photon-photon interactions at the LHC," *Nucl. Phys. B Proc. Suppl.* **179-180** (2008) 257–264, arXiv:0807.1121 [hep-ph].

[537] E. Chapon, C. Royon, and O. Kepka, "Anomalous quartic W W gamma gamma, Z Z gamma gamma, and trilinear WW gamma couplings in two-photon processes at high luminosity at the LHC," *Phys. Rev. D* **81** (2010) 074003, arXiv:0912.5161 [hep-ph].

[538] ATLAS Collaboration, "Observation of photon-induced W^+W^- production in pp collisions at $\sqrt{s} = 13$ TeV using the ATLAS detector," *Phys. Lett. B* **816** (2021) 136190, arXiv:2010.04019 [hep-ex].

[539] ATLAS Collaboration, "Sensitivity to exclusive WW production in photon scattering at the High Luminosity LHC." ATL-PHYS-PUB-2021-026, 2021. https://cds.cern.ch/record/2776764.

[540] O. Kepka and C. Royon, "Anomalous $WW\gamma$ coupling in photon-induced processes using forward detectors at the LHC," *Phys. Rev. D* **78** (2008) 073005, arXiv:0808.0322 [hep-ph].

[541] S. Fichet, G. von Gersdorff, and C. Royon, "Scattering light by light at 750 GeV at the LHC," *Phys. Rev. D* **93** no. 7, (2016) 075031, arXiv:1512.05751 [hep-ph].

[542] S. Fichet, G. von Gersdorff, and C. Royon, "Measuring the Diphoton Coupling of a 750 GeV Resonance," *Phys. Rev. Lett.* **116** no. 23, (2016) 231801, arXiv:1601.01712 [hep-ph].

[543] C. Baldenegro, S. Fichet, G. von Gersdorff, and C. Royon, "Probing the anomalous $\gamma\gamma\gamma$Z coupling at the LHC with proton tagging," *JHEP* **06** (2017) 142, arXiv:1703.10600 [hep-ph].

[544] C. Baldenegro, G. Biagi, G. Legras, and C. Royon, "Central exclusive production of W boson pairs in pp collisions at the LHC in hadronic and semi-leptonic final states," *JHEP* **12** (2020) 165, arXiv:2009.08331 [hep-ph].

[545] C. Baldenegro, A. Bellora, S. Fichet, G. von Gersdorff, M. Pitt, and C. Royon, "Searching for anomalous top quark interactions with proton tagging and timing detectors at the LHC," arXiv:2205.01173 [hep-ph].

[546] S. J. Brodsky, V. S. Fadin, V. T. Kim, L. N. Lipatov, and G. B. Pivovarov, "The QCD pomeron with optimal renormalization," *JETP Lett.* **70** (1999) 155–160, arXiv:hep-ph/9901229.

[547] S. J. Brodsky, V. S. Fadin, V. T. Kim, L. N. Lipatov, and G. B. Pivovarov, "High-energy QCD asymptotics of photon-photon collisions," *JETP Lett.* **76** (2002) 249–252, arXiv:hep-ph/0207297.

[548] F. Caporale, D. Y. Ivanov, and A. Papa, "BFKL resummation effects in the gamma* gamma* total hadronic cross section," *Eur. Phys. J. C* **58** (2008) 1–7, arXiv:0807.3231 [hep-ph].

[549] X.-C. Zheng, X.-G. Wu, S.-Q. Wang, J.-M. Shen, and Q.-L. Zhang, "Reanalysis of the BFKL Pomeron at the next-to-leading logarithmic accuracy," *JHEP* **10** (2013) 117, arXiv:1308.2381 [hep-ph].

[550] G. A. Chirilli and Y. V. Kovchegov, "$\gamma^*\gamma^*$ Cross Section at NLO and Properties of the BFKL Evolution at Higher Orders," *JHEP* **05** (2014) 099, arXiv:1403.3384 [hep-ph]. [Erratum: JHEP 08, 075 (2015)].

[551] D. Y. Ivanov, B. Murdaca, and A. Papa, "The $\gamma^*\gamma^*$ total cross section in next-to-leading order BFKL and LEP2 data," *JHEP* **10** (2014) 058, arXiv:1407.8447 [hep-ph].

[552] D. Yu. Ivanov and A. Papa, "Electroproduction of two light vector mesons in the next-to-leading approximation," *Nucl. Phys. B* **732** (2006) 183–199, arXiv:hep-ph/0508162.

[553] D. Yu. Ivanov and A. Papa, "Electroproduction of two light vector mesons in next-to-leading BFKL: Study of systematic effects," *Eur. Phys. J. C* **49** (2007) 947–955, arXiv:hep-ph/0610042.

[554] R. Enberg, B. Pire, L. Szymanowski, and S. Wallon, "BFKL resummation effects in gamma* gamma* —> rho rho," *Eur. Phys. J. C* **45** (2006) 759–769, arXiv:hep-ph/0508134. [Erratum: Eur.Phys.J.C 51, 1015 (2007)].

[555] J. Kwiecinski and L. Motyka, "Diffractive J / psi production in high-energy gamma gamma collisions as a probe of the QCD pomeron," *Phys. Lett. B* **438** (1998) 203–210, `arXiv:hep-ph/9806260`.

[556] F. G. Celiberto, D. Yu. Ivanov, B. Murdaca, and A. Papa, "High-energy resummation in heavy-quark pair photoproduction," *Phys. Lett. B* **777** (2018) 141–150, `arXiv:1709.10032 [hep-ph]`.

[557] N. Craig, C. Csaki, and A. El-Khadra, "Theory Frontier Summary Report,". Snowmass 2021 Community Study.

[558] A. Huss, J. Huston, S. Jones, and M. Pellen, "Les Houches 2021: Physics at TeV Colliders: Report on the Standard Model Precision Wishlist," `arXiv:2207.02122 [hep-ph]`.

[559] G. Heinrich, "Collider Physics at the Precision Frontier," *Phys. Rept.* **922** (2021) 1–69, `arXiv:2009.00516 [hep-ph]`.

[560] F. Febres Cordero, A. von Manteuffel, and T. Neumann, "Computational challenges for multi-loop collider phenomenology," in *2022 Snowmass Summer Study*. 4, 2022. `arXiv:2204.04200 [hep-ph]`.

[561] G. Travaglini *et al.*, "The SAGEX Review on Scattering Amplitudes," `arXiv:2203.13011 [hep-th]`.

[562] L. Chen, "A prescription for projectors to compute helicity amplitudes in D dimensions," *Eur. Phys. J. C* **81** no. 5, (2021) 417, `arXiv:1904.00705 [hep-ph]`.

[563] T. Peraro and L. Tancredi, "Physical projectors for multi-leg helicity amplitudes," *JHEP* **07** (2019) 114, `arXiv:1906.03298 [hep-ph]`.

[564] T. Peraro and L. Tancredi, "Tensor decomposition for bosonic and fermionic scattering amplitudes," *Phys. Rev. D* **103** no. 5, (2021) 054042, `arXiv:2012.00820 [hep-ph]`.

[565] F. V. Tkachov, "A Theorem on Analytical Calculability of Four Loop Renormalization Group Functions," *Phys. Lett. B* **100** (1981) 65–68.

[566] K. G. Chetyrkin and F. V. Tkachov, "Integration by Parts: The Algorithm to Calculate beta Functions in 4 Loops," *Nucl. Phys. B* **192** (1981) 159–204.

[567] T. Gehrmann and E. Remiddi, "Differential equations for two loop four point functions," *Nucl. Phys. B* **580** (2000) 485–518, `arXiv:hep-ph/9912329`.

[568] S. Laporta, "High precision calculation of multiloop Feynman integrals by difference equations," *Int. J. Mod. Phys. A* **15** (2000) 5087–5159, `arXiv:hep-ph/0102033`.

[569] P. Kant, "Finding Linear Dependencies in Integration-By-Parts Equations: A Monte Carlo Approach," *Comput. Phys. Commun.* **185** (2014) 1473–1476, `arXiv:1309.7287 [hep-ph]`.

[570] A. von Manteuffel and R. M. Schabinger, "A novel approach to integration by parts reduction," *Phys. Lett. B* **744** (2015) 101–104, `arXiv:1406.4513 [hep-ph]`.

[571] T. Peraro, "Scattering amplitudes over finite fields and multivariate functional reconstruction," *JHEP* **12** (2016) 030, `arXiv:1608.01902 [hep-ph]`.

[572] S. Weinzierl, "Feynman Integrals," `arXiv:2201.03593 [hep-th]`.

[573] S. Abreu, R. Britto, and C. Duhr, "The SAGEX Review on Scattering Amplitudes, Chapter 3: Mathematical structures in Feynman integrals," `arXiv:2203.13014 [hep-th]`.

[574] J. Blümlein and C. Schneider, "The SAGEX Review on Scattering Amplitudes, Chapter 4: Multi-loop Feynman Integrals," `arXiv:2203.13015 [hep-th]`.

[575] S. Abreu, F. Febres Cordero, H. Ita, M. Jaquier, B. Page, and M. Zeng, "Two-Loop Four-Gluon Amplitudes from Numerical Unitarity," *Phys. Rev. Lett.* **119** no. 14, (2017) 142001, `arXiv:1703.05273 [hep-ph]`.

[576] S. Abreu, F. Febres Cordero, H. Ita, B. Page, and M. Zeng, "Planar Two-Loop Five-Gluon Amplitudes from Numerical Unitarity," *Phys. Rev. D* **97** no. 11, (2018) 116014, `arXiv:1712.03946 [hep-ph]`.

[577] S. Abreu, J. Dormans, F. Febres Cordero, H. Ita, B. Page, and V. Sotnikov, "Analytic Form of the Planar Two-Loop Five-Parton Scattering Amplitudes in QCD," *JHEP* **05** (2019) 084, `arXiv:1904.00945 [hep-ph]`.

[578] A. V. Kotikov, "Differential equations method: New technique for massive Feynman diagrams calculation," *Phys. Lett. B* **254** (1991) 158–164.

[579] J. M. Henn, "Multiloop integrals in dimensional regularization made simple," *Phys. Rev. Lett.* **110** (2013) 251601, `arXiv:1304.1806 [hep-th]`.

[580] S. Abreu, H. Ita, F. Moriello, B. Page, W. Tschernow, and M. Zeng, "Two-Loop Integrals for Planar Five-Point One-Mass Processes," *JHEP* **11** (2020) 117, `arXiv:2005.04195 [hep-ph]`.

[581] H. Frellesvig, "On epsilon factorized differential equations for elliptic Feynman integrals," *JHEP* **03** (2022) 079, `arXiv:2110.07968 [hep-th]`.

[582] C. Dlapa, X. Li, and Y. Zhang, "Leading singularities in Baikov representation and Feynman integrals with uniform transcendental weight," *JHEP* **07** (2021) 227, `arXiv:2103.04638 [hep-th]`.

[583] N. Syrrakos, "Pentagon integrals to arbitrary order in the dimensional regulator," *JHEP* **06** (2021) 037, `arXiv:2012.10635 [hep-ph]`.

[584] A. Kardos, C. G. Papadopoulos, A. V. Smirnov, N. Syrrakos, and C. Wever, "Two-loop non-planar hexa-box integrals with one massive leg," *JHEP* **05** (2022) 033, `arXiv:2201.07509 [hep-ph]`.

[585] J. Henn, T. Peraro, Y. Xu, and Y. Zhang, "A first look at the function space for planar two-loop six-particle Feynman integrals," *JHEP* **03** (2022) 056, `arXiv:2112.10605 [hep-th]`.

[586] S. Abreu, H. Ita, B. Page, and W. Tschernow, "Two-loop hexa-box integrals for non-planar five-point one-mass processes," *JHEP* **03** (2022) 182, `arXiv:2107.14180 [hep-ph]`.

[587] C. G. Papadopoulos, "Simplified differential equations approach for Master Integrals," *JHEP* **07** (2014) 088, `arXiv:1401.6057 [hep-ph]`.

[588] D. D. Canko, C. G. Papadopoulos, and N. Syrrakos, "Analytic representation of all planar two-loop five-point Master Integrals with one off-shell leg," *JHEP* **01** (2021) 199, `arXiv:2009.13917 [hep-ph]`.

[589] M. Argeri and P. Mastrolia, "Feynman Diagrams and Differential Equations," *Int. J. Mod. Phys. A* **22** (2007) 4375–4436, `arXiv:0707.4037 [hep-ph]`.

[590] J. M. Henn, "Lectures on differential equations for Feynman integrals," *J. Phys. A* **48** (2015) 153001, `arXiv:1412.2296 [hep-ph]`.

[591] A. Gehrmann-De Ridder, T. Gehrmann, and E. W. N. Glover, "Antenna subtraction at NNLO," *JHEP* **09** (2005) 056, `arXiv:hep-ph/0505111`.

[592] J. Currie, E. W. N. Glover, and S. Wells, "Infrared Structure at NNLO Using Antenna Subtraction," *JHEP* **04** (2013) 066, `arXiv:1301.4693 [hep-ph]`.

[593] R. Gauld, A. Gehrmann-De Ridder, E. W. N. Glover, A. Huss, and I. Majer, "Associated production of a Higgs boson decaying into bottom quarks and a weak vector boson decaying leptonically at NNLO in QCD," *JHEP* **10** (2019) 002, `arXiv:1907.05836 [hep-ph]`.

[594] R. Gauld, A. Gehrmann-De Ridder, E. W. N. Glover, A. Huss, and I. Majer, "Predictions for Z-Boson Production in Association with a b-Jet at $\mathcal{O}(\alpha_s^3)$," *Phys. Rev. Lett.* **125** no. 22, (2020) 222002, `arXiv:2005.03016 [hep-ph]`.

[595] T. Gehrmann and R. Schürmann, "Photon fragmentation in the antenna subtraction formalism," *JHEP* **04** (2022) 031, `arXiv:2201.06982 [hep-ph]`.

[596] X. Chen, T. Gehrmann, E. W. N. Glover, M. Höfer, A. Huss, and R. Schürmann, "Single Photon Production at Hadron Colliders at NNLO QCD with Realistic Photon Isolation," `arXiv:2205.01516 [hep-ph]`.

[597] M. Czakon, "A novel subtraction scheme for double-real radiation at NNLO," *Phys. Lett. B* **693** (2010) 259–268, `arXiv:1005.0274 [hep-ph]`.

[598] M. Czakon, "Double-real radiation in hadronic top quark pair production as a proof of a certain concept," *Nucl. Phys. B* **849** (2011) 250–295, `arXiv:1101.0642 [hep-ph]`.

[599] R. Boughezal, K. Melnikov, and F. Petriello, "A subtraction scheme for NNLO computations," *Phys. Rev. D* **85** (2012) 034025, `arXiv:1111.7041 [hep-ph]`.

[600] S. Frixione, Z. Kunszt, and A. Signer, "Three jet cross-sections to next-to-leading order," *Nucl. Phys. B* **467** (1996) 399–442, `arXiv:hep-ph/9512328`.

[601] R. Frederix, S. Frixione, F. Maltoni, and T. Stelzer, "Automation of next-to-leading order computations in QCD: The FKS subtraction," *JHEP* **10** (2009) 003, `arXiv:0908.4272 [hep-ph]`.

[602] T. Binoth and G. Heinrich, "An automatized algorithm to compute infrared divergent multiloop integrals," *Nucl. Phys. B* **585** (2000) 741–759, `arXiv:hep-ph/0004013`.

[603] G. Heinrich, "A numerical method for NNLO calculations," *Nucl. Phys. B Proc. Suppl.* **116** (2003) 368–372, `arXiv:hep-ph/0211144`.

[604] C. Anastasiou, K. Melnikov, and F. Petriello, "A new method for real radiation at NNLO," *Phys. Rev. D* **69** (2004) 076010, `arXiv:hep-ph/0311311`.

[605] T. Binoth and G. Heinrich, "Numerical evaluation of phase space integrals by sector decomposition," *Nucl. Phys. B* **693** (2004) 134–148, `arXiv:hep-ph/0402265`.

[606] M. Czakon, A. Mitov, M. Pellen, and R. Poncelet, "NNLO QCD predictions for W+c-jet production at the LHC," *JHEP* **06** (2021) 100, `arXiv:2011.01011 [hep-ph]`.

[607] M. L. Czakon, T. Generet, A. Mitov, and R. Poncelet, "B-hadron production in NNLO QCD:

application to LHC t$\bar{t}$ events with leptonic decays," *JHEP* **10** (2021) 216, `arXiv:2102.08267 [hep-ph]`.

[608] S. Catani and M. Grazzini, "An NNLO subtraction formalism in hadron collisions and its application to Higgs boson production at the LHC," *Phys. Rev. Lett.* **98** (2007) 222002, `arXiv:hep-ph/0703012`.

[609] M. Grazzini, S. Kallweit, and M. Wiesemann, "Fully differential NNLO computations with MATRIX," *Eur. Phys. J. C* **78** no. 7, (2018) 537, `arXiv:1711.06631 [hep-ph]`.

[610] J. M. Campbell, R. K. Ellis, and S. Seth, "Non-local slicing approaches for NNLO QCD in MCFM," *JHEP* **06** (2022) 002, `arXiv:2202.07738 [hep-ph]`.

[611] R. Bonciani, S. Catani, M. Grazzini, H. Sargsyan, and A. Torre, "The q_T subtraction method for top quark production at hadron colliders," *Eur. Phys. J. C* **75** no. 12, (2015) 581, `arXiv:1508.03585 [hep-ph]`.

[612] R. Angeles-Martinez, M. Czakon, and S. Sapeta, "NNLO soft function for top quark pair production at small transverse momentum," *JHEP* **10** (2018) 201, `arXiv:1809.01459 [hep-ph]`.

[613] S. Catani, S. Devoto, M. Grazzini, S. Kallweit, J. Mazzitelli, and H. Sargsyan, "Top-quark pair hadroproduction at next-to-next-to-leading order in QCD," *Phys. Rev. D* **99** no. 5, (2019) 051501, `arXiv:1901.04005 [hep-ph]`.

[614] S. Catani, S. Devoto, M. Grazzini, S. Kallweit, and J. Mazzitelli, "Top-quark pair production at the LHC: Fully differential QCD predictions at NNLO," *JHEP* **07** (2019) 100, `arXiv:1906.06535 [hep-ph]`.

[615] S. Catani, S. Devoto, M. Grazzini, S. Kallweit, and J. Mazzitelli, "Bottom-quark production at hadron colliders: fully differential predictions in NNLO QCD," *JHEP* **03** (2021) 029, `arXiv:2010.11906 [hep-ph]`.

[616] R. Boughezal, X. Liu, and F. Petriello, "*N*-jettiness soft function at next-to-next-to-leading order," *Phys. Rev. D* **91** no. 9, (2015) 094035, `arXiv:1504.02540 [hep-ph]`.

[617] R. Boughezal, C. Focke, X. Liu, and F. Petriello, "*W*-boson production in association with a jet at next-to-next-to-leading order in perturbative QCD," *Phys. Rev. Lett.* **115** no. 6, (2015) 062002, `arXiv:1504.02131 [hep-ph]`.

[618] J. Gaunt, M. Stahlhofen, F. J. Tackmann, and J. R. Walsh, "N-jettiness Subtractions for NNLO QCD Calculations," *JHEP* **09** (2015) 058, `arXiv:1505.04794 [hep-ph]`.

[619] R. Boughezal, J. M. Campbell, R. K. Ellis, C. Focke, W. Giele, X. Liu, F. Petriello, and C. Williams, "Color singlet production at NNLO in MCFM," *Eur. Phys. J. C* **77** no. 1, (2017) 7, `arXiv:1605.08011 [hep-ph]`.

[620] J. Campbell and T. Neumann, "Precision Phenomenology with MCFM," *JHEP* **12** (2019) 034, `arXiv:1909.09117 [hep-ph]`.

[621] V. Del Duca, C. Duhr, G. Somogyi, F. Tramontano, and Z. Trócsányi, "Higgs boson decay into b-quarks at NNLO accuracy," *JHEP* **04** (2015) 036, `arXiv:1501.07226 [hep-ph]`.

[622] S. Catani and M. H. Seymour, "A General algorithm for calculating jet cross-sections in NLO QCD," *Nucl. Phys. B* **485** (1997) 291–419, `arXiv:hep-ph/9605323`. [Erratum: Nucl.Phys.B 510, 503–504 (1998)].

[623] F. Caola, K. Melnikov, and R. Röntsch, "Nested soft-collinear subtractions in NNLO QCD computations," *Eur. Phys. J. C* **77** no. 4, (2017) 248, `arXiv:1702.01352 [hep-ph]`.

[624] F. Caola, M. Delto, H. Frellesvig, and K. Melnikov, "The double-soft integral for an arbitrary angle between hard radiators," *Eur. Phys. J. C* **78** no. 8, (2018) 687, `arXiv:1807.05835 [hep-ph]`.

[625] M. Delto and K. Melnikov, "Integrated triple-collinear counter-terms for the nested soft-collinear subtraction scheme," *JHEP* **05** (2019) 148, `arXiv:1901.05213 [hep-ph]`.

[626] L. Magnea, E. Maina, G. Pelliccioli, C. Signorile-Signorile, P. Torrielli, and S. Uccirati, "Local analytic sector subtraction at NNLO," *JHEP* **12** (2018) 107, `arXiv:1806.09570 [hep-ph]`. [Erratum: JHEP 06, 013 (2019)].

[627] L. Magnea, E. Maina, G. Pelliccioli, C. Signorile-Signorile, P. Torrielli, and S. Uccirati, "Factorisation and Subtraction beyond NLO," *JHEP* **12** (2018) 062, `arXiv:1809.05444 [hep-ph]`.

[628] M. Cacciari, F. A. Dreyer, A. Karlberg, G. P. Salam, and G. Zanderighi, "Fully Differential Vector-Boson-Fusion Higgs Production at Next-to-Next-to-Leading Order," *Phys. Rev. Lett.* **115** no. 8, (2015) 082002, `arXiv:1506.02660 [hep-ph]`. [Erratum: Phys.Rev.Lett. 120, 139901 (2018)].

[629] T. Carli, D. Clements, A. Cooper-Sarkar, C. Gwenlan, G. P. Salam, F. Siegert, P. Starovoitov, and M. Sutton, "A posteriori inclusion of parton density functions in NLO QCD final-state calculations

at hadron colliders: The APPLGRID Project," *Eur. Phys. J. C* **66** (2010) 503–524, `arXiv:0911.2985 [hep-ph]`.

[630] T. Kluge, K. Rabbertz, and M. Wobisch, "FastNLO: Fast pQCD calculations for PDF fits," in *14th International Workshop on Deep Inelastic Scattering*, pp. 483–486. 9, 2006. `hep-ph/0609285`.

[631] S. Carrazza, E. R. Nocera, C. Schwan, and M. Zaro, "PineAPPL: combining EW and QCD corrections for fast evaluation of LHC processes," *JHEP* **12** (2020) 108, `arXiv:2008.12789 [hep-ph]`.

[632] A. Abdesselam *et al.*, "Boosted objects: a probe of beyond the standard model physics," *EPHJA,C71,1661.2011* **C71** (2011) 1661, `arXiv:1012.5412 [hep-ph]`.

[633] A. Altheimer *et al.*, "Jet Substructure at the Tevatron and LHC: New results, new tools, new benchmarks," `arXiv:1201.0008 [hep-ph]`. Long author list - awaiting processing.

[634] A. Altheimer *et al.*, "Boosted Objects and Jet Substructure at the LHC. Report of BOOST2012, held at IFIC Valencia, 23rd-27th of July 2012," *Eur. Phys. J. C* **74** no. 3, (2014) 2792, `arXiv:1311.2708 [hep-ex]`.

[635] D. Adams *et al.*, "Towards an Understanding of the Correlations in Jet Substructure," *Eur. Phys. J. C* **75** no. 9, (2015) 409, `arXiv:1504.00679 [hep-ph]`.

[636] R. Kogler, B. Nachman, A. Schmidt (editors), *et al.*, "Jet Substructure at the Large Hadron Collider: Experimental Review," *Rev. Mod. Phys.* **91** no. 4, (2019) 045003, `arXiv:1803.06991 [hep-ex]`.

[637] R. Kogler, *Advances in Jet Substructure at the LHC: Algorithms, Measurements and Searches for New Physical Phenomena*, vol. 284 of *Springer Tracts Mod. Phys.* Springer, 2021.

[638] C. H. Yeh, S. V. Chekanov, A. V. Kotwal, J. Proudfoot, S. Sen, N. V. Tran, and S. S. Yu, "Studies of granularity of a hadronic calorimeter for tens-of-TeV jets at a 100 TeV pp collider," *JINST* **14** no. 05, (2019) P05008, `arXiv:1901.11146 [physics.ins-det]`.

[639] E. Coleman, M. Freytsis, A. Hinzmann, M. Narain, J. Thaler, N. Tran, and C. Vernieri, "The importance of calorimetry for highly-boosted jet substructure," *JINST* **13** no. 01, (2018) T01003, `arXiv:1709.08705 [hep-ph]`.

[640] J. R. Andersen *et al.*, "Les Houches 2017: Physics at TeV Colliders Standard Model Working Group Report," 2018.

[641] **CMS** Collaboration, A. M. Sirunyan *et al.*, "Identification of heavy-flavour jets with the CMS detector in pp collisions at 13 TeV," *JINST* **13** no. 05, (2018) P05011, `arXiv:1712.07158 [physics.ins-det]`.

[642] **ATLAS** Collaboration, G. Aad *et al.*, "ATLAS b-jet identification performance and efficiency measurement with $t\bar{t}$ events in pp collisions at $\sqrt{s} = 13$ TeV," *Eur. Phys. J. C* **79** no. 11, (2019) 970, `arXiv:1907.05120 [hep-ex]`.

[643] **CMS** Collaboration, "A new calibration method for charm jet identification validated with proton-proton collision events at $\sqrt{s} =$13 TeV," 11, 2021.

[644] **ATLAS** Collaboration, G. Aad *et al.*, "Measurement of the c-jet mistagging efficiency in $t\bar{t}$ events using pp collision data at $\sqrt{s} = 13$ TeV collected with the ATLAS detector," *Eur. Phys. J. C* **82** no. 1, (2022) 95, `arXiv:2109.10627 [hep-ex]`.

[645] J. Erdmann, O. Nackenhorst, and S. V. Zeißner, "Maximum performance of strange-jet tagging at hadron colliders," *JINST* **16** no. 08, (2021) P08039, `arXiv:2011.10736 [hep-ex]`.

[646] Y. Nakai, D. Shih, and S. Thomas, "Strange Jet Tagging," `arXiv:2003.09517 [hep-ph]`.

[647] J. Erdmann, "A tagger for strange jets based on tracking information using long short-term memory," *JINST* **15** no. 01, (2020) P01021, `arXiv:1907.07505 [physics.ins-det]`.

[648] W. H. Chiu, Z. Liu, M. Low, and L.-T. Wang, "Jet timing," *JHEP* **01** (2022) 014, `arXiv:2109.01682 [hep-ph]`.

[649] S. Chatterjee, R. Godbole, and T. S. Roy, "Jets with electrons from boosted top quarks," *JHEP* **01** (2020) 170, `arXiv:1909.11041 [hep-ph]`.

[650] M. Mitra, R. Ruiz, D. J. Scott, and M. Spannowsky, "Neutrino Jets from High-Mass W_R Gauge Bosons in TeV-Scale Left-Right Symmetric Models," *Phys. Rev. D* **94** no. 9, (2016) 095016, `arXiv:1607.03504 [hep-ph]`.

[651] M. Nemevšek, F. Nesti, and G. Popara, "Keung-Senjanović process at the LHC: From lepton number violation to displaced vertices to invisible decays," *Phys. Rev. D* **97** no. 11, (2018) 115018, `arXiv:1801.05813 [hep-ph]`.

[652] K. du Plessis, M. M. Flores, D. Kar, S. Sinha, and H. van der Schyf, "Hitting two BSM particles

with one lepton-jet: search for a top partner decaying to a dark photon, resulting in a lepton-jet," `arXiv:2112.08425 [hep-ph]`.

[653] S. Dube, D. Gadkari, and A. M. Thalapillil, "Lepton-Jets and Low-Mass Sterile Neutrinos at Hadron Colliders," *Phys. Rev. D* **96** no. 5, (2017) 055031, `arXiv:1707.00008 [hep-ph]`.

[654] D. Wang, L. Wu, J. M. Yang, and M. Zhang, "Photon-jet events as a probe of axionlike particles at the LHC," *Phys. Rev. D* **104** no. 9, (2021) 095016, `arXiv:2102.01532 [hep-ph]`.

[655] B. Sheff, N. Steinberg, and J. D. Wells, "Higgs boson decays into narrow diphoton jets and their search strategies at the Large Hadron Collider," *Phys. Rev. D* **104** no. 3, (2021) 036009, `arXiv:2008.10568 [hep-ph]`.

[656] D. Kar and S. Sinha, "Exploring jet substructure in semi-visible jets," *SciPost Phys.* **10** no. 4, (2021) 084, `arXiv:2007.11597 [hep-ph]`.

[657] F. Canelli, A. de Cosa, L. L. Pottier, J. Niedziela, K. Pedro, and M. Pierini, "Autoencoders for Semivisible Jet Detection," `arXiv:2112.02864 [hep-ph]`.

[658] **CMS** Collaboration, A. Tumasyan *et al.*, "Search for a right-handed W boson and a heavy neutrino in proton-proton collisions at $\sqrt{s} = 13$ TeV," `arXiv:2112.03949 [hep-ex]`.

[659] **ATLAS** Collaboration, M. Aaboud *et al.*, "Search for a right-handed gauge boson decaying into a high-momentum heavy neutrino and a charged lepton in pp collisions with the ATLAS detector at $\sqrt{s} = 13$ TeV," *Phys. Lett. B* **798** (2019) 134942, `arXiv:1904.12679 [hep-ex]`.

[660] **CMS** Collaboration, A. Tumasyan *et al.*, "Search for resonant production of strongly coupled dark matter in proton-proton collisions at 13 TeV," `arXiv:2112.11125 [hep-ex]`.

[661] **ATLAS** Collaboration, G. Aad *et al.*, "Search for light long-lived neutral particles produced in pp collisions at $\sqrt{s} = 13$ TeV and decaying into collimated leptons or light hadrons with the ATLAS detector," *Eur. Phys. J. C* **80** no. 5, (2020) 450, `arXiv:1909.01246 [hep-ex]`.

[662] **CMS** Collaboration, A. M. Sirunyan *et al.*, "Search for long-lived particles using nonprompt jets and missing transverse momentum with proton-proton collisions at $\sqrt{s} = 13$ TeV," *Phys. Lett. B* **797** (2019) 134876, `arXiv:1906.06441 [hep-ex]`.

[663] H. Chen, I. Moult, J. Sandor, and H. X. Zhu, "Celestial Blocks and Transverse Spin in the Three-Point Energy Correlator," `arXiv:2202.04085 [hep-ph]`.

[664] H. Chen, I. Moult, and H. X. Zhu, "Spinning Gluons from the QCD Light-Ray OPE," `arXiv:2104.00009 [hep-ph]`.

[665] H. Chen, I. Moult, and H. X. Zhu, "Quantum Interference in Jet Substructure from Spinning Gluons," *Phys. Rev. Lett.* **126** no. 11, (2021) 112003, `arXiv:2011.02492 [hep-ph]`.

[666] H. Chen, M.-X. Luo, I. Moult, T.-Z. Yang, X. Zhang, and H. X. Zhu, "Three point energy correlators in the collinear limit: symmetries, dualities and analytic results," *JHEP* **08** no. 08, (2020) 028, `arXiv:1912.11050 [hep-ph]`.

[667] H. Chen, I. Moult, X. Zhang, and H. X. Zhu, "Rethinking jets with energy correlators: Tracks, resummation, and analytic continuation," *Phys. Rev. D* **102** no. 5, (2020) 054012, `arXiv:2004.11381 [hep-ph]`.

[668] J. Holguin, I. Moult, A. Pathak, and M. Procura, "A New Paradigm for Precision Top Physics: Weighing the Top with Energy Correlators," `arXiv:2201.08393 [hep-ph]`.

[669] P. T. Komiske, I. Moult, J. Thaler, and H. X. Zhu, "Analyzing N-point Energy Correlators Inside Jets with CMS Open Data," `arXiv:2201.07800 [hep-ph]`.

[670] M. Kologlu, P. Kravchuk, D. Simmons-Duffin, and A. Zhiboedov, "The light-ray OPE and conformal colliders," *JHEP* **01** (2021) 128, `arXiv:1905.01311 [hep-th]`.

[671] M. Dasgupta, A. Fregoso, S. Marzani, and G. P. Salam, "Towards an understanding of jet substructure," *JHEP* **1309** (2013) 029, `arXiv:1307.0007 [hep-ph]`.

[672] A. J. Larkoski, S. Marzani, G. Soyez, and J. Thaler, "Soft Drop," *JHEP* **1405** (2014) 146, `arXiv:1402.2657 [hep-ph]`.

[673] G. Luisoni, P. F. Monni, and G. P. Salam, "C-parameter hadronisation in the symmetric 3-jet limit and impact on α_s fits," *Eur. Phys. J. C* **81** no. 2, (2021) 158, `arXiv:2012.00622 [hep-ph]`.

[674] F. Caola, S. Ferrario Ravasio, G. Limatola, K. Melnikov, and P. Nason, "On linear power corrections in certain collider observables," *JHEP* **01** (2022) 093, `arXiv:2108.08897 [hep-ph]`.

[675] F. Caola, S. Ferrario Ravasio, G. Limatola, K. Melnikov, P. Nason, and M. A. Ozcelik, "Linear power corrections to e^+e^- shape variables in the three-jet region," `arXiv:2204.02247 [hep-ph]`.

[676] A. H. Hoang, S. Mantry, A. Pathak, and I. W. Stewart, "Nonperturbative Corrections to Soft Drop

Jet Mass," *JHEP* **12** (2019) 002, `arXiv:1906.11843 [hep-ph]`.

[677] L. J. Dixon, I. Moult, and H. X. Zhu, "Collinear limit of the energy-energy correlator," *Phys. Rev. D* **100** no. 1, (2019) 014009, `arXiv:1905.01310 [hep-ph]`.

[678] L. J. Dixon, M.-X. Luo, V. Shtabovenko, T.-Z. Yang, and H. X. Zhu, "Analytical Computation of Energy-Energy Correlation at Next-to-Leading Order in QCD," *Phys. Rev. Lett.* **120** no. 10, (2018) 102001, `arXiv:1801.03219 [hep-ph]`.

[679] M.-X. Luo, V. Shtabovenko, T.-Z. Yang, and H. X. Zhu, "Analytic Next-To-Leading Order Calculation of Energy-Energy Correlation in Gluon-Initiated Higgs Decays," *JHEP* **06** (2019) 037, `arXiv:1903.07277 [hep-ph]`.

[680] M. A. Ebert, B. Mistlberger, and G. Vita, "The Energy-Energy Correlation in the back-to-back limit at N³LO and N³LL'," *JHEP* **08** (2021) 022, `arXiv:2012.07859 [hep-ph]`.

[681] A. Kardos, A. J. Larkoski, and Z. Trócsányi, "Groomed jet mass at high precision," *Phys. Lett. B* **809** (2020) 135704, `arXiv:2002.00942 [hep-ph]`.

[682] Z. Bern, L. J. Dixon, F. Febres Cordero, S. Höche, H. Ita, D. A. Kosower, and D. Maitre, "Ntuples for NLO Events at Hadron Colliders," *Comput. Phys. Commun.* **185** (2014) 1443–1460, `arXiv:1310.7439 [hep-ph]`.

[683] K. Cranmer *et al.*, "Publishing statistical models: Getting the most out of particle physics experiments," *SciPost Phys.* **12** (2022) 037, `arXiv:2109.04981 [hep-ph]`.

[684] X.-L. Meng, "Statistical paradises and paradoxes in big data (I): Law of large populations, big data paradox, and the 2016 US presidential election," *The Annals of Applied Statistics* **12** no. 2, (2018) 685.

[685] HEP ML Community, "A Living Review of Machine Learning for Particle Physics." `https://iml-wg.github.io/HEPML-LivingReview/`.

[686] S. Badger *et al.*, "Machine Learning and LHC Event Generation," `arXiv:2203.07460 [hep-ph]`.

[687] D. Boyda *et al.*, "Applications of Machine Learning to Lattice Quantum Field Theory," in *2022 Snowmass Summer Study*. 2, 2022. `arXiv:2202.05838 [hep-lat]`.

[688] P. Shanahan *et al.*, "Snowmass 2021 Computational Frontier CompF03 Topical Group Report: Machine Learning," `arXiv:2209.07559 [physics.comp-ph]`.

[689] A. V. Manohar, "Effective field theories," *Lect. Notes Phys.* **479** (1997) 311–362, `arXiv:hep-ph/9606222`.

[690] I. Brivio and M. Trott, "The Standard Model as an Effective Field Theory," *Phys. Rept.* **793** (2019) 1–98, `arXiv:1706.08945 [hep-ph]`.

[691] I. Brivio, S. Bruggisser, F. Maltoni, R. Moutafis, T. Plehn, E. Vryonidou, S. Westhoff, and C. Zhang, "O new physics, where art thou? A global search in the top sector," *JHEP* **02** (2020) 131, `arXiv:1910.03606 [hep-ph]`.

[692] J. Ellis, M. Madigan, K. Mimasu, V. Sanz, and T. You, "Top, Higgs, Diboson and Electroweak Fit to the Standard Model Effective Field Theory," *JHEP* **04** (2021) 279, `arXiv:2012.02779 [hep-ph]`.

[693] **SMEFiT** Collaboration, J. J. Ethier, G. Magni, F. Maltoni, L. Mantani, E. R. Nocera, J. Rojo, E. Slade, E. Vryonidou, and C. Zhang, "Combined SMEFT interpretation of Higgs, diboson, and top quark data from the LHC," *JHEP* **11** (2021) 089, `arXiv:2105.00006 [hep-ph]`.

[694] T. Corbett, A. Helset, A. Martin, and M. Trott, "EWPD in the SMEFT to dimension eight," *JHEP* **06** (2021) 076, `arXiv:2102.02819 [hep-ph]`.

[695] R. Boughezal, E. Mereghetti, and F. Petriello, "Dilepton production in the SMEFT at $O(1/\Lambda 4)$," *Phys. Rev. D* **104** no. 9, (2021) 095022, `arXiv:2106.05337 [hep-ph]`.

[696] J. J. Ethier, R. Gomez-Ambrosio, G. Magni, and J. Rojo, "SMEFT analysis of vector boson scattering and diboson data from the LHC Run II," *Eur. Phys. J. C* **81** no. 6, (2021) 560, `arXiv:2101.03180 [hep-ph]`.

[697] V. Miralles, M. M. López, M. M. Llácer, A. Peñuelas, M. Perelló, and M. Vos, "The top quark electro-weak couplings after LHC Run 2," *JHEP* **02** (2022) 032, `arXiv:2107.13917 [hep-ph]`.

[698] G. Durieux, A. G. Camacho, L. Mantani, V. Miralles, M. M. López, M. Llácer Moreno, R. Poncelet, E. Vryonidou, and M. Vos, "Snowmass White Paper: prospects for the measurement of top-quark couplings," in *2022 Snowmass Summer Study*. 5, 2022. `arXiv:2205.02140 [hep-ph]`.

[699] A. Greljo, S. Iranipour, Z. Kassabov, M. Madigan, J. Moore, J. Rojo, M. Ubiali, and C. Voisey, "Parton distributions in the SMEFT from high-energy Drell-Yan tails," *JHEP* **07** (2021) 122, `arXiv:2104.02723 [hep-ph]`.

[700] S. Iranipour and M. Ubiali, "A new generation of simultaneous fits to LHC data using deep learning," *JHEP* **05** (2022) 032, `arXiv:2201.07240 [hep-ph]`.

[701] D. Liu, C. Sun, and J. Gao, "Machine learning of log-likelihood functions in global analysis of parton distributions," `arXiv:2201.06586 [hep-ph]`.

[702] S. Carrazza, C. Degrande, S. Iranipour, J. Rojo, and M. Ubiali, "Can New Physics hide inside the proton?," *Phys. Rev. Lett.* **123** no. 13, (2019) 132001, `arXiv:1905.05215 [hep-ph]`.

[703] **ZEUS** Collaboration, H. Abramowicz *et al.*, "Limits on contact interactions and leptoquarks at HERA," *Phys. Rev. D* **99** no. 9, (2019) 092006, `arXiv:1902.03048 [hep-ex]`.

[704] **CMS** Collaboration, A. Tumasyan *et al.*, "Measurement and QCD analysis of double-differential inclusive jet cross sections in proton-proton collisions at $\sqrt{s} = 13$ TeV," *JHEP* **02** (2022) 142, `arXiv:2111.10431 [hep-ex]`.

[705] R. Boughezal, F. Petriello, and D. Wiegand, "Removing flat directions in standard model EFT fits: How polarized electron-ion collider data can complement the LHC," *Phys. Rev. D* **101** no. 11, (2020) 116002, `arXiv:2004.00748 [hep-ph]`.

[706] R. Boughezal, F. Petriello, and D. Wiegand, "Disentangling Standard Model EFT operators with future low-energy parity-violating electron scattering experiments," *Phys. Rev. D* **104** no. 1, (2021) 016005, `arXiv:2104.03979 [hep-ph]`.

[707] **GEANT4** Collaboration, S. Agostinelli *et al.*, "GEANT4–a simulation toolkit," *Nucl. Instrum. Meth. A* **506** (2003) 250–303.

[708] **CALICE** Collaboration, G. Eigen *et al.*, "Characterisation of different stages of hadronic showers using the CALICE Si-W ECAL physics prototype," *Nucl. Instrum. Meth. A* **937** (2019) 41, `arXiv:1902.06161 [physics.ins-det]`.

[709] T. Han, Y. Ma, and K. Xie, "High energy leptonic collisions and electroweak parton distribution functions," *Phys. Rev. D* **103** no. 3, (2021) L031301, `arXiv:2007.14300 [hep-ph]`.